

Runa Berstad Frengen

# Assessment of swelling pressure on sprayed concrete lining at the headrace tunnel of Moglice Hydropower Project.

Master's thesis in Geotechnology

Supervisor: Bjørn Nilsen

June 2020

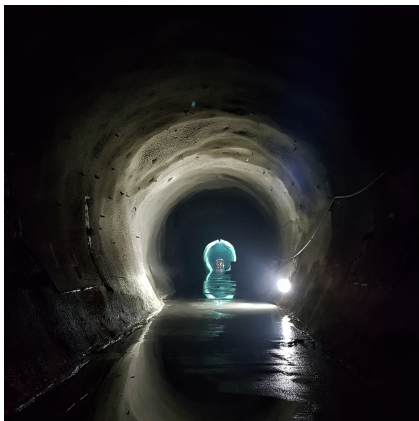
NTNU  
Norwegian University of Science and Technology  
Faculty of Engineering  
Department of Geoscience and Petroleum





Runa Berstad Frengen

# **Assessment of swelling pressure on sprayed concrete lining at the headrace tunnel of Moglice Hydropower Project.**



Master's thesis in Geotechnology  
Supervisor: Bjørn Nilsen  
June 2020

Norwegian University of Science and Technology  
Faculty of Engineering  
Department of Geoscience and Petroleum



Norwegian University of  
Science and Technology





**Assessment of swelling pressure on sprayed concrete lining at the headrace tunnel of**  
**Moglice Hydropower Project**

**Program for MSc-thesis**

**Runa Berstad Frengen**

As part of her specialization project, the candidate has carried out extensive laboratory testing with main focus on assessment of swelling and slaking properties of rocks from Moglice Hydropower Project. She also did extensive literature review of laboratory testing methodology and case studies of tunnels associated with collapse due to swelling and slaking. This MSc assignment is a continuation of her project assignment, with main emphasis to be placed on the following tasks:

- Evaluation of engineering geological conditions along the headrace tunnel at the Moglice Project, and in particular the conditions of the instrumented area of the tunnel.
- Discussion of results from laboratory testing of rock and sprayed concrete samples from the headrace tunnel.
- Assessment on the impact of swelling pressure on the applied rock support, consisting of reinforced ribs of sprayed concrete and systematic bolting.
- Prediction of extent of deformation and discussion of potential long-term impact on the stability of the headrace tunnel due to deformation caused by swelling pressure.
- Numerical modelling is to be used as a tool for analyzing stresses and deformations.

The work is to be carried out in cooperation with Statkraft, with MSc Thomas Schönborn as contact person. PhD research fellow Lena Selen is appointed co-supervisor. Background material for this study, such as reports, maps, information and data from supervisors, will be made available by Statkraft.

The thesis work is to be completed by June 1<sup>st</sup> 2020.

Norwegian University of Science and Technology (NTNU)  
Department of Geoscience and Petroleum  
August 22, 2019/revised 12.5.2020

Prof. Bjørn Nilsen  
Professor of geological engineering, main supervisor



---

## Abstract

Moglice hydropower tunnel is excavated through flysch rock. Flysch rock is a severely heterogeneous rock type comprised of weak and strong layers of clay, silt and sandstone with varying thickness. Another characteristic of flysch rock is the varying slake durability and the potential to disintegrate and/or swell in contact with water. A combination of these characteristics may cause deterioration of the rock mass and in worst case collapse.

The swelling and slaking characteristics of flysch rock collected in the headrace tunnel have been investigated in Frengen (2019), a specialisation project conducted as a precursor to this master thesis. All the specimens tested showed some degree of swelling, with an average swelling pressure of 0.18 MPa. The slake durability index of flysch rock ranged from 43% to 98% with an average of 70%.

Further laboratory investigations conducted during this thesis work included the UCS test, the Point load index test, the Brazil test as well as measurements of material density and sound velocity. For the rock specimens, some tests could not be performed due to poor quality or lack of sufficient material. Strong specimens dominated by sandstone and conglomerate had an average dry UCS of 137 MPa. Clay dominated specimens could only be tested with the point load test, from which an estimated UCS of 8 MPa was found. Sprayed concrete from the cores were also tested and had a dry UCS of 41 MPa and a tensile strength of 4.9 MPa.

Following up on these findings, the effect of swelling on the tunnel support consisting of reinforced ribs of sprayed concrete (RRS) have been evaluated by use of numerical modelling in RS<sup>2</sup>, a two dimensional FEM model. The aforementioned laboratory results have been used as material parameters in this analysis.

Two versions of flysch rock, a strong and a weak flysch and two versions of the RRS have been modelled. Extensive yielding of the rock mass was found for the weak flysch. The deformations of the tunnel wall prior to swelling was found to be 7 mm. The strong flysch showed deformations of the wall up to 2 mm, and a minimal yielded zone around the excavation.

Accurate levels of swelling are hard to model due to the uncertainty in how laboratory values relates to in-situ pressure. A range of pressures from 0.06 MPa to 5 MPa were tested by applying a uniform load onto the lining. This method produced an additional displacement of 0.4 mm for a swelling pressure of 0.5 MPa, which was evaluated to be a reasonable value. No RRS elements yielded for any pressure applied in the model.

The direct application of the swelling pressure did however not affect the encompassing rock mass in a realistic manner, which caused a reduction of rock stresses. Tensile forces thus yielded bolts and the rock mass around the tunnel, which seeds doubts to the validity of the results. Additional research is thus needed to confidently predict the extent swelling affect the long term stability. Furthermore, the combined effect of swelling and slaking may be a cause for concern. This effect should thus also be investigated further.





---

## Sammendrag

Tilløpstunellen ved Moglice vannkraftverk er drevet gjennom bergarten flysch. Denne bergarten er sterkt heterogen og består av sterke lag av sandstein og konglomerat som veksler med svake lag dominert av leir og siltstein. Slike bergarter kan svulle og har lav motstandsdyktighet mot vekslinger i vannmetning (slake durability). Desintegrasjon og svelling i slike bergarter kan i verste fall føre til tunnelkollaps.

Svelle og «slake durability» egenskapene til flysch hentet fra tilløpstunellen har blitt vurdert iCITE, som er forløperen til denne masteroppgaven. Alle flysch-prøvene viste en viss grad av svelling med ett gjennomsnittlig svelletrykk på 0.25 MPa. Prøvenes gjennomsnittlige «slake durability index» var 70%, med en variasjon fra 43% til 98%.

I denne masteroppgaven har de bergmekaniske egenskapene til flysch og sprøytebetong fra tilløpstunellen blitt vurdert ved bruk av UCS test, punktlasttest, braziltest samt målinger av tetthet og lyd hastighet. Sterke konglomerat og sandsteinslag hadde en gjennomsnittlig trykkfasthet på 137 MPa. Trykkfastheten til silt og leirsteinseksemplarene ble estimert til å være 8 MPa ved bruk av punktlasttesten, da materialet var for svakt til å prepareres for UCS test. Sprøytebetongen hadde en trykkfasthet på 41 MPa og strekkfasthet på 4.9MPa.

Det numeriske modelleringsverktøyet RS<sup>2</sup>, et todimensjonal FEM program ble brukt for å evaluere effekten svelling har på stabiliteten til tunellen. Laboratorieresultatene ble brukt som inngangsparametere i denne modellen.

To versjoner av flysch, en sterk og en svak ble evaluert samt to versjoner av sikringen bestående av sprøytebetongbuer. Den svake flyschen gikk i brudd for ett omfattende område rundt tunellen før svelling var lagt til. Deformasjonene av veggene var på dette punktet 7 mm. Den sterke flyschen hadde en mindre bruddsone og kun en deformasjon på 2mm.

Det er vanskelig å vurdere hvor mye svelling og hva slags svelletrykk som kan forventes in situ. Svelletrykk fra 0.06 MPa til 5 MPa var derfor testet i en sensitivitetsanalyse. Trykket ble ført på sikringen som en konstant uniform last rundt profilet. Svelletrykket som ble vurdert som et sannsynlig maks, 0.5 MPa, resulterte i en ekstra deformasjon på 0.4 mm i veggene. Ingen sprøytebetongelementer gikk i brudd i modellen.

Metoden brukt til å simulere svelling påvirket ikke den omliggende bergmassen på en realistisk måte, og førte til strekkbrudd i både bergmassen og etter hvert bolter. Gyldigheten til resultatene er derfor tvilsomme. Videre modellering er nødvendig for å vurdere effekten svelling har på bergsikring. I tillegg bør den kombinerte effekten av svelling og lav «slake durability» undersøkes nærmere for å vurdere den langsiktige stabiliteten av tunellen.



---

## Preface

This paper concludes the final work of my Master of Science degree in Geotechnology with a specialisation towards Engineering Geology and Rock Mechanics. The thesis work was initiated in the autumn semester of 2019 and is submitted to the Department of Geosciences and Petroleum at the Norwegian University of Science and Technology (NTNU).

The thesis focus has been to conduct an assessment of the stability of the headrace tunnel at Moglice Hydropower Project. The effect of swelling rock on installed support and long term stability related to squeezing deformation has been the main focus.

This thesis is building on the specialisation project "Study on the swelling and slaking properties of rocks from Moglice Hydropower Project" that was submitted in June 2019. The findings from this project is summarised in Chapter 2.

Initially, Professor Krishna Panthi was intended to supervise this thesis, considering he had already supervised the specialisation project. However, as he was not available at NTNU due to his sabbatical work, other options eventually had to be explored. Professor Bjørn Nilsen was understanding of the situation and agreed to supervise an extra student on short notice, and has supervised the thesis work as of March 2020.

Lena Selen has been the co-supervisor for the specialisation project and questions regarding swelling and slaking. Statkraft has been the cooperating partner for this thesis from which Thomas Schönborn has been the contact person at the company.

Trondheim, 01.06.2020

A handwritten signature in black ink, reading "Runa Berstad Frengen". The signature is written in a cursive, flowing style.

Runa Berstad Frengen



---

## Acknowledgements

First I would like to thank Bjørn Nilsen for kindly taking on the additional responsibility and time to supervise an extra student this spring. Although we did not have many meetings in person as the coronavirus pandemic unfolded shortly after he agreed to supervise me, the weekly discussions over Skype have been essential to finish this master's thesis.

I would also like to thank Krishna Panthi for being my supervisor during the specialisation project and Lena Selen, Gunnar Vistnes, Jon Runar Drotninghaug and Laurentius Tjihuis for their time, guidance and interesting discussions regarding the the laboratory testing both in the specialisation project and this thesis.

The cooperating partner of this project has been Statkraft, where Thomas Schönborn has been the contact person. I would like to extend my gratitude for his hospitality and enlightening conversations when visiting the project site at Moglice during the specialisation project.

Most importantly, I would like to thank Ingeborg and Jomar for being the worlds best and most loving parents. Without their support, comforting words and proof readings, this thesis would never have been finalised. Additional thanks to Jeras and my siblings Eira and Trym for their encouragement during the writing process. Of course, my cat Hermine deserves a thank you for (although with limited success) attempting to write parts of this text.

At last, I would like to thanks my friends and fellow students from the study association Bergstuderendes Forening for an excellent time as a student at NTNU. Practices and events with song, music and Dahl's pilsner with the girls choir Spinell and Berseblæsten Student Orchestra have been the foundation for many of my best memories as a student.

R.B.F.



# Contents

<b>Abstract</b>	<b>i</b>
<b>Sammendrag</b>	<b>ii</b>
<b>Preface</b>	<b>iii</b>
<b>Acknowledgements</b>	<b>iv</b>
<b>1 Introduction</b>	<b>1</b>
1.1 Background . . . . .	1
1.2 Thesis scope . . . . .	2
1.3 Methodology . . . . .	3
1.3.1 Numerical modelling . . . . .	3
1.3.2 Laboratory investigations . . . . .	3
1.3.3 Literature studies . . . . .	3
1.3.4 Context from the specialisation project . . . . .	4
1.4 Limitations . . . . .	4
<b>2 Considerations from the Specialisation project</b>	<b>5</b>
2.1 Swelling and slaking . . . . .	6
2.1.1 Swelling . . . . .	6
2.1.2 Slaking . . . . .	8
2.2 Tunnel collapse in the Chingaza Project in Colombia . . . . .	9
2.3 Testing methodologies . . . . .	11
2.3.1 The slake durability index test . . . . .	12
2.3.2 Swelling tests . . . . .	13
2.4 Determining mineral content by use of XRD . . . . .	15
2.5 Sample description . . . . .	16
2.5.1 Flysch . . . . .	16
2.6 Results from the laboratory testing . . . . .	17
2.6.1 Mineralogical content . . . . .	17
2.6.2 Swelling and slaking . . . . .	17
2.7 Main findings from the specialisation project . . . . .	18

---

<b>3</b>	<b>Rock mass characteristics and stability</b>	<b>19</b>
3.1	Introduction . . . . .	19
3.2	Rock mechanical properties . . . . .	19
3.2.1	Intact rock strength . . . . .	20
3.2.2	Elasticity and deformability of rocks . . . . .	22
3.2.3	Tensile strength . . . . .	23
3.2.4	Factors influencing rock mechanical laboratory results . . . . .	24
3.3	Rock mass strength and deformability . . . . .	28
3.3.1	Rock mass strength . . . . .	28
3.3.2	Rock mass deformability . . . . .	28
3.4	Geological setting . . . . .	29
3.4.1	Stress situation . . . . .	29
3.4.2	Discontinuities . . . . .	32
3.4.3	The effect of water . . . . .	34
3.5	Failure criteria . . . . .	35
3.5.1	Mohr-Coulomb criterion . . . . .	35
3.5.2	Hoek Brown criterion . . . . .	36
3.5.3	Applicability of the Hoek-Brown criteria . . . . .	37
<b>4</b>	<b>Moglice hydropower project</b>	<b>39</b>
4.1	Project description . . . . .	39
4.2	Engineering geological conditions . . . . .	40
4.2.1	Regional geology . . . . .	40
4.2.2	Ground investigations . . . . .	41
4.2.3	Geological conditions at the area instrumented with flat jacks . . . . .	42
4.3	Design of the headrace tunnel . . . . .	44
<b>5</b>	<b>Laboratory testing</b>	<b>45</b>
5.1	Material description . . . . .	45
5.1.1	Sprayed concrete and rock material cores . . . . .	45
5.2	Specimen preparation . . . . .	48
5.3	Uniaxial compression strength test and deformability . . . . .	49
5.4	Point load index test . . . . .	50
5.5	Brazil test . . . . .	53
5.6	Density and velocity . . . . .	53
<b>6</b>	<b>Methodology of numerical modelling</b>	<b>55</b>
6.1	Introduction to methods of analysing stability . . . . .	55
6.2	Numerical analysis . . . . .	55
6.2.1	Types of numerical models . . . . .	56
6.2.2	The process of a numerical analysis . . . . .	56



---

<b>7 Evaluating the effect of swelling by use of RS<sup>2</sup></b>	<b>59</b>
7.1 Problem definition . . . . .	59
7.2 Choice of numerical method . . . . .	59
7.3 Model geometry . . . . .	60
7.3.1 Mesh and boundary conditions . . . . .	60
7.3.2 Stages . . . . .	61
7.4 Determining input parameters . . . . .	62
7.4.1 Material parameters . . . . .	62
7.4.2 In-situ stresses . . . . .	64
7.4.3 Support . . . . .	67
7.4.4 Load splitting . . . . .	69
7.4.5 Swelling pressure . . . . .	70
<b>8 Results from the numerical model</b>	<b>73</b>
8.1 General stresses and deformations prior to swelling . . . . .	73
8.1.1 Stresses and yielded zones . . . . .	73
8.1.2 Deformation reduction due to the additional support . . . . .	75
8.1.3 Yielded bolts . . . . .	78
8.2 Swelling . . . . .	78
8.2.1 Deformations and yielded support in weak rock . . . . .	78
8.2.2 Deformations and yielded support in strong flysch . . . . .	80
8.2.3 Comments on the effect of swelling in weak and strong flysch . . . . .	82
<b>9 Discussion</b>	<b>85</b>
9.1 General rock characteristics . . . . .	85
9.2 Numerical analysis . . . . .	86
9.2.1 Input values . . . . .	86
9.2.2 Iterations and changes to the model . . . . .	88
9.3 Long term stability . . . . .	88
9.3.1 Deformations at the excavation and support stage . . . . .	88
9.3.2 The effect of swelling . . . . .	89
9.3.3 Swelling and slaking . . . . .	90
<b>10 Conclusion and recommendations</b>	<b>91</b>
10.1 Conclusion . . . . .	91
10.2 Recommendations for further work . . . . .	92
<b>Bibliography</b>	<b>92</b>
<b>Appendices</b>	<b>i</b>
Appendix A: Laboratory results . . . . .	i
Appendix B: Standard charts and Figures . . . . .	xi

# Chapter 1

## Introduction

### 1.1 Background

After a tumultuous political century, the Albanian energy sector is in a crisis. Due to poor investments in the 1990's the energy sector has been neglected while the demand for energy has been rising due to increased modernisation of households, causing capacity shortfalls sometimes leads to daily power outages or grid instabilities (Rickerson and Perroy, 2005). Together with the threat of climate change, the demand for clean energy in Albania is evident.

As of 2005, only 35% of the major hydropower potential was exploited in Albania (NAE, 2003). In IISD (2014) the president of Albania Bujar Faik Nishani declared that the country has implemented new climate policies in line with the EU regulations for 2020. Thus, a reduction of green house gas emissions of 20% compared to the level in 1990 is to be obtained (EU, 2014). As a part of this initiative, the Devoll hydropower project (DHPP) is now under development.

The DHPP is located southeast in Albania along the Devoll river around 50 - 70 km from the capital Tirana. The project location is shown in Figure 1.1. When completed the project will produce an annual 705 GWh (Statkraft, 2019). This will increase the Albanian electricity production by 17% (Statkraft, 2014). The lower plant in this project, Banja is already in operation, while a second plant, Moglice is currently under construction.

Both this master's thesis, and the specialisation project that it builds upon, is written in cooperation with Statkraft, which since 2013 held the concession to the DHPP through their daughter company Devoll Hydropower Sh.A.

Statkraft has a long history of developing hydropower in Norway. After the year 2000 they have started to expand their practice and are developing hydropower projects in the Andes Mountains, Albania and elsewhere in the world (Statkraft, 2015). Some of these projects have experienced tunnel collapses and Statkraft is now funding a PhD project through HydroCen to

assess the potential swelling and slaking behaviour of weak rock such as flysch, serpentinite, andesite and clay rich rocks.

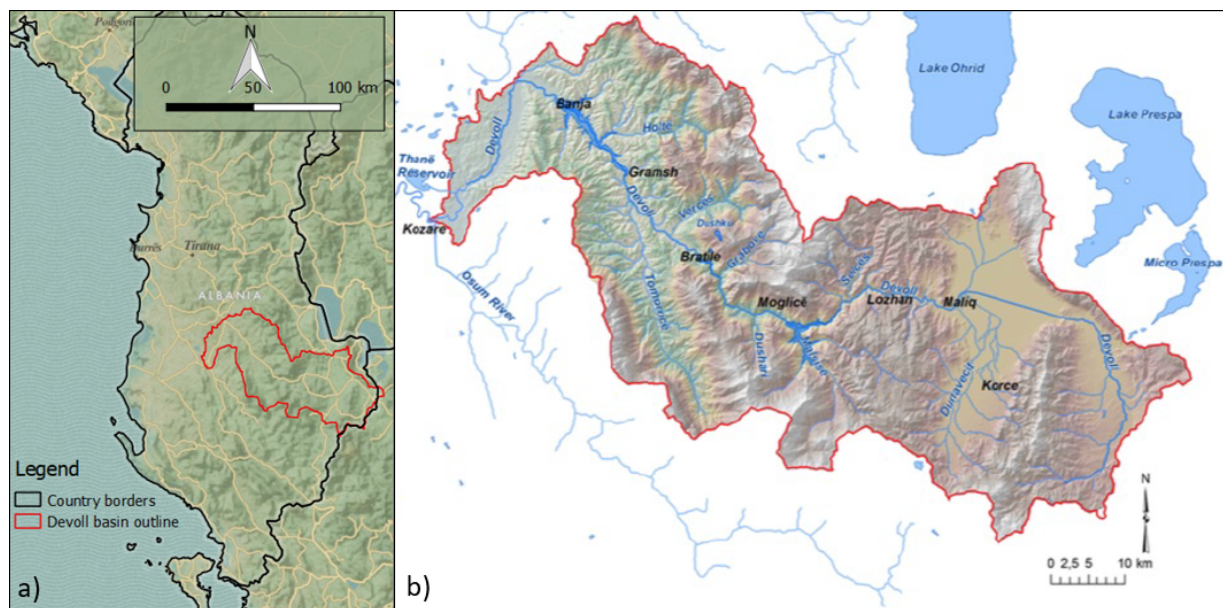


Figure 1.1. a) Overview of the location of the Devoll catchment within Albania (Frengen, 2019). b) Closeup of the Devoll catchment and the location of Moglice (Statkraft, 2017).

Where Moglice HPP is being constructed, rocks as flysch and serpentinite is commonplace. Such rocks may display swelling and slaking behaviour. Hence, the relationship between mineralogy, slaking and swelling of rocks brought from Moglice HPP has been discussed in the specialisation project that is written as a precursor for this master's thesis (Frengen, 2019).

Building on this, the mechanical properties of flysch and sprayed concrete samples from the headrace tunnel will be tested in the lab. Furthermore, the results from these tests will be used to evaluate what impact swelling will have on the applied support and on long term stability of the tunnel.

## 1.2 Thesis scope

The following points describes the main tasks for this master's thesis:

- Evaluation of engineering geological conditions along the headrace tunnel at the Moglice Project, and in particular the conditions of the instrumented area of the tunnel.
- Discussion of results from laboratory testing of rock and shotcrete samples from the headrace tunnel.
- Assessment of the impact of swelling pressure on the applied rock support, consisting of reinforced ribs of sprayed concrete and systematic bolting.
- Prediction of the extent of deformation and discussion of potential long-term impact on the stability of the headrace tunnel due to deformations caused by swelling pressure.
- Numerical modelling is to be used as a tool for analysing stresses and deformations.

## **1.3 Methodology**

The following tools and practices have been used to deliver the aforementioned scopes:

### **1.3.1 Numerical modelling**

The software RS<sup>2</sup> has been used for the following purposes:

- Evaluating in-situ stresses in the area.
- Determining the effect of different support designs.
- Conducting a sensitivity analysis on the effect of different swelling pressures.

### **1.3.2 Laboratory investigations**

The main source of input data for the swelling characteristics are determined from laboratory investigations during the specialisation project (Frengen, 2019). Further investigations on the mechanical properties of flysch rock and sprayed concrete was performed for this thesis to produce the necessary material input data. The following tests and measurements have been conducted in the laboratory for this thesis:

- Uniaxial compression test
- Point load strength test
- Brazil test
- Sound velocity measurements
- Density measurements

### **1.3.3 Literature studies**

To evaluate and choose reasonable input parameters for the numerical model, a literature study of relevant rock mass characteristics and relevant laboratory methods have been conducted. The topics that have been researched for this thesis are:

- Rock mechanical properties and laboratory practices to determine these.
- Empirical relationship between rock and rock mass properties.
- The effect of geological features.
- Failure criteria and appropriate settings to apply them.

A review of numerical modelling tools and a suggested methodology is also performed to make an informed choice of software and modelling procedure.

### **1.3.4 Context from the specialisation project**

Several parts of the specialisation project are relevant for this thesis and is referred to throughout the text. Because the specialisation project is unpublished, sections that are of importance have been assembled in Chapter 2 together with a presentation of the main findings from the project.

From the literature study, theory on swelling and slaking characteristics of rocks and the validity of different laboratory practices determining these have been included. A case study highlighting the issue of swelling and slaking in water tunnels is also presented.

## **1.4 Limitations**

The laboratory work conducted in the specialisation project is limited to rocks collected from two rock drill cores. The rock samples are therefore only representing of one section of the headrace tunnel and cannot without caution be used to illustrate the condition of the rock types as a whole. Swelling and slaking results may therefore not be fully transferable to other parts of the tunnel. Another point of caution is the limited amount of tested rock samples. Only four serpentinite samples and six flysch samples are tested, thus the reliability of the results are somewhat reduced.

During the initial phase of this thesis work, it was discovered that only thirteen out of the sixty cores available was suitable for laboratory testing, which significantly reduced the available material. Due to this, the Brazil test could not be performed on rock material. Furthermore, it was discovered that none of the cores containing the weaker flysch were in a state where material strength could be obtained through the UCS test. Even with the point load test, many clay flysch samples gave invalid results, rendering the material strength uncertain. Serpentinite was also to be tested, but no pieces were of high enough quality to allow the mechanical properties to be studied.

The tool used to analyse the effect of swelling on the installed rock support and long term stability was numerical modelling. A model is never more accurate than the input data used. Limited information about rock stresses and difficulty modelling 3D structures in a 2D software, in addition to uncertainty in the material input parameters were the main limitations concerning the numerical model.

## Chapter 2

# Considerations from the Specialisation project

This master's thesis is a continuation of the specialisation project "Study on the swelling and slaking properties of rocks from Moglice Hydropower Project" (Frengen, 2019). During this project, the swelling and slaking properties of flysch and serpentinite collected at Devoll HPP. The NTNU swelling pressure test and the free swelling test and the slake durability test was used for this purpose. X-ray diffraction was used to determine the rocks mineralogical content. The following research questions were answered in the project:

- What is the mineral content of the flysch and serpentinite rock?
- Is there a relationship between mineral content and swelling potential?
- Is there a relationship between mineral content and slaking?
- Is there a correlation between the swelling and slaking values of the tested rocks?

As a part of the specialisation project, a literature study was conducted. The main focus was the swelling and slaking properties of rocks and what minerals are likely to cause these issues. Additionally, the laboratory methods used to determine swelling and slaking was evaluated. A case study of projects where failure occurred due to swelling and/or slaking was also performed. Important sections from the literature and case study are reproduced in this chapter to give the reader the necessary background.

At last, the result of the analysis is presented. Serpentinite results are not presented in this chapter, as they are not of interest for this thesis. For additional information about laboratory methodology and more in-depth theory, the reader is referred to Frengen (2019).

## 2.1 Swelling and slaking

Swelling and slaking are both the result of water-rock interaction and are thus of interest when evaluating the stability of a hydropower tunnel. Depending on the mineral content and texture of the rock mass, swelling and slaking may occur simultaneously or independently. The main mineralogical culprit responsible for swelling is clay minerals. In Norway, swelling clays are associated with 75% of the cost related to reinforcement installed after a tunnel has been put into operation (Selmer-Olsen et al., 1989). Slaking may occur in all types of rock, but sedimentary rocks are generally prone to experience high levels. In such rock, minerals may be loosely bound due to insufficient compaction or cementation and thus slake when exposed to the elements (Nilsen and Palmström, 2000).

In a hydropower tunnel environment, both swelling and slaking may pose a threat to stability as both running water, and cycles of wetting and drying are present conditions. To plan sufficient support, knowing what minerals are likely to cause such problems are important.

### 2.1.1 Swelling

Swelling is a term that describes an expansion that occurs as a time dependent volume increase (Einstein, 1996). In a tunnel, swelling manifests as ground deformations or advancement into the tunnel as the rock absorbs water. Although the result is similar to that of squeezing, there is an important distinction to be made. For swelling, a reaction between water and the rock must occur to cause the deformation (Nilsen and Palmström, 2000). Squeezing on the other hand, is a mechanical process where shearing of the rock material caused by stress, leading to inward movement of the tunnel perimeter (Einstein, 1996).

Naturally, the degree of swelling is determined by the type and content of swelling material in the rock. Nilsen and Palmström (2000) lists the following minerals as the main reason for swelling:

- Smectite clay minerals (montmorillonite, vermiculite, ect.)
- Anhydrite
- Pyrrhoite (Found in some scists and shales)

#### **Clay minerals: Smectite**

Structurally, clay minerals are composed of sheets of alumina octahedral (O-layer) and silica tetrahedral (T-layer) layers. In a non-swelling clay such as kaolinite, seen in Figure 2.1 the T and O layer is condensed, forming a 1:1 structure. The compact structure remains uncharged, and water is thus not absorbed between the sheets. Montmorillonite is a swelling clay with a 1:2 structure. Typically the  $Al^{+3}$  and  $Si^{+4}$  in the structure are replaced with cations of lower valency, resulting in a permanently negatively charged surface. Intracrystalline swelling may then occur as water is absorbed between the sheets.

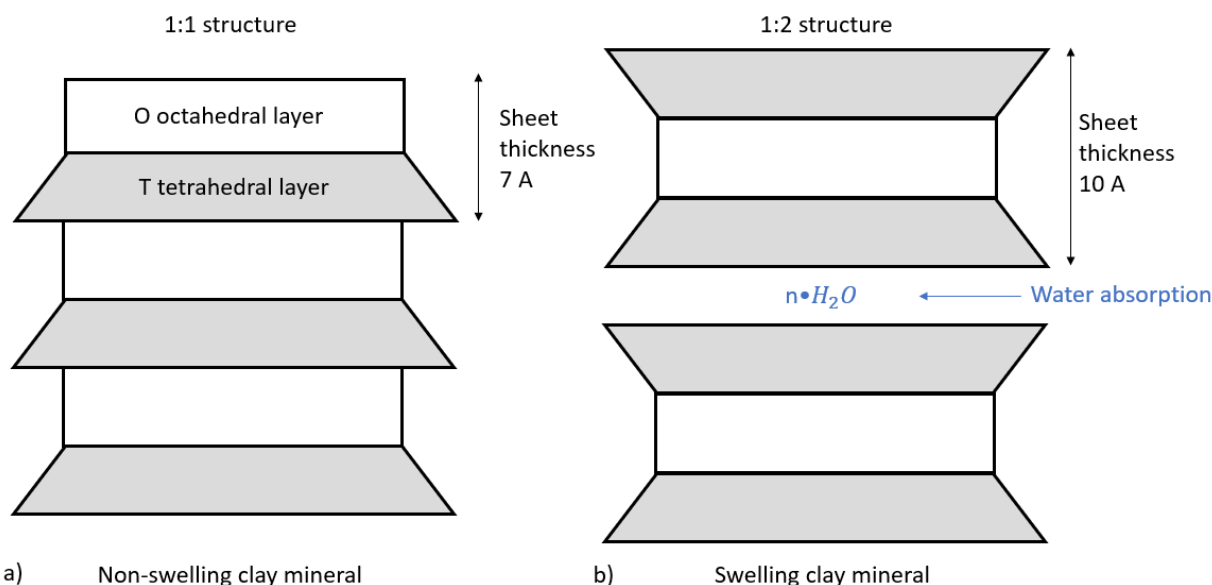


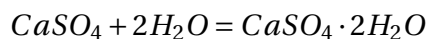
Figure 2.1. Structural differences between non-swelling clay such as kaolinite (a) and swelling clay exemplified by montmorillonite (b). The sheet thickness is given in Angstrom,  $1\text{Å}=10^{-7}\text{m}$  (Frenge, 2019).

Depending on which cation, the quantity of replaced cations, and access to water, the degree of swelling will vary (Madsen and Müller-Vonmoos, 1989). A montmorillonite that is fully saturated by  $\text{Na}^+$  or  $\text{Li}^+$ , may swell and give an interlayer separation of several nanometers (Theng, 2012). In pure montmorillonite the pressure created by swelling may reach as high as 400 MPa (Madsen and Müller-Vonmoos, 1989).

In addition to cation exchange, cations are also attracted to the negative surface of the clay minerals (Theng, 2012). The increased concentration causes osmotic swelling, an effect where water will flow to a higher concentration of cations (Theng, 2012).

### Anhydrite

Anhydrite ( $\text{CaSO}_4$ ) is an evaporite mineral commonly formed by the dehydration of gypsum or a residue after evaporating seawater (Dyar, 2008). Thus, rocks of sedimentary origin may contain this mineral (Nilsen and Palmström, 2000). When subjected to water, the mineral is transformed back to gypsum through the following chemical reaction (Madsen and Müller-Vonmoos, 1989).



Through this process water is incorporated into the crystal structure and causes an expansion of 60% as visible in Figure 2.2. Swelling pressures of up to 4 MPa may occur in anhydrite containing rock formations (Madsen and Müller-Vonmoos, 1989).



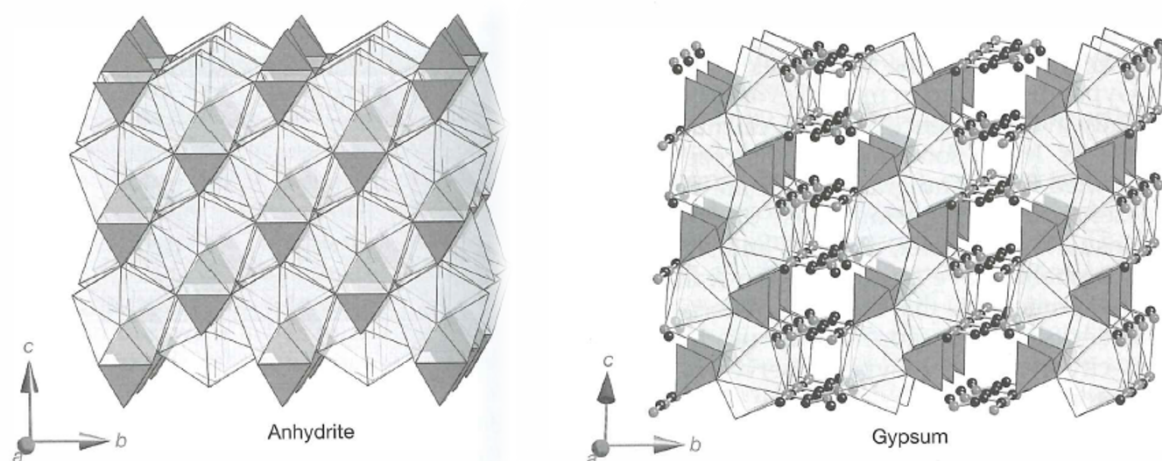


Figure 2.2. The structures of anhydrite and gypsum. The mineral structure occupy a visibly larger volume in the gypsum structure. Image from Dyar (2008).

### Pyrrhoite

Pyrrhotite is a term that is used to describe a collection of several variations of iron sulphides with compositions ranging from  $Fe_6S_7$  through  $Fe_{11}S_{12}$ . Certain pyrrhoites can expand when exposed to oxygen in the atmosphere or in water (Nilsen and Palmström, 2000). The byproduct of the oxidation, an acid, can cause clays and carbonates in the rock to transform to anhydrite which as described may swell when exposed to water (Taylor and Spears, 1970).

### 2.1.2 Slaking

Nilsen and Palmström (2000) defines slaking as a disintegration or weathering in response to changes in humidity and temperature. Furthermore, a rocks slake durability is defined as its resistance to disintegration or slaking when exposed to weathering processes. A current trend in hydropower is to produce electricity after demand (Bråtveit et al., 2016). Water tunnels are thus subjected to cycles of wetting and drying to a larger extent than before, which may amplify the slaking effect.

Franklin and Chandra (1972) mentions the following rock characteristics as influential to the degree of slaking:

- Permeability and porosity.
- Reactions between the rock and penetrating fluids.
- The capacity of the rock to resist disruptive forces.

Franklin and Chandra (1972) explains that increased permeability and porosity increases the possibility for fluids to enter a rock and and the fluids mobility. Reactions like ion exchange, capillary effects and stress relief are then affecting the rock at a faster rate. Typical durable rocks are thus impermeable, or non-reactive or has high intergranular strength (Franklin and Chandra, 1972).

As with swelling, the mineralogy is of importance. Clay minerals as described in the previous section are in general a common denominator for slaking rocks. Shales and mudstones are thus some of the rocks most susceptible to slaking. In addition clay bearing rocks as weathered igneous rocks or some sandstones can also experience slaking (Franklin and Chandra, 1972). Due to the similarity in mineralogy, slaking is observed alongside swelling in several cases (Selen, Panthi et al. (2018), Brattli and Broch (1995), Franklin and Chandra (1972)).

An example of total effect of clay content and permeability is illustrated in Brattli and Broch (1995). The slake durability of two rocks, a homogeneous siltstone and a shale with a penetrative slaty cleavage were compared. Upon submersion the clay containing and more permeable shale disintegrated almost immediately. On the other hand the siltstone did not visibly disintegrate after two hours covered in water.

## **2.2 Tunnel collapse in the Chingaza Project in Colombia**

To highlight the potential consequences of swelling and slaking, the failure that occurred at the Chingaza project is described. The background for the project was the massive population growth in the city of Bogota in the period from 1938 to 1984. During this period, the population grew from 350 000 to 6 million inhabitants. Increasing the water supply was a necessary project to facilitate the growth. In 1970, the Chingaza project was initiated to add 14 m<sup>3</sup>/s of water to the city (Broch, 1984).

The longest tunnel in the project was the 28.4 km long Palacio-Rioblanco tunnel. This tunnel had a diameter of 3.7 m and went through a series of sedimentary rocks, mainly of Cretaceous age (Broch, 1984). A 4 km section of the tunnel was excavated through the Fomeque formation, dominated by shales interbedded with silt and limestones. The rock was folded and sheared, which resulted in localised crushing and fracturing. Depending on the local geological condition different support mechanisms were installed along the tunnel. Sprayed concrete with a thickness of 5- 15 cm was used as lining for 2 km of this section and 2.2 km was lined with plain concrete. Four sections of a total of 64 m was covered with steel linings (Brattli and Broch, 1995).

After four months use, the water supply was stopped when it was discovered that the tunnel was about to be completely blocked. At this time, the capacity was as low as 1 m<sup>3</sup>/s (Broch, 1984). From an inspection, more than 40 fall-outs and slides were observed in the tunnel. One of these is illustrated in Figure 2.3 and shows a near total closure of the tunnel. Most of these were located in the shotcrete lined part in the Fomeque formation (Brattli and Broch, 1995).



Figure 2.3. Debris from fallout and slides in the Chingaza tunnel. Note the broken shotcrete lining (Brattli and Broch, 1995).

A study of rocks from the Fomeque formation was conducted by Brattli and Broch (1995). Results from swelling tests on powder and disks as well as the samples reaction with water is displayed in Table 2.1, shows a clear relationship between disk swelling pressure and disintegration in water, which indicates a low SDI. The result of submersing sample G in water for two hours is shown in Figure 2.4.

Table 2.1. Results from swelling pressure tests on both powder and disk samples as well as their reaction in water on rocks from the Fomeque formation (Brattli and Broch, 1995). Rock type has been added where descriptions of the samples are given in the text.

Station no	Sample (rock type)	Swelling pressure [MPa]		Reaction in water
		Powder	Disk	
K1 + 553	A	0.05	0.56	No reaction
K2 + 760	D (siltstone)	-	0.14	No reaction
K2 + 875	F	-	3.2	Moderate disintegration
K3 + 037	G (Shale)	0.06	4.5	Complete disintegration

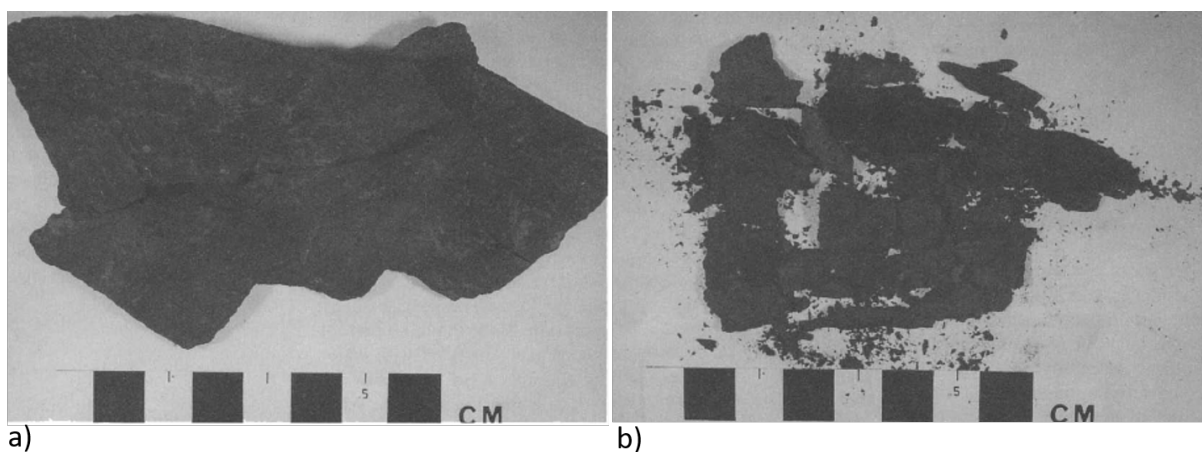


Figure 2.4. Sample G (shale) a) before and b) after submersion in water for about 2 hours. The rock is almost completely disintegrated into small fragments (Brattli and Broch, 1995).

To highlight the differences between the rocks, Brattli and Broch (1995) conducted further testing on sample D, a massive siltstone, and G, a fissible partly slickensided shale as the difference in swelling pressure and level of disintegration were the largest for these materials. It is also noted that the problematic areas in the tunnels were characterised by rocks similar to the shale, while no fall-outs occurred in the siltstone areas.

The mineralogy was studied both in thin sections and by XRD testing. An important distinction is that sample G consisted of 20% swelling clays, almost the double of the amount in sample D, which only had 11%. The content of illite/muscovite and chlorite was also much higher at 28% and 17% in sample G compared to 11 and 7% in sample D. Both samples had similar levels of pyrite around 10 %, while sample D contained 18% dolomite while sample G only consisted of 5%.

Three possible factors were evaluated by Brattli and Broch (1995) to influence the rock mass stability. First, the changes of rock texture during the construction period. The excavation of the tunnel was conducted over a 10 year period. It is believed that the excessive drying out that happened in this period caused fissures and cracks to form in the shale, increasing its permeability. The drying is further believed to have reduced the strength of the rock. Secondly, weathering of pyrite and formation of gypsum or sulphate minerals was discussed. However, gypsum was not found in the samples and the oxidation of pyrite is too slow at the conditions found in the tunnel to be a likely cause. At last the high content of swelling clays was determined to be a significant factor. Brattli and Broch (1995) mentions that the swelling pressures measured in sample G is high enough to crack a normal shotcrete lining.

In conclusion Brattli and Broch (1995) explains that the strength reduction and increased permeability and exposed rock surface caused by the drying created an environment where the problems of swelling of clay minerals were enhanced upon filling of the tunnel, causing fall-outs where these conditions were present.

### **2.3 Testing methodologies**

Measuring swelling and slaking can be a challenge. There are several tests that can be used to quantify swelling and slaking, but depending on the condition in which the result is to be used, one test may give more valid results than others. Some lab testing methodologies and their applications are therefore reviewed. A short description of mineralogical testing is also provided. For a more thorough description of the methodology used, see Frengen (2019).

### 2.3.1 The slake durability index test

Slake durability is a rocks resistance to disintegration when subjected to repeated cycles of drying and wetting (Franklin and Chandra, 1972). The most commonly used test used to determine this index is the slake durability test developed by Franklin and Chandra (1972). The test is performed by subjecting rock samples to cycles of wetting and drying, where the wetting sequence is performed by rotating a steel drum containing the rock samples in a water bath. The percentage of the mass remaining in the drum after two cycles are used to classify the slake durability index in accordance with Table 2.2.

Table 2.2. Suggested classification for two slaking cycles after (ISRM, 1979b).

Classification	Slake durability index, $I_{d2}$ [%]
Very high	98 - 100
High	95 - 98
Medium high	85 - 95
Medium	60 - 85
Low	30 - 60
Very low	0 - 30

Most rocks are extremely durable, so unequal subdivisions are used to distinguish slight differences in resistance to breakdown (Franklin and Chandra, 1972). In Figure 2.5 the variability of degradation after multiple rounds of slaking for some samples is shown. Rocks of sedimentary show a wide variety in slaking characteristics. In Figure 2.5a, the tested rocks has a slake durability index varying from 5 to 99 after two cycles.

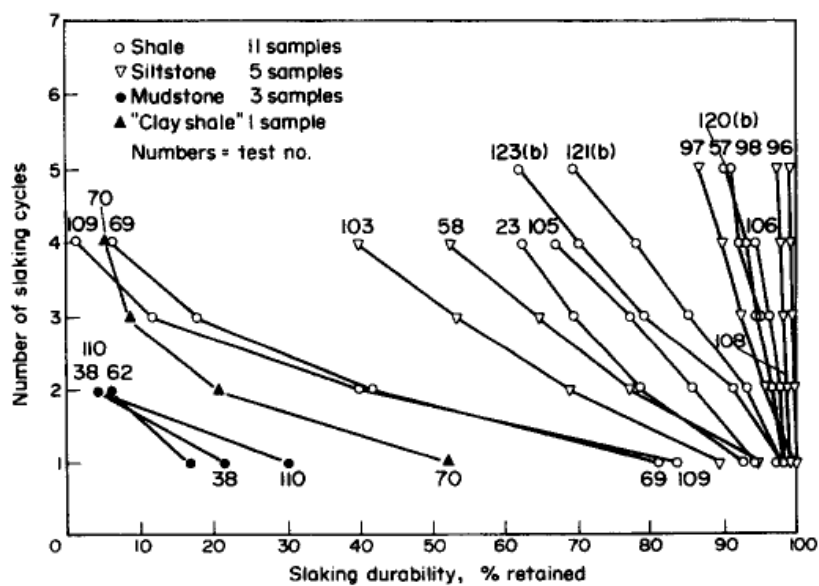


Figure 2.5. The effect of repeated slaking cycles on a) Sedimentary rocks (ISRM, 1979b) and b) igneous rocks. Modified from Panthi (2006).

After the test was first described by Franklin and Chandra (1972), it has become the standard for measuring slake durability in the industry and is recommended by both ISRM (1979*b*) and ASTM (1992). However, a possible weakness of the test when applied to hydropower tunnelling might be that the test relies on complete drying between the cycles. Hydropower tunnels on the other hand experience some drying, but not to the same extent. Research on whether or not a modified slake durability test with moderate drying is more applicable to these conditions is being conducted by Lena Selen for her PhD (Selen, 2019).

### **2.3.2 Swelling tests**

Swelling is harder to quantify than slaking due to the numerous testing methodologies and is further exacerbated by different testing procedures used at different labs (Selen, Panthi and Vergara, 2018).

A common way to quickly determine the swelling potential of a powder is the free swelling test, which measures the free swell index of a powder or a soil (Statens vegvesen, 2014). Additionally, two main swelling characteristics can be determined in a laboratory. Swelling strain under the condition of no change in pressure is found by measuring the displacement of a submerged specimen in three axis. This method is unsuitable for this project as flysch rock disintegrates in water. The maximum swelling pressure can be measured under the condition of no volume change with radial and axial restraint. The two conditions are also sometimes combined (Rauh et al., 2006).

In this project the free swelling test and the NTNU swelling pressure test utilising the zero volume change condition was used. A more thorough description of the methodology and limitations are provided below.

#### **Free swelling test**

The free swelling test is a simple test that is widely used to obtain information on whether or not a powder expands when suspended in water. 10 cm<sup>3</sup> of a <20 μm powder is sprinkled into water and the percentage increase in volume is recorded (Statens vegvesen, 2014). In the specialisation project, the rock specimens were crushed to 2.5mm and further milled down to 20 μm.

Although the test is cheap and easy, it has certain limitations. Sivapullaiah et al. (1987) mentions that measuring 10 cm<sup>3</sup> is difficult due to the soils sensitivity to moisture and method of pouring into the cylinder. Furthermore, the kaolinite clay is observed to shrink and cause negative swelling.

#### **NTNU swelling pressure test**

Under the condition of zero volume change, the maximum swelling pressure can be found. Following ISRM (1979*b*) recommendations, the machine displayed in Figure 2.6 is used at NTNU. In the test, the specimen rests upon a porous glass filter and is radially constrained by

a metal ring. On top of the specimen a copper plate and a stamp is placed. As water enters the specimen through the filter, a change in height is logged by the height transducer. To maintain zero volume change a pressure is exerted on the specimen. The pressure is logged over a period of 24 hours or until the pressure is constant after which the maximum pressure is noted.

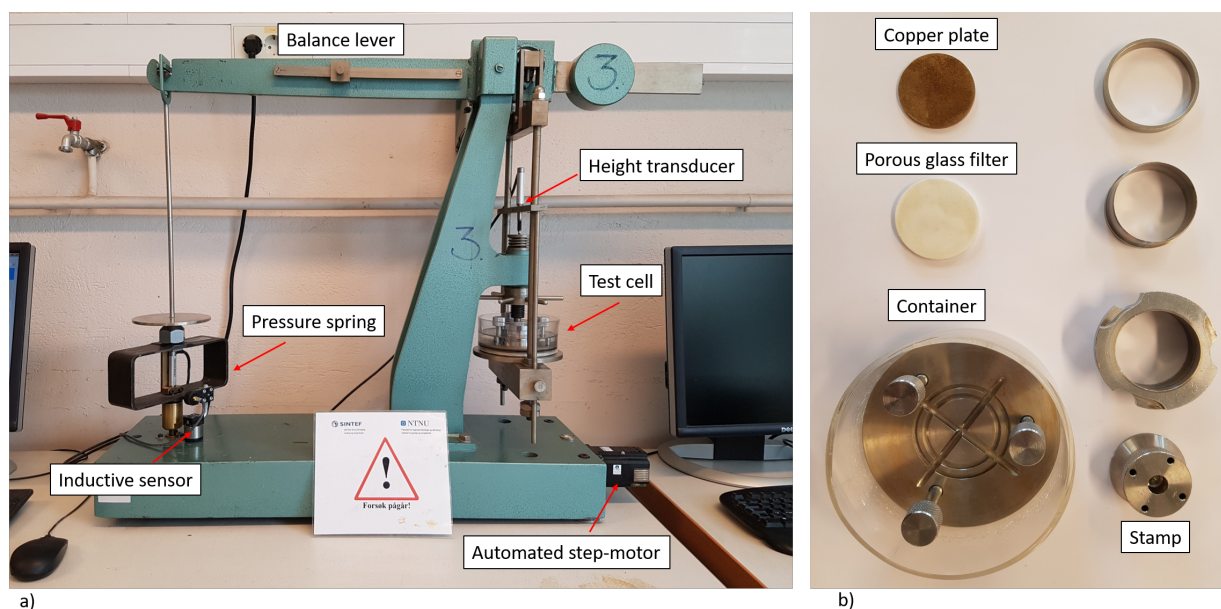


Figure 2.6. a) Swelling test apparatus setup during the swelling sequence.

b) The parts making up the cell of the oedometer apparatus. Unnamed parts are used to keep the sample in place between the porous filter and copper plate (Frengen, 2019).

Although the procedure is standardised by ISRM (1979*b*), different interpretations of this document results in uncertain measurement of maximum swelling pressure. In Selen (2017) the methodology of the NTNU and KiT laboratory is compared. Differences in methodology is found in mass, diameter and height used in both powder and disk samples, degree of preloading, climatic control, number of cycles and preparation of rock specimens. One notable difference is that NTNU only tests 20  $\mu\text{m}$  powder (the same as in the free swelling test), while KiT tests both intact rock disks and powder specimens.

Selen (2017) further tested the same samples at the two labs which showed drastically different results. The powder samples tested at Kit showed levels of swelling 2-4 times higher than that at NTNU. A contrast between swelling pressures of powder and disk test were also observed, with disks generally showing a higher swelling pressure than powder samples. Higher swelling pressure in rock disk specimens has also been observed by Brattli and Broch (1995).

### Comparing free swelling and swelling pressure

Both free swelling and the swelling pressure test has been performed to determine swelling properties of some samples in this project. This calls for a further review of the correlation between the two, especially since the swelling pressure test is more time consuming and requires higher precision of the equipment. The classification used for the two tests are shown in Table

2.3. For both tests the classifications very high, high, moderate and low are used.

Table 2.3. Classification of swelling and free swelling pressures from Nilsen and Palmström (2000).

<b>Classification</b>	<b>Free swelling index [%]</b>	<b>Swelling Pressure [MPa]</b>
Very high	>200	>0.75
High	140 - 200	0.30 - 0.75
Moderate	100 - 140	0.1 - 0.3
Low	<100	<0.10

Several papers compares results from free swelling and swelling pressure tests. In Brekke and Selmer-Olsen (1965) material from montmorillonite-carrying joints and faults from different tunnels in Norway are tested. Brekke (1965) is unable to establish a relation between the two parameters and finds it necessary to consider the parameters as independent. In Selen (2017) a correlation is also absent. Forouzan (2016) on the other hand finds a clear correlation between the two parameters. It must however be noted that the samples used in this study is artificial samples with varying bentonite content and not natural soil samples.

## 2.4 Determining mineral content by use of XRD

X-ray diffraction (XRD) is a method that is among other applications, used to quantitatively determine a rocks mineral content (Nilsen and Broch, 2012). In the Specialisation project this test was performed on the same powder used for the swelling test, but further milled to 6  $\mu m$ . To perform an XRD-test, an x-ray with a given wavelength  $\lambda$  is directed at a sample at an incidence angle  $\theta$  varying from 0 to 45°, as seen in Figure 2.7. Within a given crystal structure, atoms are fixed in a repeating lattice with several identifiable planes. The incident ray will be reflected from atoms with the distance  $d$ , but constructive interference, will only happen if the path difference  $2d \sin \theta$  of waves reflected from different atoms are equal to a whole number of wavelengths  $n\lambda$ , thus fulfilling Braggs law (Equation 2.1) (Waseda et al., 2011).

As the angle of incidence increases, the intensity of the reflected wave is continuously recorded. Every mineral have characteristic peaks that then can be identified. Taller peaks are a result of more reflections and is thus proportional to the mineral quantity (Waseda et al., 2011). An important note is that the a mineral must be sufficiently large for the wave to be reflected. Small or weathered minerals, the so-called amorph content is thus not identified. The quantification of minerals is thus determined from the crystalline content of the specimen. There are also uncertainties related to overlapping peaks or small peaks that are completely masked by larger peaks (Will, 2006).



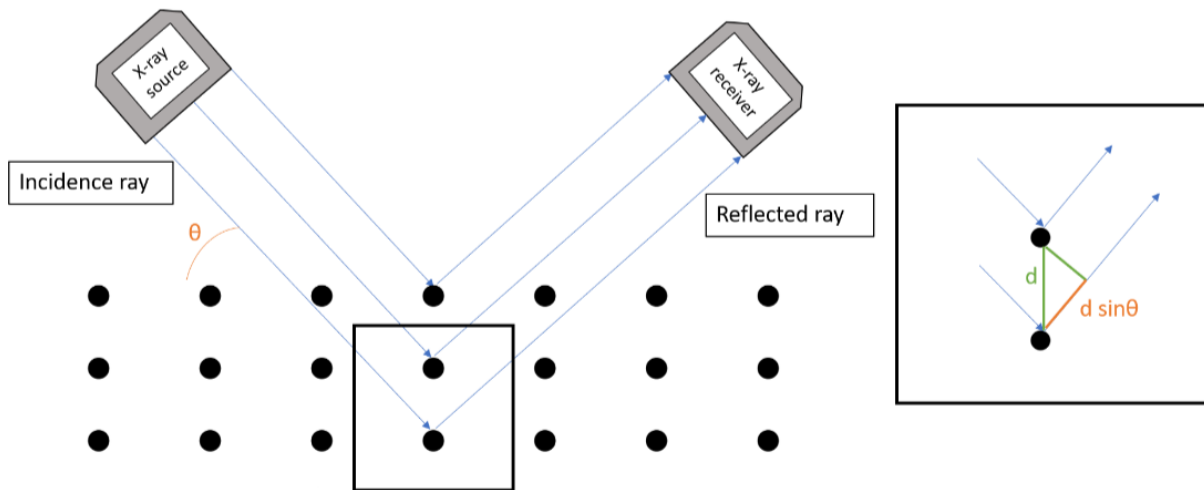


Figure 2.7. Schematic drawing of diffraction of X-rays by crystals (Frengen, 2019).

$$n\lambda = 2d \sin \theta \quad (2.1)$$

A way to identify swelling minerals by XRD is to compare a sample to one subjected to gaseous ethylene-glycol. Swelling clay absorbs the ethylene-glycol between the charged layers, effectively increasing the atom spacing. This causes a visible left-shift in the recorded intensity which confirms the presence of swelling minerals (Brekke, 1965).

## 2.5 Sample description

The rocks tested in the specialisation project were collected from core drillings from the head-race tunnel at Moglice HPP. From the flysch cores, six sections have been selected for this study by Lena Selen. For each of the sections, representative samples has been chosen for each of the tests.

### 2.5.1 Flysch

The flysch at Moglice HPP is heterogeneous and consists of alternating bands of clay-, silt- and sandstone. Figure 2.8 shows a typical example of the rock present at Moglice with some stronger and some weak sections. To perform the SDI test intact lumps of 40-50 g are needed. As seen in Figure 2.8 the rock clearly is of too poor quality in some sections to satisfy this requirement. Selecting representative specimens for the SDI test was thus not achievable. The resulting SDI might therefore be exaggerated.

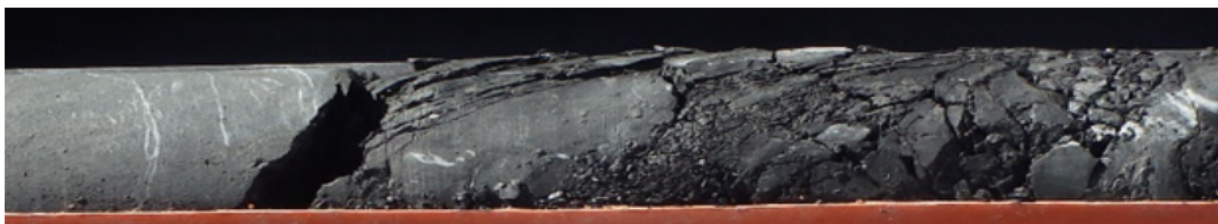


Figure 2.8. Example of flysch rock from Moglice (Selen, Panthi et al., 2018)

## 2.6 Results from the laboratory testing

### 2.6.1 Mineralogical content

The flysch rock mineralogical content was consistent and was generally composed of quartz, feldspars (plagioclase and k-feldspar), sheet silicates (muscovite and chlorite) calcite and pyrite, where >50% of the content is quartz and sheet silicates. Table 2.4 shows the makeup of the individual specimens. Information on the equipment used and a visual representation of the mineral distribution of the crystalline fraction are found in Appendix A. Up to 47.9% of the rock is amorphous content, indicating some level of weathering or mineral alteration. Swelling clays could be identified in four out of the six specimens.

Table 2.4. Mineral content, crystalline/amorphous content and identification of swelling minerals in the <math><6 \mu\text{m}</math> for flysch 6-11. Mineral content is given as percentage of the crystalline phase. Average values are presented as mean  $\pm$  standard deviation

Flysch nr.	6	7	8	9	10	11	Average
Mineral content [%]							
Quartz	48.0	43.3	22.7	25.4	24.1	22.0	30.9 $\pm$ 10.6
Plagioclase	17.2	17.1	5.8	10.7	10.7	12.1	12.3 $\pm$ 4.0
Muscovite	4.6	6.4	6.9	14.4	14.4	19.4	11.0 $\pm$ 5.4
Chlorite	8.1	11.6	23.4	27.2	32.0	29.8	22.0 $\pm$ 9.1
Calcite	18.6	18.7	40.0	20.6	17.2	15.1	21.7 $\pm$ 8.4
K-Feldspar	3.5	2.5	1.0	1.5	1.4	1.4	1.9 $\pm$ 0.8
Pyrite	0.1	0.4	0.1	0.2	0.2	0.2	0.2 $\pm$ 0.1
Crystalline content [%]	77.1	72.4	62.9	60.3	56.7	52.1	63.6 $\pm$ 8.7
Amorphous content [%]	22.9	27.6	37.1	39.7	43.3	47.9	36.4 $\pm$ 8.7
Swelling clay	yes	yes	yes	no	yes	no	

### 2.6.2 Swelling and slaking

Table 2.5 shows the resulting swelling pressure, free swelling, and Slaked durability results from the laboratory investigation. The swelling tests were conducted by Frengen (2019), while results from the SDI analysis were provided by Lena Selen. All specimens show varying degrees of swelling which may be classified moderate to high according to Table 2.3, with the

exception of Flysch 7 displaying a low swelling pressure.

Table 2.5. Swelling pressure, swelling potential and slake durability results for flysch 6-11. Average values are presented as mean  $\pm$  standard deviation.

<b>Flysch nr.</b>	<b>6</b>	<b>7</b>	<b>8</b>	<b>9</b>	<b>10</b>	<b>11</b>	<b>Average</b>
Swelling pressure [Mpa]	0.17	0.07	0.25	0.16	0.16	0.24	0.18 $\pm$ 0.06
Free swelling [%]	111	133	158	135	147	120	134 $\pm$ 2
SDI [%]	97.6	93.4	70.8	48.9	64.9	43.3	70 $\pm$ 20

In Appendix A the results are plotted. From this visual representation no definitive correlation between results from the three tests are apparent, although free swelling and SDI values follow a similar pattern. A possible reason why no clear linkage is found may be the relatively few specimens tested.

## 2.7 Main findings from the specialisation project

On the basis of the discussed laboratory results, the following main findings can be stated:

### 1) Mineral content of flysch rock and its general properties

The flysch rock consists of quartz, sheet silicates, feldspars and calcite and some pyrite, and has a varying amorph content. Great variation is found in levels of slake durability, while the rock generally has moderate swelling properties.

### 2) Relationship between mineral content and swelling

From the comparison of mineral content and swelling and slaking results, there seem to be some indication that flysch specimens with more feldspars and amorph content are more susceptible to swelling. The correlation is however weak.

### 3) Relationship between mineral content and slaking

For the flysch samples, slake durability does seem to be influenced by the content of quartz, which is the strongest of the minerals found in the rock. Specimens showing low slake durability are the ones with higher levels of amorph content and sheet silicates, both weak constituents of the rock.

### 4) Relationship between swelling and slaking

Although the theory discussed on this topic suggests a linkage between the two, the correlation found in this study is weak, possibly due to the low number of samples.

# Chapter 3

## Rock mass characteristics and stability

### 3.1 Introduction

For engineering geological purposes, rock and rock mass are terms that are not interchangeable. A rock can be described as a fabric of mineral grains that are bound or welded together, which usually contains microscopic cracks or fissures. (Nilsen and Palmström, 2000). The rock mass is however usually made up of a matrix consisting of interlocking discrete blocks of rocks (Hoek, 2000). Consequently, mechanical properties of rock and rock mass is usually influenced by scaling effects and the relationship between results obtained in the lab on rock specimens and in-situ values are important to evaluate.

There are several factors related to the geological setting that an engineering geologist must be aware of when planning an underground structure. The regional stress situation could enhance squeezing in a tunnel. Joints or faults may cross at an unfavourable direction or have fillings of adverse character. Water may also affect the rock mass by influencing strength and stress situation.

Knowing these characteristics is of key importance to evaluate underground stability. Theoretical failure criteria have been developed to predict when failure will occur, utilising knowledge about the rock (mass) properties and the underground stress situation. Two of the most common failure criteria used for rock engineering purposes are the Mohr-Coulomb criterion and the generalised Hoek-Brown criterion.

### 3.2 Rock mechanical properties

The main mechanical properties of a rock is it's compressive and tensile strength and its deformability. These qualities are of importance when planning support for an underground structure and must be quantified by use of laboratory investigations. A rocks intact strength

can be found by the point load strength test or the uniaxial compression strength test. The latter test is also used to determine the deformability of rocks. Tensile strength is usually indirectly found using the Brazil test.

### 3.2.1 Intact rock strength

According to Singh et al. (2012), the most important mechanical property of rock is the uniaxial compression strength (UCS), denoted as  $\sigma_c$ . The most common way to determine the intact rock strength is by use of the uniaxial compression strength test. A cylindrical core of rock is compressed between two plates as shown in Figure 3.1a) until failure, upon which the maximum load,  $P_{max}$  sustained by the rock specimen is noted. The UCS of a rock is then calculated by Equation 3.1, where  $A$  is the cross-sectional area of the specimen (Li, 2017).

$$\sigma_c = \frac{P_{max}}{A} \quad (3.1)$$

For some projects, cylindrical cores cannot be gathered. It may be that the rock is too jointed to provide a core of sufficient length or the material may be of too poor strength to be prepared to a core. For such rocks the point load index (PLi) test may give an indication of the rock strength. The test is performed by loading a sample between two spherically truncated, conical platens until failure, as shown in Figure 3.1b).

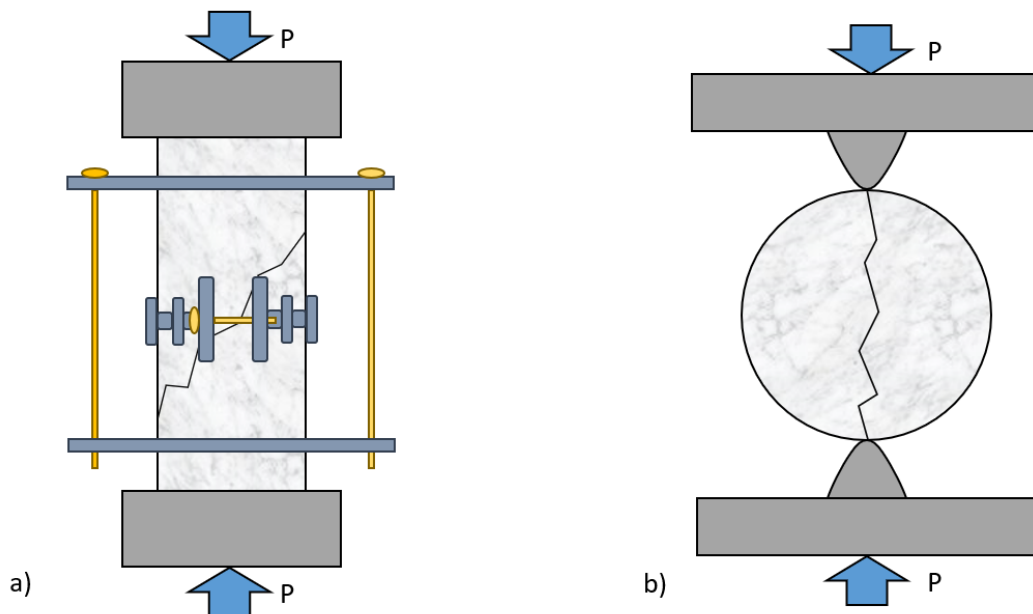


Figure 3.1. a) Sketch of the setup of a UCS test. An increasing load  $P$  compresses the specimen until failure. Axial and radial deformations are logged by extensometers (yellow pins). b) Sketch of the point load index test setup. A disk or a core is loaded between two spherically truncated conical platens.

The point load strength,  $I_s$  can be calculated using Equation 3.2, where  $D_e^2$  is the equivalent core diameter. For axial tests  $D_e^2 = 4WD/\pi$ , where  $WD$  is the cross sectional area of the plane

through the platen points. An estimate of the UCS value can then be found using Equation 3.3, where  $k_s$  is a correlation factor (ISRM, 1985).

$$I_s = \frac{P}{D_e^2} \quad (3.2)$$

This test can be performed on irregular shapes and blocks, as well as cores. Performing the test in both diametral and axial orientation also gives an indication of the strength anisotropy of the rock (Nilsen and Palmström, 2000). Another advantage of this test is that the equipment is comparatively lightweight and allows for the test to be performed on site (Palmström and Stille, 2010). A table with classification of UCS and Pli values is found in Table 3.1.

$$\sigma_c = k_s \cdot I_s \quad (3.3)$$

Table 3.1. Classification of rocks based on uniaxial compression strength and point load index ( <sup>1</sup>ISRM (1978a) and <sup>2</sup>Bieniawski (1984) in Nilsen and Palmström (2000)).

Type	Classification	UCS <sup>1)</sup> [MPa]	Pli <sup>2)</sup> [MPa]
Soil	Extremely low strength	<0.25-1	N/A
Rock	Very low strength	1-5	<1
	Low strength	5-25	1-2
	Medium strength	25-50	2-4
	High strength	50-100	4-8
	Very high strength	100-250	>8
	Extremely high strength	>250	N/A

For the classification of Pli, the classification of extremely low and extremely high is not used.

The value of  $k_s$  is not set. Several studies have been conducted to give a guideline on how to best define  $k_s$  depended on the tested rock specimen. ISRM (1985) states that k on average is 20-25. It has been suggested that the correlation factor increases with the rock strength (Nilsen and Palmström, 2000). Singh et al. (2012) suggest using 14-16 for softer rock, and 20-24 for rocks of high strength. Nilsen and Palmström (2000) further divides the rock mass into four categories as shown in Table 3.2.

Table 3.2. Suggested values of the factor  $k_s$  (Nilsen and Palmström, 2000).

Compressive strength $\sigma_c$ [MPa]	Point load strength $I_s$ [MPa]	Suggested value of $k_{50}$
25* -50	1.8-3.5	14
50-100	3.5-6	16
100-200	6-10	20
>200	>10	25

\*Bieniawski (1973) in Nilsen and Palmström (2000) suggests that the point load strength test should not be used on rocks having  $\sigma_c < 25$ MPa.

### 3.2.2 Elasticity and deformability of rocks

When subjected to a load, a material will deform. In contrast to the UCS, this aspect of a rock can be measured directly and may thus be a better basis for assessing the stability of rock masses (Bieniawski, 1978). Deformability and elasticity of a rock is calculated based on the stress-strain curve from a uniaxial compression test where both axial and radial deformations are measured as the axial stress increases. A typical curve is shown in Figure 3.2. In addition, the Poisson's ratio; the ratio between radial and axial deformation, is another parameter that can be found using this test.

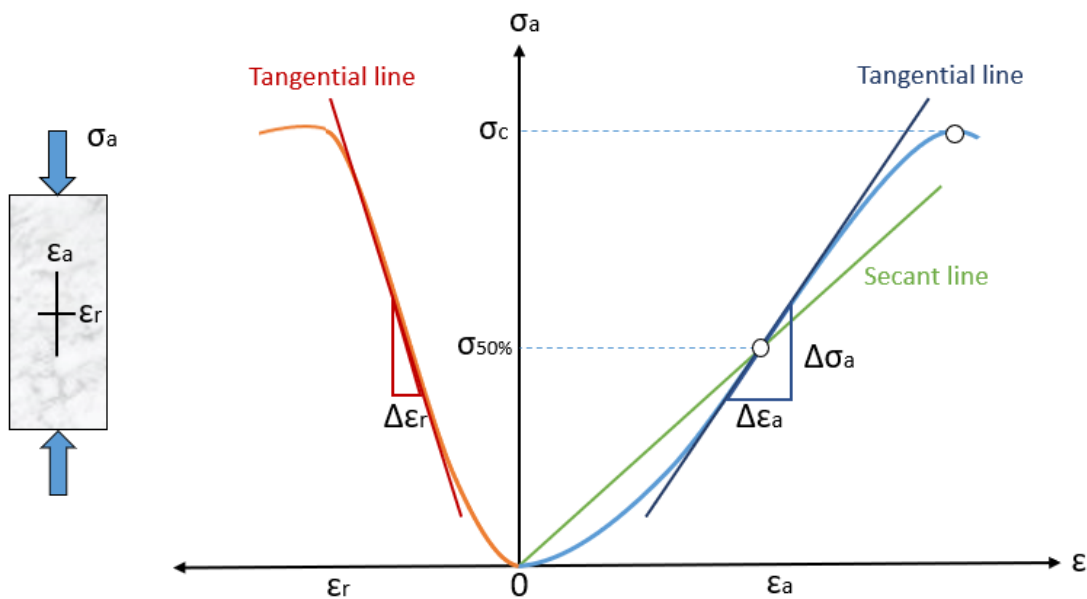


Figure 3.2. Stress-strain curves of a rock specimen during a uniaxial compression test. The axial stress-strain curve is coloured in light blue and the radial in orange.

The deformability of a rock can be described by either the elastic modulus or Young's modulus,  $E_t$  described by the axial tangential line or the deformation modulus,  $E_{sec}$  described by the secant line in Figure 3.2. The elastic modulus is determined from the linear portion of the stress/strain curve when conducting a UCS test. When the curve is considered as a whole, there are sections that are not linear. At the beginning of the curve, small fissures in the rock are closed, causing higher axial strain. After the rock starts to fail, plastic deformation occurs in the specimen. To calculate the deformation modulus the absolute axial stress and strain at a given point on the curve are used. In the secant modulus, plastic deformation is included in addition to the elastic strain. Similarly a secant and elastic Poisson's ratio,  $\nu$  can be calculated (Li, 2017).

Depending on what part of the curve is used to create a tangential line, the values of the Young's modulus and Poisson's ratio will change. It is observed that most rocks have a linear portion of the stress-strain curve at 50% of its maximum axial stress value (Li, 2017). ISRM (1979a) thus recommends to measure  $E$  and  $\nu$  at  $\sigma_{50\%}$  as described in Equation 3.4 and 3.5.

$$E = \frac{\Delta\sigma_{a,50\%}}{\Delta\epsilon_{a,50\%}} \quad (3.4)$$

$$\nu = -\frac{\Delta\epsilon_{r,50\%}}{\Delta\epsilon_{a,50\%}} \quad (3.5)$$

### 3.2.3 Tensile strength

Although tensile stresses are rarely found underground, they may be induced around a tunnel profile if the difference between the maximum and minimum stress is large enough. In the case of induced tensile stress, the tensile strength  $\sigma_t$  of a rock must be sufficient to avoid fracturing (Li, 2017). For high-pressure hydropower tunnels this is especially important. Secondary jointing may in these cases lead to water leakage out of the tunnel and lower production of electricity (Nilsen and Palmström, 2000).

Tensile strength may be found by the direct tensile test, shown in Figure 3.3a. A specimen is glued to two steel platens which are pulled apart until the specimen fractures. Due to difficult specimen preparation, it is not a common way to measure a rock's tensile strength (Li, 2017).

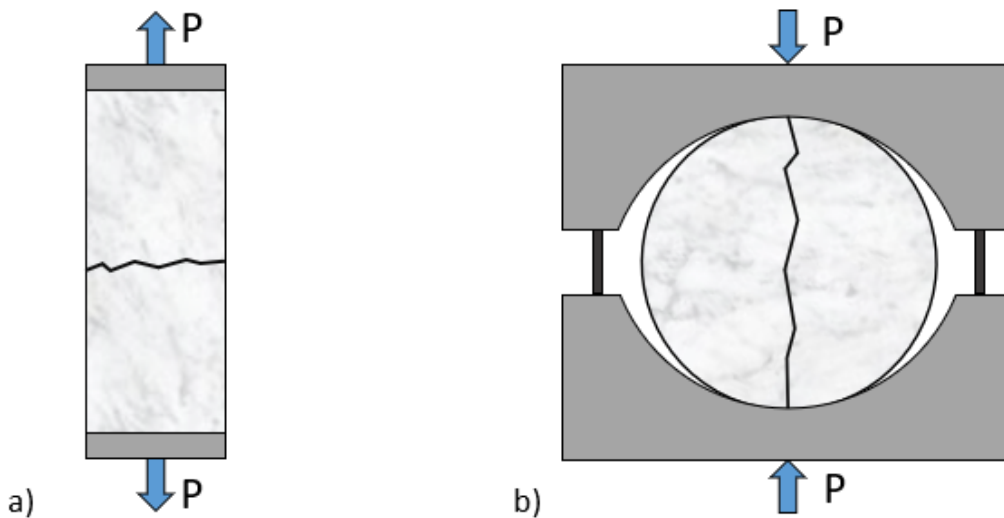


Figure 3.3. a) Direct tensile test setup. The specimen is pulled apart until failure occurs. b) Brazilian test setup. Tensile forces are induced in the specimen, causing tensile failure.

A more common way to determine the tensile strength of a specimen is by the Brazilian test (Li, 2017). The setup of the test is shown in Figure 3.3b. A disk specimen is loaded axially between two cylindrical metal caps. The tensile strength  $\sigma_t$  can be calculated with Equation 3.6, where  $P$  is the maximum pressure sustained by a circular specimen with thickness  $t$  and diameter  $D$  (ISRM, 1978b).

$$\sigma_t = 0.636 \frac{P}{D \cdot t} \quad (3.6)$$



### 3.2.4 Factors influencing rock mechanical laboratory results

The accuracy of the mentioned rock mechanical tests are influenced by several factors. Using results from these tests in further calculations without correcting the results may lead to error. Some of the most common factors are the size of the tested specimen, level of saturation and rock anisotropy.

#### Specimen size

As the specimen size increases, the chance of it containing a weak plane or irregularities increases. Consequently, the strength of a large specimen is weaker than a small one. Figure 3.4 shows how increasing the diameter of a specimen results in a lower UCS. This is due to the increased number of micro cracks and other flaws in the specimen (Hoek and Brown, 1980).

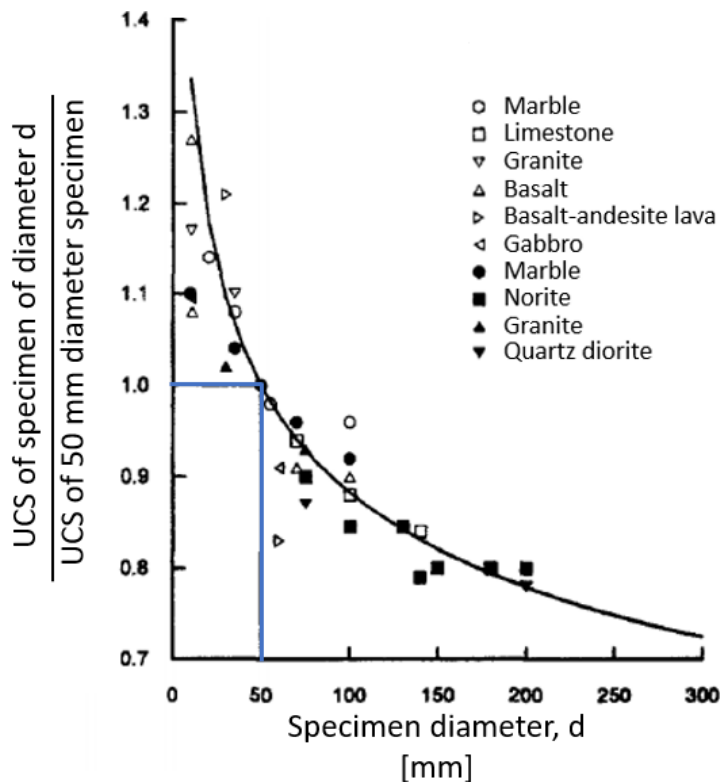


Figure 3.4. Influence of specimen size on the uniaxial compression strength of intact rock. Modified after (Hoek and Brown, 1980).

To set a standard for testing ISRM (1979*a*) suggests a core diameter of approximately 54 mm. Based upon an analysis of published data, Hoek and Brown (1980) suggested that the uniaxial compression strength  $\sigma_{cd}$  of a specimen with the diameter  $d$  can be adjusted to the uniaxial compression strength  $\sigma_{c50}$  of a 50 mm specimen using Equation 3.7.

$$\sigma_{c,50} = \frac{\sigma_{c,d}}{\left(\frac{50}{d}\right)^{0.18}} \quad (3.7)$$

For the point load index test, the same principle is valid. Equation 3.8 relates the PLi  $I_{s(d)}$  of a specimen with the diameter  $d$  to the PLi  $I_{s(50)}$  of a 50 mm diameter specimen by the factor  $F$ .  $F$  is dependent on the equivalent diameter  $D_e^2$  of the specimen and the (ISRM, 1985).

$$I_{s(50)} = F \cdot I_{s(d)} \quad \text{where} \quad F = \left(\frac{D_e}{50}\right)^{0.45} \quad (3.8)$$

In addition to the specimen diameter, the relationship between the height,  $H$  and the diameter,  $d$  of a specimen will influence the result of a UCS test. Short specimens will be affected by end effects that may give an erroneously high reading (Hawkes and Mellor, 1970). Figure 3.5 shows that specimens with a low  $H/d$  ratio will give an uncertain value.

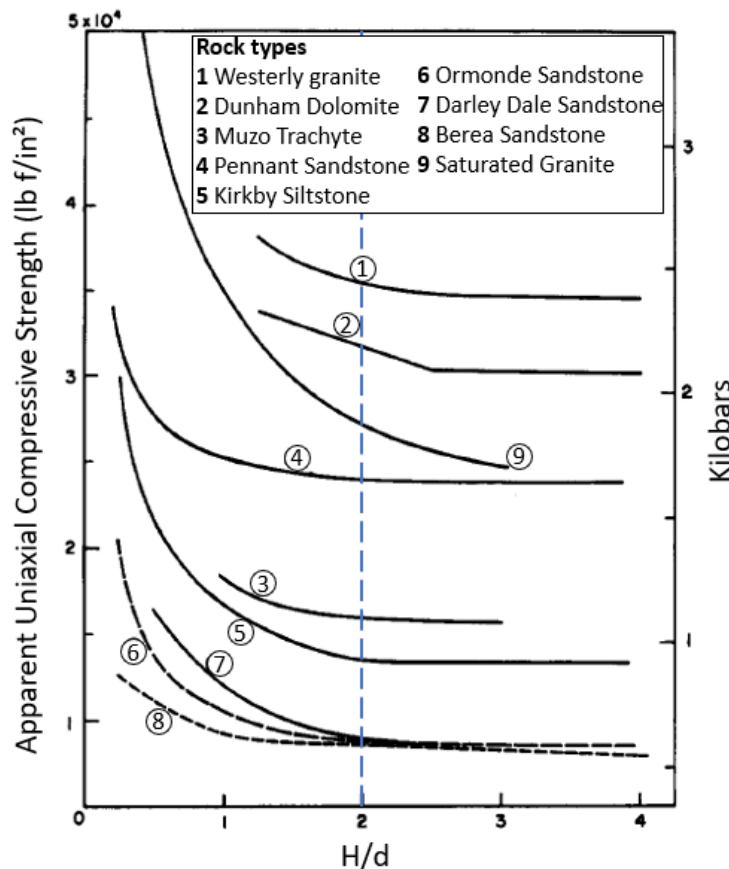


Figure 3.5. Influence of height/diameter ( $H/d$ ) on uniaxial compression strength. The blue line highlights a  $H/d$  ratio of 2, which is the recommended absolute minimum by Hawkes and Mellor (1970). Modified after Hawkes and Mellor (1970).

For this reason, ISRM (1979a) recommends a  $H/d$  ratio of 2.5-3.0. Hawkes and Mellor (1970) suggests that the point on the  $H/d$  curve flattens out, stipulated in Figure 3.5 at 2 should be the absolute minimum. Granite and other hard rocks shows end effects for  $H/d$  ratios up to 2.5. For sedimentary rocks the curve flattens out earlier, at values as low as 1 and display a stable character at  $H/d$  values over 2.

**Saturation of the specimen**

Water plays a great influence on the properties of rock, as illustrated in Figure 3.6. Hawkins

and McConnell (1992) demonstrated that a change in water content as low as 1 % from dry state may have a significant effect on both strength and deformability. Broch (1979) states that the reason for the reduction in strength is a reduction of the internal friction of the rock. Another reason, as Hawkins and McConnell (1992) explains, is that water has a weakening effect on the cement or matrix of the rock, causing microfractures to propagate along grains with more ease. Especially, sedimentary rocks with a high content of clay, show a softening when saturation levels are increased.

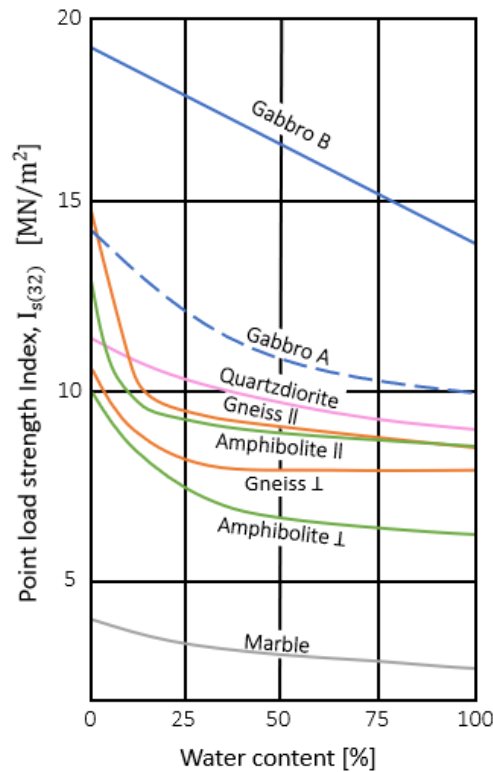


Figure 3.6. Point load strength of six different rocks as a function of the water content in rock cores of 32 mm diameter. Modified after Broch (1979).

Several studies have been conducted to try to establish a relationship between dry and saturated strength of rocks. Broch (1979) found that the point load strength was reduced between 20 and 45 % with an 34% average, when testing six different magmatic rocks. Upon testing 35 British sandstones, Hawkins and McConnell (1992) found a maximum decrease of 78%, while the minimum decrease was 8% with an 31% average loss in strength. The main outliers in this study were clay rich samples, which showed an increased strength reduction compared to more quartz dominated rocks.

A statistical analysis of the data from Hawkins and McConnell (1992) by Vásárhelyi (2003), showed an overall best fit linear regression equation between dry and saturated uniaxial compression strength as shown in Equation 3.9.

$$\sigma_{c,sat} = 0.759 \cdot \sigma_{c,dry} \quad (3.9)$$

For a reliable result, when testing a rock specimens strength, the importance of maintaining constant saturation of a sample collected in the field during storage and testing must not be ignored. Clay rich rocks are especially sensitive to moisture changes, as drying of such rocks may cause irreversible micro-cracking. Hawkins and McConnell (1992) argues that rocks should be tested in wet condition as standard procedure to combat the issue of saturation levels.

### Strength anisotropy

For some rocks, the intact rock strength is dependent on the orientation. Schistosity, foliation, layering or bedding are common causes of strength anisotropy in rock (Nilsen and Palmström, 2000). Minerals such as mica, chlorite, amphiboles and pyroxenes are flaky and are often orientated in the same direction in sedimentary or metamorphic rock, causing weak planes (Palmstrom, 1996). Figure 3.7 illustrates how the intact rock strength of various rocks changes, depending on the direction of loading relative to the schistosity.

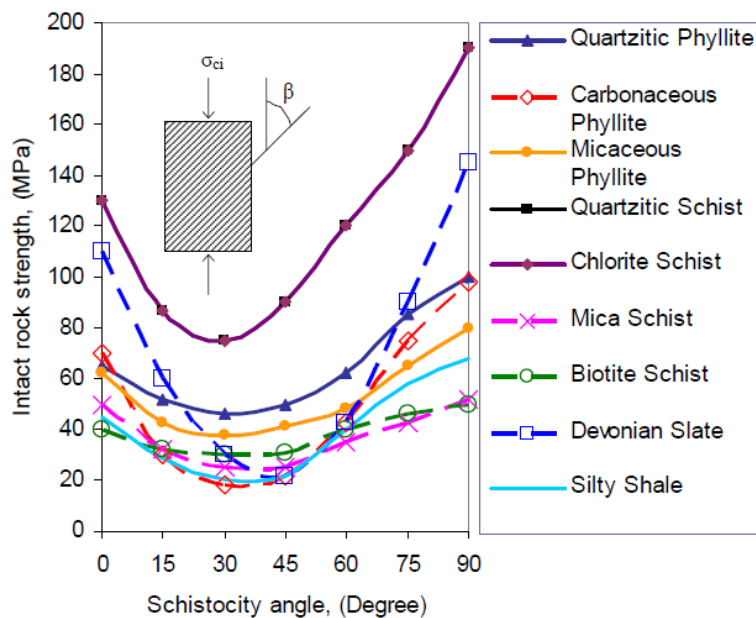


Figure 3.7. The intact rock strength of different Himalayan rocks loaded at different angles ( $\beta$ ) relative to the schistosity plane during a uniaxial compression test (Panthi, 2006).

The highest compressive strength is found when a specimen is loaded perpendicular to the schistosity or bedding. When a specimen is loaded at an angle of approximately 30 degrees to the schistosity the rock will be weakest (Panthi, 2006).

When specimens are prepared for strength tests from rock samples, anisotropy must be taken into account. For both compressive strength tests, as the UCS and Pli test, and tensile strength tests like the Brazil test, care must be taken to ensure that the desired orientation is tested. However, when cores are supplied from the field, it is not always possible to achieve ideally oriented specimens. In such cases one must evaluate the orientation of the weak layers relative to the loaded direction when discussing the results.

### 3.3 Rock mass strength and deformability

Rock mass strength can be defined as the ability a rock mass has to withstand stress and deformation (Panthi, 2006). Intact rock strength and elasticity are commonly measured on rock specimen. A relationship between laboratory results and in-situ values is thus necessary to predict the stability of a underground construction such as a tunnel or cavern.

#### 3.3.1 Rock mass strength

Intact rock strength is in most cases a parameter that is easy to find in the laboratory. The small, homogeneous and strong specimens, are however not representative of the rock mass (Panthi, 2006). In a rock mass, blocks of rock are separated by discontinuities, which reduces the strength (Nilsen and Palmström, 2000). It is difficult to test the strength of the rock mass in the field, and the required specimen size required to test the strength in the lab is impractical (Panthi, 2006). Still, the rock mass strength is a parameter necessary in the design of almost any underground excavation (Hoek, 2000). Several authors have proposed empirical relationships between rock mass strength  $E_M$  and rock mass classifications and/or intact rock strength. Some of these are presented in Table 3.3.

Table 3.3. Some empirical relationships between rock mass strength  $\sigma_{cm}$  and rock mass classifications.

Proposed by	Empirical relationship
Bieniawski (1993)	$\sigma_{cm} = \sigma_{ci} \times \exp\left(\frac{RMR-100}{18.75}\right)$
Hoek et al. (2002)	$\sigma_{cm} = \sigma_{ci} s^a = \sigma_{ci} \times \left[\exp\left(\frac{GSI-100}{9-3D}\right)\right]^a$
Barton (2002)	$\sigma_{cm} = 5\gamma \left(Q \frac{\sigma_{ci}}{100}\right)^{1/3}$
Panthi (2006)	$\sigma_{cm} = \frac{\sigma_{ci}^{1.5}}{60}$ for schistose rock mass
Panthi (2017)	$\sigma_{cm} = \frac{\sigma_{ci}^{1.6}}{60}$ for brittle rock mass

The rock mass classifications mentioned are: GSI is the Geological Strength Index, RMR stands for Rock Mass Rating and Q is the Q-value. a and s are parameters from the Hoek Brown criterion.

#### 3.3.2 Rock mass deformability

As discussed previously, intact rock has both an elastic modulus and a deformation modulus. In a rock mass, it is not only the intact rock that deforms, but additional deformation will occur due to the presence of joints and discontinuities. Consequently, rock mass is not deforming elastically. Bieniawski (1978) recommends that the term modulus of deformation, denoted as  $E_m$  is more accurate than modulus of elasticity in the context of rock mass. The effect of jointing is that the deformability modulus of the rock mass is significantly lower than

that of intact rock, meaning the rock mass will deform more than a rock specimen. Compared to the intact rock elasticity modulus, the rock mass deformation modulus may be as low as 10% (Panthi, 2006).

The deformability of the rock mass can be found by in-situ measurements. Bieniawski (1978) mentions compression tests, borehole jacking, flat jacks and shear tests as possible in-situ methods. However, such tests are both time consuming and expensive. Furthermore, Nilsen and Palmström (2000) states that values obtained from different procedures may differ as much as 100% as another disadvantage.

Alternatively, the rock mass deformability modulus may be estimated using correlations to rock mass classifications systems. Table 3.4 lists some proposed relationships. Nilsen and Palmström (2000) suggests using multiple relationships so that the results can be compared. Thus, the reliability of the results may be evaluated accordingly.

Table 3.4. Some empirical relationships between rock mass deformability  $E_m$  and rock mass classifications.

Proposed by	Empirical relationship
Bieniawski (1978)	$E_m = 2RMR - 100$
Hoek and Brown (1997)	$E_m = \sqrt{\frac{\sigma_{ci}}{100}} \cdot 10^{(GSI - \frac{10}{40})}$
Barton (2002)	$E_m = 10 \times Q_c^{1/3}$
Panthi (2006)	$E_m = E_{ci} \times \frac{\sigma_{cm}}{\sigma_{ci}}$

The rock mass classifications mentioned are: GSI is the Geological Strength Index, RMR stands for Rock Mass Rating and Q is the Q-value.

## 3.4 Geological setting

Beside the parameters of the rock mass, there are qualities of the local geological setting that may influence an engineering geologists decision making. The terrain may influence the local stresses, discontinuities may be present as weakness zones or joints with various qualities. In the same manner that water affects the intact rock strength, it also has an influence on a larger scale.

### 3.4.1 Stress situation

At any given point in a rock mass there are three principal stresses. These are the rock stresses that are in a direction with no shear stresses and are perpendicular to each other. These are referred to as the major  $\sigma_1$ , intermediate  $\sigma_2$  and minor  $\sigma_3$  principal stresses. The natural stress

state in a rock mass is influenced by several factors. Prior to excavation the virgin stresses are the sum of the following constituents (Nilsen and Palmström, 2000):

- Gravitational stresses
- Topographic stresses
- Tectonic stresses
- Residual stresses

### **Gravitational stresses**

Gravitational stresses increases with depth and are the result of the weight of the overburden. At a depth  $z$  Equation 3.10 can be used to calculate the vertical stress  $\sigma_v$ , assuming a horizontal surface (Palmström and Stille, 2010).

$$\sigma_v = \rho \cdot g \cdot z \quad (3.10)$$

where  $\rho \cdot g$  is the specific gravity of the rock.

Although the horizontal stresses  $\sigma_h$ , may be identical to the vertical stress, this is often not the case. In an elastic rock mass, the horizontal stresses are influenced by the rock's Poisson's ratio  $\nu$  follows the relationship in equation 3.11 (Nilsen and Palmström, 2000):

$$\sigma_h = \frac{\nu}{1 - \nu} \sigma_v \quad (3.11)$$

A common Poisson's ratio for a rock mass is 0.25 (Nilsen and Palmström, 2000). Horizontal stresses are in this case 1/3 of the vertical stress. For soils, which have low strength this relation describes the horizontal stresses well (Sheorey, 1994). Nilsen and Palmström (2000) notes that the gravitational stress in rock only account for a small portion of the horizontal stresses and that this idealised relation does not correspond well with reality where the rock mass is jointed.

### **Topographic and tectonic stresses**

The terrain has a considerable influence on the rock stresses when the surface is not horizontal. Scandinavian experience from tunnelling indicates that peaks closer than  $30^\circ$  from a tunnel may influence the stress (Palmström and Stille, 2010). Figure 3.8 shows typical directions and magnitudes of principal stresses as affected by topography. Horizontal stresses at the bottom of the valley are influenced by nearby peaks, resulting in a stress concentration at this location. Horizontal de-stressing is happening at the peaks where there is less material at the same elevation to cause horizontal pressure. Along the valley sides, the minor principle stress aligns with the surface. With increasing depth, the stress directions return to the vertical or horizontal (Li, 2017).

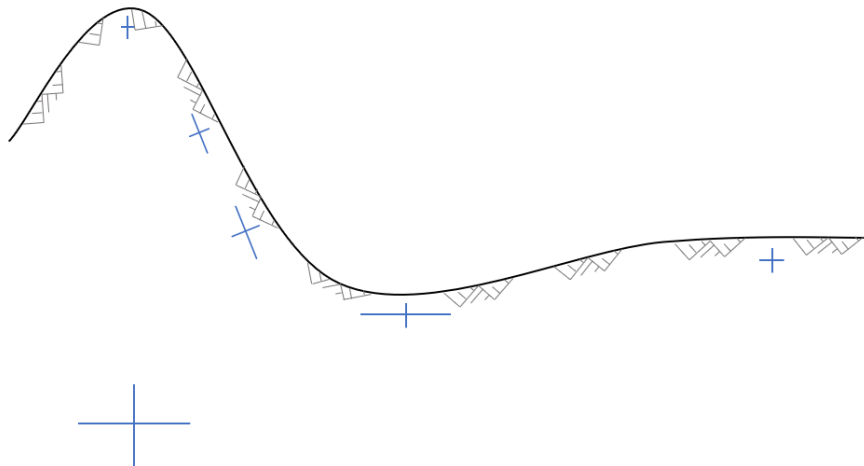


Figure 3.8. Principal stresses as affected by topographic features.

Tectonic stresses may also add to the horizontal stresses experienced by the rock. The main cause of tectonic stresses are plate tectonics (Nilsen and Palmström, 2000). Due to the topographic and tectonic stresses, horizontal stresses are usually higher than the vertical, especially at low depths (Li, 2017). To illustrate the anisotropy, the  $k$  value is often used, defined as the horizontal stress divided by the vertical stress (Palmström and Stille, 2010). Figure 3.9 shows that a  $k$  value of 1 to 3 is common for low depths. Materials with a low  $E$  modulus generally also have a lower  $k$  value (Sheorey, 1994).

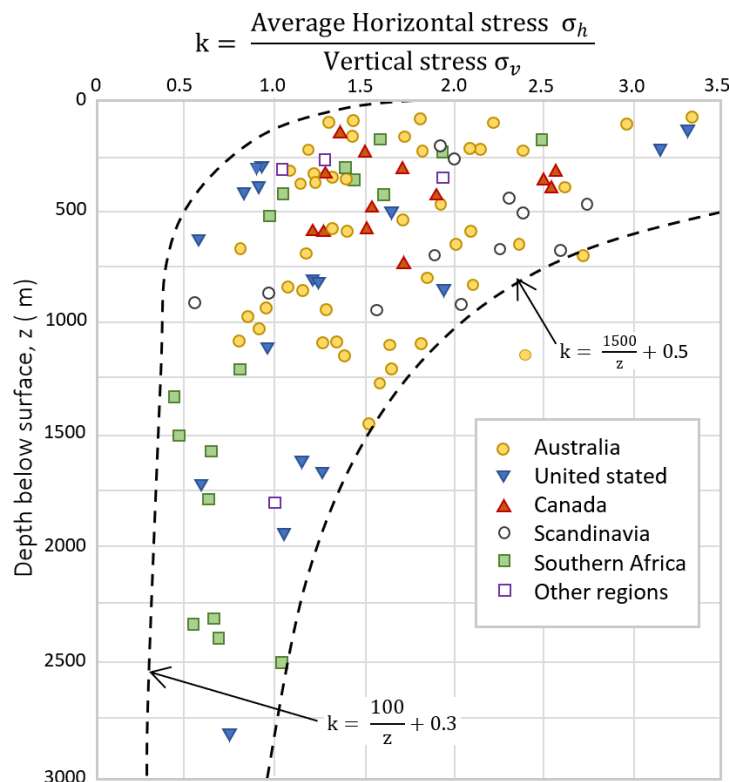


Figure 3.9. Variations of ratio of average horizontal to vertical stress with depth below surface. (Modified after Hoek and Brown (1980) in Nilsen and Palmström (2000)).

### Residual stresses

In the early stages of a rock's geological history, stresses may be locked into the rock mass.



These are called residual or remnant stresses. Stress caused by contraction during cooling of magma is an example of this Palmström and Stille (2010).

### 3.4.2 Discontinuities

A discontinuity can be defined as a structural or geological feature that alters the homogeneity of the rock mass (Nilsen and Palmström, 2000). ISRM (1978*a*) separates discontinuities into joints and faults. Joints do not show any signs of displacements and are often accompanied by parallel joints, forming a joint set. Intersecting joint sets further form a joint system. Terms of various types of joints in Figure 3.10 are chosen from their size, composition and origin (Palmström and Stille, 2010). Joints following rock structures as bedding planes and foliation and cleavage are named accordingly, while cracks and fissures are describing the character of the joint. Faults are large discontinuities that do show recognisable displacement (ISRM, 1978*a*). Fault walls are often affected by the displacement and may be slickensided and smooth. Where joints usually have a limited thickness, faults may create zones with crushed and altered rock material.

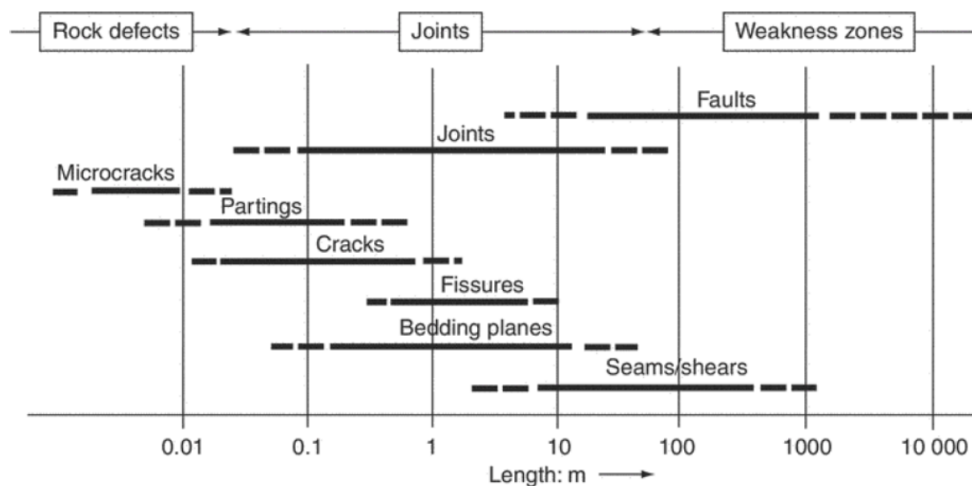


Figure 3.10. The main types of discontinuities and their lengths (Palmström, 1995)

The character of the discontinuities will affect the quality and stability of a rock mass. Thus the quantity and quality of joints are used in several rock classification schemes used to determine the rock mass quality and/or need for rock support. Table 3.3 and 3.4 shows how such classifications may be used to estimate the rock mass strength from intact rock strength. Some common classification systems are the Rock quality designation (RQD) system, the Geological strength index (GSI) and the Q-system.

#### Rock quality designation (RQD)

According to Nilsen and Palmström (2000) Rock quality designation is the most commonly used method for characterising the degree of jointing in a borehole core. It is defined as the percentage of the core that is composed of core bits larger than 10 cm. The relative ease of

determining a cores RQD make it a commonly used as a parameter for block size or jointing density in more advanced rock classification systems.

### **The Geological strength index (GSI) system**

The geological strength index, developed by (Hoek, 1994), Hoek and Brown (1997) and Marinós and Hoek (2001) offers a means to estimate the reduction of intact rock properties in the Hoek-Brown failure criterion based on the visual inspection of a rock in terms of block structure and joint surface conditions. Previously the Rock mass rating (RMR) system was used for this purpose, but it was deemed too unreliable for this failure criteria, especially in poor rock mass (Hoek, 2000). Appendix B.1 shows how the GSI system is constructed, where poorer rock surface conditions and increased jointing results in a lower GSI.

However, not all rock masses are easily classified by this Table. Flysch rock is known to be a heterogenous material with may have a complex structure due to its deposition and tectonic history (Marinos and Hoek, 2001). The Table found in Appendix B.1, Figure B.2. was thus created for the estimation of rock mass parameters and classification of flysch and other heterogeneous rock masses. Similarly to the original chart, the GSI is reduced as the structure becomes less intact and with a poorer softer surface of joints. Additionally, categories of rock depending on the composition of clay, sand and sandstone layers and rates of tectonic deformation is indicated, to easily identify the rock mass on the chart.

### **The Q-system**

The Q-system was first developed by Barton et al. (1974) in cooperation with the Norwegian Geotechnical Institute (NGI) and is based on empirical data from over 2000 examples from existing tunnels and underground structures. The Q-value of a rock mass typically ranges from 0.001 and 1000 which can be calculated using Equation 3.12 . Each fraction of the equation describes a factor that's important for underground stability.  $\frac{RQD}{J_n}$  describes the degree of jointing,  $\frac{J_r}{J_a}$  describes the joint friction and  $\frac{J_w}{SRF}$  describes the active stress situation. The reader is referred to NGI (2015) for in-depth description on how these factors are determined for a rock mass.

$$Q = \frac{RQD}{J_n} \cdot \frac{J_r}{J_a} \cdot \frac{J_w}{SRF} \quad (3.12)$$

Where :

- RQD = Rock quality designation
- $J_n$  = joint set number
- $J_r$  = Joint roughness number
- $J_a$  = Joint alteration number
- $J_w$  = Joint water reduction factor
- SRF = Stress reduction factor

An advantage of the Q-system is that it can be used directly to estimate the needed support of an underground structure. Figure 3.11 illustrated how the span of a tunnel, adjusted for the Excavation support ratio (ESR), coupled with the rock mass Q value indicates a support class from 1 to 9. It is noted by NGI (2015) that these classes are not to be used as definitive support classes. Instead the chart should be used as a continuous scale for the different types of support.

For structures with a low span, where the rock mass has a high Q-values, indicating strong rock, a support regime relying on the strength of the rock mass and spot bolting is suggested. For poorer rock and higher spans the suggested support increases and the support regime is intensified with more and longer bolts, as well as thicker layers of (reinforced) sprayed concrete, reinforced ribs of sprayed concrete, or even cast concrete linings.

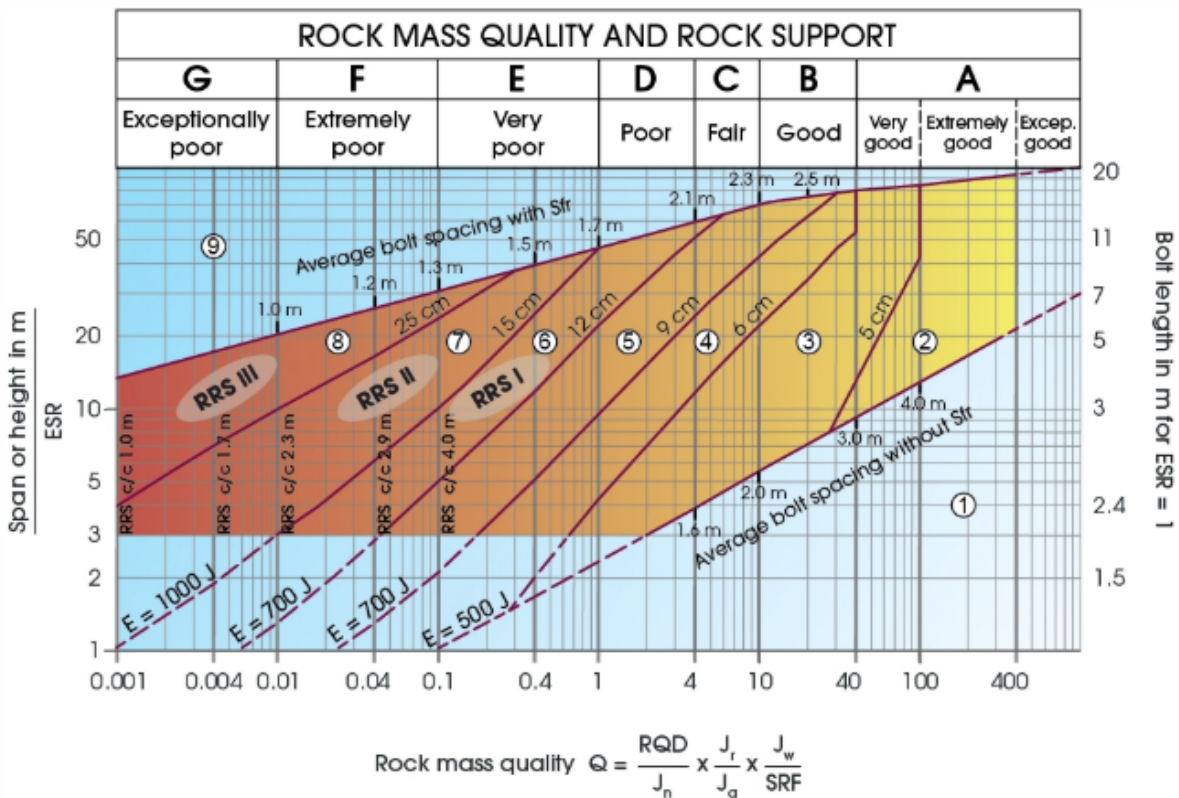


Figure 3.11. Permanent support recommendations based on Q-values and span/ESR (NGI, 2015).

### 3.4.3 The effect of water

For intact rock, higher saturation of water often weakens the material and results in a lower intact compressive strength (Broch, 1979). Water is also influential on a larger scale, especially since joints and cavities allows for more mobility in the rock mass. Palmström and Stille (2010) mentions the following problems water may cause when excavating an underground structure.

The main effect water on stability other than that of the intact rock strength is the reduction

of shear strength along discontinuities. Close to the surface, the rock mass is generally more jointed, causing this type of problems to be more pronounced in shallow structures. Secondly, when a swelling material comes into contact with water, swelling related instabilities may occur as investigated in Chapter 2. At last, the excavation logistics are affected as the capacity on site may be reduced due to drilling and charging becoming more difficult, the need for pumping and worsening roadway conditions.

### 3.5 Failure criteria

Depending on the rock properties and the stress situation, different failure criteria have been developed to estimate when failure will occur in a rock or rock mass. Traditionally, the Mohr-Coulomb criteria, a linear principal stress criteria describing the conditions for failure in an isotropic material (Labuz and Zang, 2012).

In 1980, a non-linear failure criterion was developed by Hoek and Brown (1980), based on experimental failure data Hoek (2000).

#### 3.5.1 Mohr-Coulomb criterion

The Mohr–Coulomb (MC) failure criterion is a set of linear equations where the major and minor principle stress describes the conditions for which an isotropic material will fail. Coulomb assumed that failure in an isotropic material occurs due to shear stress  $\tau$  acting along a plane. The shear stress envelope is described by Equation 3.13, where  $c$  is the cohesion,  $\sigma_n$  is the stress acting normal to the plane and  $\phi$  is the internal friction angle of the material.

$$\tau = c + \sigma_n \tan \phi \quad (3.13)$$

In order to create a Mohr-Coulomb criterion envelope a triaxial compression test must be performed on a rock core. A core is loaded with a constant radial pressure  $\sigma_r$  and an increasing axial load  $\sigma_a$ , which are equal to  $\sigma_3$  and  $\sigma_1$  respectively. The black half circle in Figure 3.12 shows the stress and shear force acting at different planes in the loaded rock, related by the angle  $\beta$ . Equation 3.14 and 3.15 relates the internal friction angle to the failure angles  $\beta$  and  $\theta$  (Labuz and Zang, 2012).

$$\beta = \frac{\pi}{4} + \frac{\phi}{2} \quad (3.14)$$

$$\theta = \frac{\pi}{4} - \frac{\phi}{2} \quad (3.15)$$

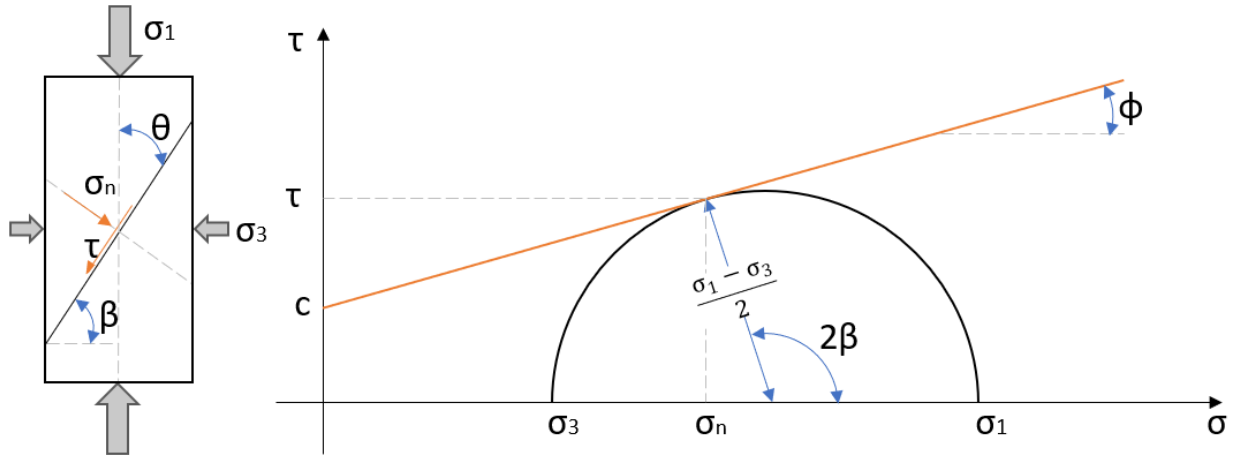


Figure 3.12. Load, forces and fracture plane of a loaded rock core with the associated Mohr-Coulomb failure criterion envelope.

### 3.5.2 Hoek Brown criterion

An important limitation of the Mohr-Coulomb criterion is that it does not realistically describe the non-linear behaviour of rock when the confining stress varies in a large span (Li, 2017). The criterion is also known to predict an exaggerated tensile strength of a material, when all forces are compressive, as is the case in a rock mass (Labuz and Zang, 2012). To better describe a realistic behaviour of rock, Hoek and Brown (1980) created a criterion which accounts for the non-linear failure envelope witnessed during triaxial tests on intact rock samples (Hoek and Brown, 2019):

$$\sigma_1 = \sigma_3 + \sigma_{ci} \sqrt{m_i \frac{\sigma_3}{\sigma_{ci}} + 1} \quad (3.16)$$

where  $\sigma_1$  and  $\sigma_3$  are the major and minor principal stresses and  $\sigma_{ci}$  is the unconfined compressive strength.  $m_i$  is an arbitrary constant that is used to fit the criterion to experimental data (Hoek and Brown, 2019). For projects where triaxial tests have not been conducted Appendix B.2. suggests values for different types of rocks.

Later revisions generalised the Hoek-Brown criterion and made it suitable for jointed rock masses (Hoek et al., 2002):

$$\sigma_1 = \sigma_3 + \sigma_{ci} \left( m_b \frac{\sigma_3}{\sigma_{ci}} + s \right)^a \quad (3.17)$$

The parameters  $m_b$ ,  $s$  and  $a$  are material constants which are calculated as shown in Equation 3.18 to 3.20. For intact rock,  $s$  and  $a$  are set to 1 and 0.5. The GSI system is implemented to reduce the value of the material parameters depending on the rock mass quality.  $D$  is a factor introduced to account for the area around an excavation that is disturbed due to blasting. This factor can be determined using Appendix B.3.

$$m_b = m_i \exp\left(\frac{GSI - 100}{28 - 14D}\right) \quad (3.18)$$

$$s = \exp\left(\frac{GSI - 100}{9 - 3D}\right) \quad (3.19)$$

$$a = \frac{1}{2} + \frac{1}{6}(e^{-GSI/15} - e^{-20/3}) \quad (3.20)$$

When the hoek-brown criteria is used for flysch rock, some additional care must be taken when the parameters  $\sigma_{ci}$  and  $m_i$  are determined. Flysch rock is heterogeneous and contains layers of both sandstone, which is generally strong, and weak silt or clay dominated rock.

In such cases the sandstone layers are usually separated by weak layers, and the contact between the strong layers is limited. Using the material values for the sandstone is thus not appropriate. Neither is using the properties of the weak layers, which would give a too conservative estimate as the sandstone certainly contributes to the rock mass strength (Marinos and Hoek, 2001). Marinos and Hoek (2001) suggests that Table 3.5 should be used to estimate the parameters of the sandstone and siltstone layers. Furthermore a weighted average of these values should be used to determine the final rock mass values.

Table 3.5. Suggested proportions of parameters  $\sigma_{ci}$  and  $m_i$  for estimating rock mass properties for flysch.

Flysch Type*	Proportions of values for each rock type to be included in rock mass property determination
A and B	Use values for sandstone beds
C	Reduce sandstone values by 20% and use full values for siltstone
D	Reduce sandstone values by 40% and use full values for siltstone
E	Reduce sandstone values by 40% and use full values for siltstone
F	Reduce sandstone values by 60% and use full values for siltstone
G	Use values for siltstone or shale
H	Use values for siltstone or shale

\* See Appendix B for flysch rock.

### 3.5.3 Applicability of the Hoek-Brown criteria

The Hoek-Brown criterion assumes an isotropic material. Both intact rock and a closely jointed rock, where the individual pieces of rock are sufficiently small compared to the structure in question, are situations where the Hoek-brown criterion is especially suitable. For a rock mass with several discontinuities, where the joint sets are of similar strength the Hoek-Brown criterion may also be considered as illustrated in Figure 3.13 (Hoek, 2000).

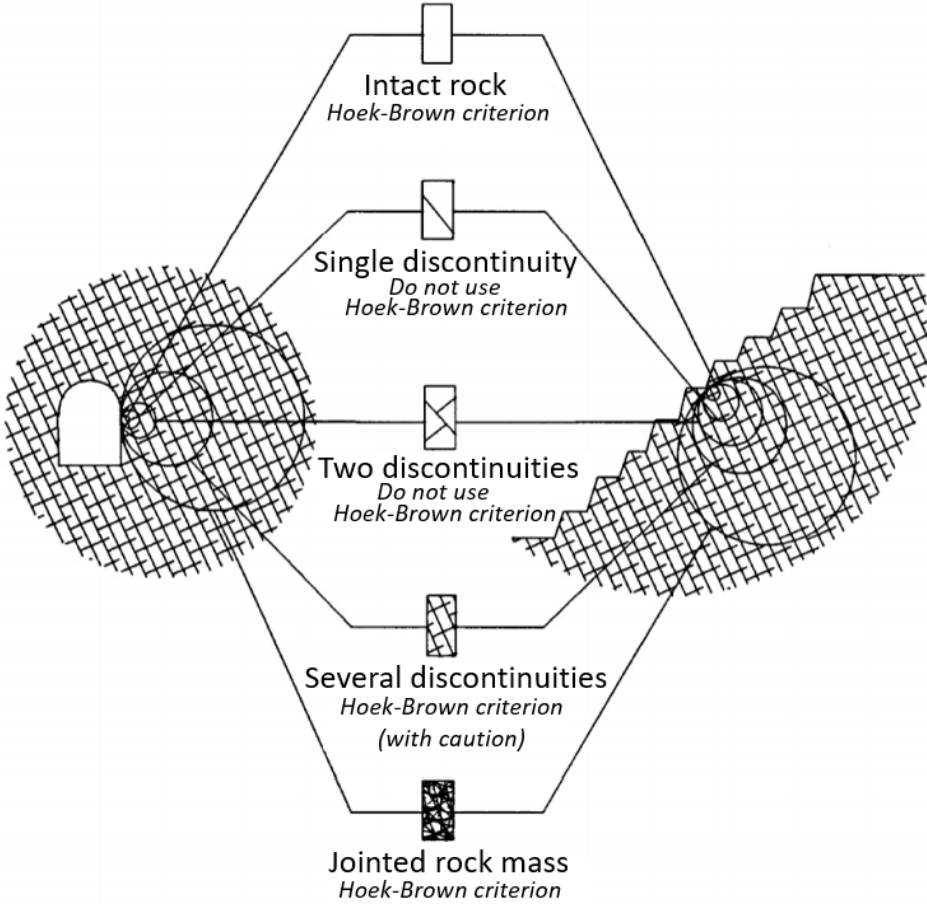


Figure 3.13. Applicability of the Mohr-Coulomb and the Hoek-Brown criterion. Modified from Hoek (2000).

# Chapter 4

## Moglice hydropower project

### 4.1 Project description

Moglice hydropower project is one out of two planned hydropower plants in the Devoll hydropower project. The DHP is located in southeast Albania, around 50 to 70 km from the capital Tirana (Devoll HPP, 2011). In Figure 1.1 in Chapter 1, the location of Moglice dam within the catchment of the Devoll river is shown as well as the location of the catchment in Albania.

Within the project, Moglice is the largest powerplant. The dam (shown in Figure 4.1) is 168 m tall and is the tallest asphalt core dam constructed by Statkraft to this date (Statkraft, 2019). In total the water head is 300 m. When filled, the reservoir will have a storage capacity of 362x10 million m<sup>3</sup> and a surface area of 7.21 km<sup>2</sup>. To transport the water there has been built approximately 11.8 km of tunnel. At last the powerhouse will be located in an underground cavern of 60 m length, 15 m width and a height of 30 m (Statkraft, 2017).



Figure 4.1. Moglice dam and spillway (Photo: Runa B. Frengen 27.03.2019)



## 4.2 Engineering geological conditions

### 4.2.1 Regional geology

The Albanides mountain range is a prominent feature in the Albanian landscape covering most of the east half of the country. It is joined by the Dinarides to the north and Hellenides to the south to form the south branch of the Mediterranean Alpine Belt. The two main divisions of the country is the external Albanides in the west and the internal Albanides to the east which are related through a southwest nappe character. The internal Albanides, where Moglice HPP is located are dominated by a ophiolitic belt which is overthrust from east to west (Frashëri, 2005).

Figure 4.2 shows the geology in the project area. Both the origin and mechanical properties of the encountered rock types varies greatly within the project. The upper parts of the headrace tunnel is dominated by a flysch rock (pink) of sedimentary origin while the penstock tunnels, the cavern and the tailrace tunnel are situated in an igneous ophiolite (dark green). Due to tectonic activity, the border between the two rocks, the melange zone (light blue) is of very poor quality (Aasen et al., 2013). In addition to these zones, the dam and intake are situated in a conglomerate (light yellow) (Devoll HPP, 2011).

The term flysch was first used by the German geologist B.Studer and comes from the German word "fliessen", meaning flow. It is thought that this related to the frequent landslides which are common in areas consisting of such rock (Hoek and Marinos, 2000). Flysch type rock is very heterogenous and consists of alternating layers of clay-, silt-, sandstone and instances of conglomerates. The mechanical properties of the different layers varies greatly depending not only on the characteristics of the individual layers, but also the proportion of the different rock types (Aasen et al., 2013).

Ophiolites are formed at oceanic ridges and are dominated by mafic to ultramafic rocks. Ophiolites are thus considered pieces of oceanic crust but are found in mountains as the Albanides due to orogenesis. An ophiolitic complex is characterised by peridotitic rocks covered by gabbroic/peridotitic rocks, underlying basalts or sponges, where the basalts are either massive or in the form of pillow lavas (Marinos et al., 2006).

Marinos et al. (2006) states that ophiolites are associated with large overthrusts and that tectonic melanges such as the one found at Moglice HPP can form at the base of such structures. In such zones minerals often change. A type of metamorphism that can occur in ophiolites is serpentinisation where ferromagnesian minerals, especially olivine is transformed into serpentines. This is unfavourable as the strength is drastically reduced as the formed minerals are relatively soft and can easily shear by tectonic processes.

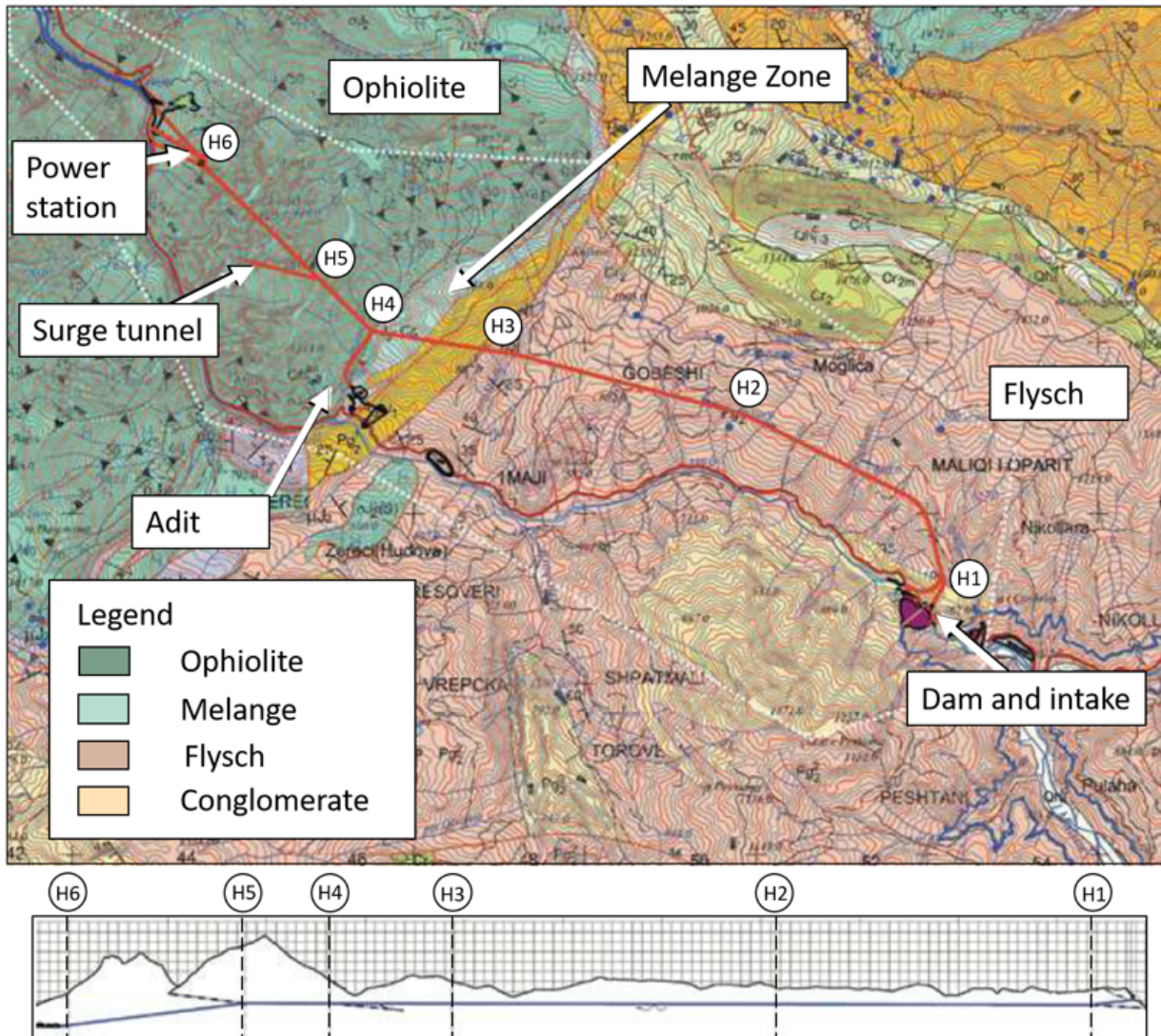


Figure 4.2. Regional geology and topology along the headrace tunnel. The tunnel is highlighted with a red line in the geological map and a blue in the topological map. Modified from Aasen et al. (2013) by Frengen (2019).

#### 4.2.2 Ground investigations

Several investigation methods have been utilised during the planning phase of Moglice HPP. Rotary core drilling and refraction seismic investigations have been conducted as a part of the geological mapping of the area. Representative core samples are illustrated alongside the longitudinal profile of Moglice HPP in Figure 4.3. The rock mass quality has been mapped using the Q and GSI system (Aasen et al., 2013).

Laboratory testing has been performed on representative samples from the different sections. Among these are uniaxial compression tests, slake durability index test and swelling tests (Aasen et al. (2013), Selen, Panthi et al. (2018) and Sweco (2018)). The slake durability test and some swelling tests are described in Chapter 2.

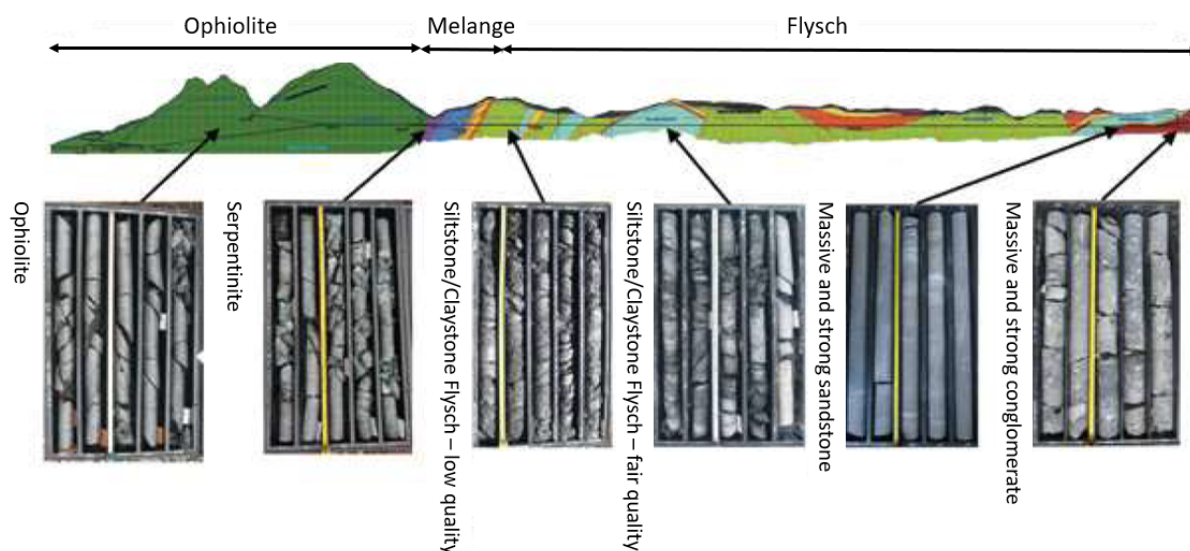


Figure 4.3. Longitudinal profile of the headrace tunnel with core samples from the different geological sections. Edited for clarity after Aasen et al. (2013) by Frengen (2019).

Flat jacks have also been installed in the tunnel around chainage 7+500, located between H3 and H4 in Figure 4.2 after the tunnel was excavated. This is a tool used to determine ground stresses (Li, 2017). By comparing stresses before filling the tunnel and after, changes in the stress conditions caused by swelling or deformations can be measured. Convergence measurements have also been conducted after the excavation.

### 4.2.3 Geological conditions at the area instrumented with flat jacks

In this thesis, rocks from the area instrumented with flat jacks are collected and used as the basis for a numerical analysis. A closer look at the conditions at this location is thus necessary.

Figure 4.4 shows the geology around chainage 7+500, where the flat jacks have been installed. The rock types in the area are flysch of varying quality, classified after the GSI system for flysch rock. Lenses of Flysch B are sandstone with interlayers of siltstone and flysch C contains approximately equal amounts of sand and siltstone. Flysch of E, F and H qualities are weak siltstone or clayey shale with sandstone interlayers of increasing tectonic folding and faulting (Marinos and Hoek, 2001).

A likely reason for the varying quality and local folding and faulting is the proximity to the ophiolitic fault breccia, separating the flysch and the ophiolitic complex. The melange zone separating the ophiolitic and flysch complex is comprised of ophiolitic fault breccia and serpentinites can in its entirety be considered a fault zone and is heavily disturbed by tectonic activity (Sweco, 2018).

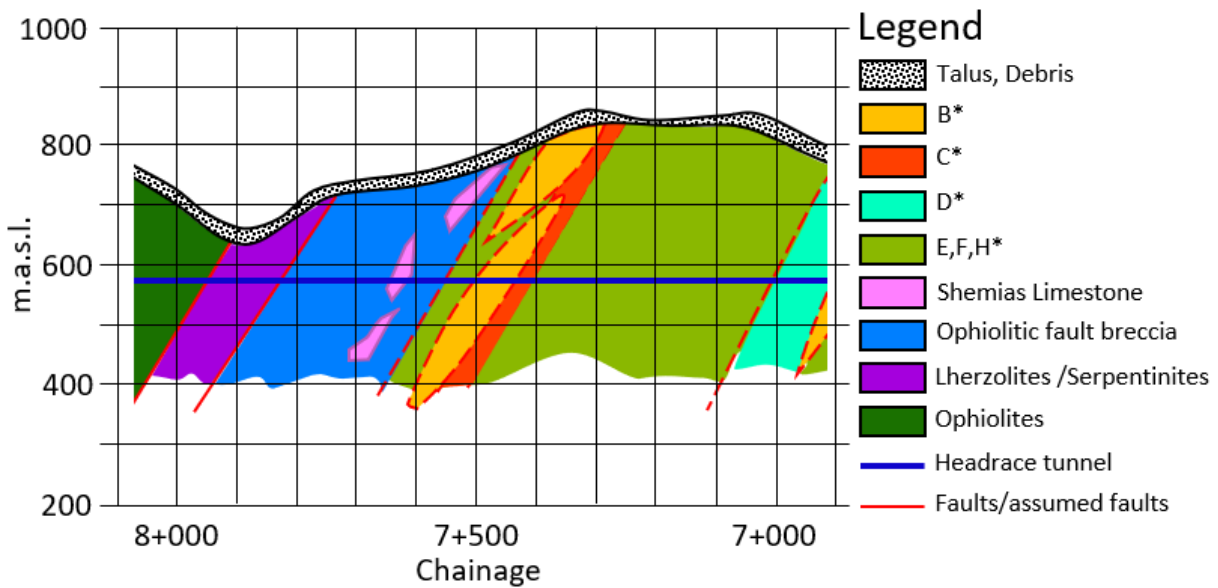


Figure 4.4. Longitudinal profile highlighting the geological conditions of the instrumented area. Rock types annotated with an asterisks are flysch rock of different qualities as described in Appendix B. This profile is a drawing by the author based on a detailed geological profile supplied by Statkraft, and does not claim to be entirely accurate.

The area between chainage 7+410 and 7+510 is described in Devoll HPP (2011) and are according to the GSI classification table for flysch rock in Appendix B. The rock mass in this region contains sandstone and clayey shale/siltstone in approximately equal amounts, with 40% to 60% of each fraction. Generally, the rock is classified as flysch of grade C or B, but folding and faulting may shift parts of the rock to grade F. Layers of strong and weak rock are of thin and medium thickness. The discontinuities in the rock mass is mostly attributed to bedding planes of fair to poor quality depending on the level of folding and faulting.

Investigations by Sweco (2018) suggests a general UCS of 25 to 55 MPa for the strong layers, while deformed sections dominated by silt and clay has UCS <25 MPa. Due to the high content of weak material, the weaker bands control the mechanical properties of the flysch. Mapped Q-values in the flysch rock is as low as 0.38, which is classified as extremely poor rock mass after Figure 3.12 (Sweco, 2018).

The varying rock mass quality is also evident in the convergence reading in the area. Convergence measurements in the region varies greatly. At chainage 7+453 the convergence stabilised after 190 days at 7.6 mm. Further down at 7+531 the convergence ended up being 46 mm.

Stability issues in the flysch rock is attributed to swelling and slaking. Sweco (2018) reports fissuring in dried up sections of the tunnel. The case study of the Chingaza Project shows how this can lead to increased slaking and swelling when clay rich rock is later subjected to water.

### 4.3 Design of the headrace tunnel

From the early stages of the planning of Moglice HPP, a "Norwegian" unlined design was chosen as both the topographical and geological conditions were satisfactory. The design of the waterways is unlined in the sense that concrete linings are only used where necessary along with rock bolts (Aasen et al., 2013).

Depending on the local geological conditions, different excavation methods and support have been installed as listed in Table 4.1. The intake is located in a strong conglomerate (Devoll HPP, 2011). The need for support is thus low. A weak section of flysch from H1 to H3 is excavated by use of TBM and supported by segmental concrete lining (Aasen et al., 2013). At H3 the excavation method changes to drill and blast. The support is adjusted to local rock mass conditions along this part. The photos in Figure 4.5 show the two excavation methods and support mechanisms. Contours of the reinforced ribs of sprayed concrete (RRS) are visible in the right photo.

Table 4.1. Tunnel support concept for the sections of the headrace tunnel. Based on information from Aasen et al. (2013) and Devoll HPP (2011).

Headrace tunnel section	General rock formation	Tunnel design support	Excavation method
Intake to H1	Conglomerate	Unlined/sprayed concrete	Drill and blast
H1-H3	Flysch	Segmental lining	TBM
H3-H4	Flysch/Melange	Concrete lining/ RRS	Drill and blast



Figure 4.5. Tunnel profiles along the headrace tunnel. The left photo is from the part excavated by TBM, while the right is from the drill and blast section (Photo: Runa B.Freng 27.03.2019).

# Chapter 5

## Laboratory testing

The tested samples has been collected from the flysch section at Moglice headrace tunnel through the sprayed concrete lining. Most of the material has been extracted during a flat jack installation in the tunnel in the area 7+492 to 7+501. An additional three flysch cores from an unknown chainage were supplied by Lena Selen.

Rock mechanical testing has been performed by the author together with Gunnar Vistnes and Jon Runar Drotninghaug. The tests have been conducted in line with ISRM's recommendations. For theoretic background to the testing procedures the reader is referred to the ISRM standards.

### 5.1 Material description

Two rock types were tested in the preliminary project: a serpentinite and a flysch type rock. As only the flysch rock is of interest for this thesis, the serpentinite is not described. The flysch rock cores were collected from the headrace tunnel at Moglice HPP. Some sections of the cores were selected for this study by Lena Selen. Six flysch sections were tested in total (flysch 6-11). For each of the sections, representative samples were chosen for each of the tests.

Testing conducted during this thesis had been performed on cored out sections from the headrace tunnel at chainage 7+492 to 7+501. These consists of shotcrete and varied flysch material.

#### 5.1.1 Sprayed concrete and rock material cores

The investigated cores were originally drilled during a flat jack installation in the area. Due to this, some cores overlapped with the hole from the previously drilled core, leaving a crescent shape core. As a result, only 13 of the around 60 provided cores were cylindrical and thus

suitable for testing. These cores are presented in Figure 5.1, and classification of the material is presented in Table 5.1 in the same order as presented in the image. In order to relate rock material to a core during testing, the cores have been given an ID number. The 13 cores are numbered related to their chainage location.

The four main material types present in the cores are sprayed concrete and flysch rock dominated by conglomerate, clay or sand. The sprayed concrete section varies in thickness, but is in general around 40 cm thick.

Some cores, especially number 10 and 14 shows signs of a more porous boundary between layers of shotcrete. The layer thickness could not be measured directly as no piece contained two layer boundaries, but seem to be around 15 cm. Individual sprayed concrete cores show different characteristics. All of them are containing steel fibre, but based on a visual inspection the size of the stone aggregate and porosity of the material seem to vary. Core 8 displayed the poorest sprayed concrete quality as it looks to be the most porous of them and shows rusted steel fibres.

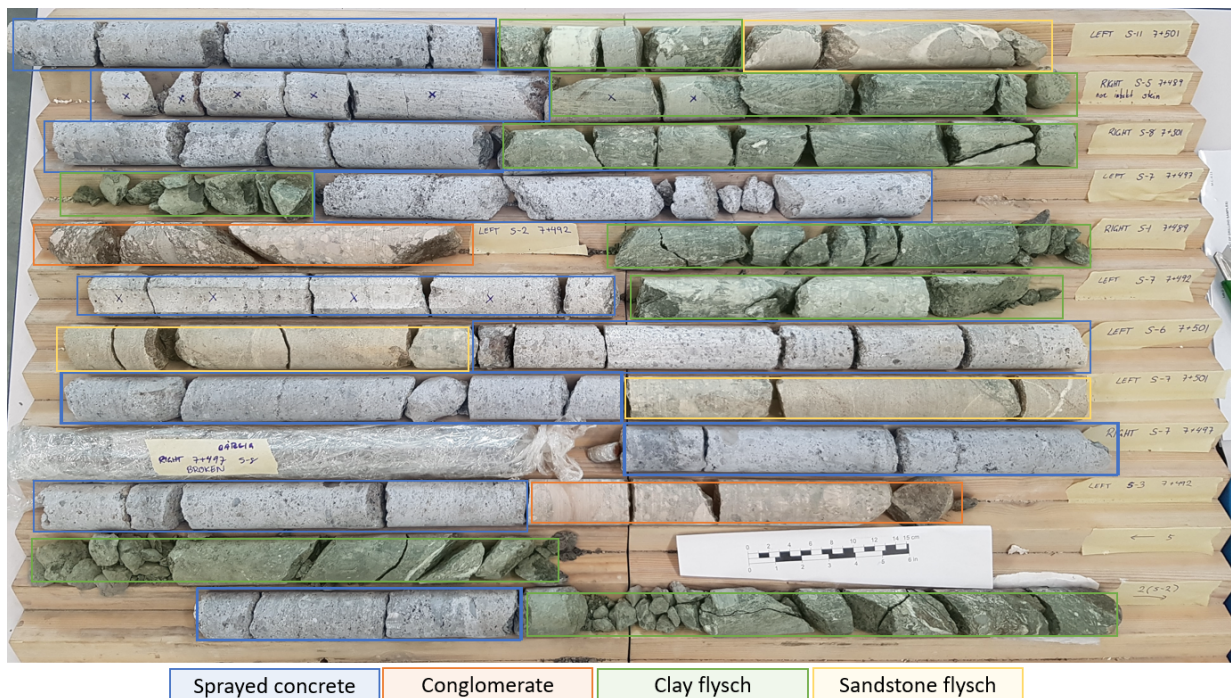


Figure 5.1. Sprayed concrete and rock material cores extracted from chainage 7+492 to 7+501 at Moglice HPP headrace tunnel. Sections marked with an x, are of crescent shape and unsuitable for testing.

The main rock type found in the cores are clayrich flysch, followed by sandstone flysch and a few sections of conglomerate. The clay flysch was generally broken into smaller pieces along the foliation. Smaller pieces could easily be broken in two by hand indicating low strength. Pieces of this quality that were submerged in water, disintegrated with ease. The sandstone and conglomerate sections were in general longer and stronger. No visible disintegration was observed after 24 hours of submersion.

Both the rock and sprayed concrete are broken into pieces that are unrelated to the foliation. These may be the result of rough handling during boring or transport. Pieces were sorted by length to identify sections that were suitable for the different rock mechanical tests.

Due to the limited rock material, some remaining cores from the preliminary project were also included. These are pictured in Figure 5.2 Two of these, flysch 6 and flysch 7, were sandstone flysch which could be prepared for the uniaxial compression test. Flysch 10 was more akin to a claystone, and was tested using the point load test. These are identified in tests and results as F6, F7 and F10, to distinguish them from the cores in Figure 5.1.



Figure 5.2. Flysch cores from Moglice headrace tunnel. F6 and F7 are sandstone flysch, while F10 is a clay flysch.



Table 5.1. Description of tested core material. L/R (left/right) indicates from which side of the tunnel the core is extracted. The table is sorted in the same manner as the rock cores in Figure 5.1 for easy comparisons.

Chainage L/R	ID	Rock content	Comment	
7+501	L	10	Clay/Sandstone flysch	
7+501	L	11	Clay flysch	
7+489	R	2	Clay flysch	Non-cylindrical sprayed concrete
7+501	R	8	Clay flysch	
7+497	L	7	Clay flysch	
7+492	L	3	Conglomerate	
7+489	R	1	Clay flysch	
7+492	L	5	Clay flysch	Non-cylindrical sprayed concrete
7+501	L	9	Sandstone flysch	
7+497	R	6	N/A	Only sprayed concrete
7+492	L	4	Conglomerate	
-	-	12	Clay flysch	Unknown chainage, rock only
-	-	13	Clay flysch	Unknown chainage
		F6	Sanstone flysch	Material from preliminary project
		F7	Sanstone flysch	Material from preliminary project
		F10	Clay flysch	Material from preliminary project

## 5.2 Specimen preparation

The initial plan was to conduct all rock mechanical tests (UCS, PLi and Brazil) as well as sound velocity and density measurements on both the sprayed concrete and the rock material. For the sprayed concrete, the preparation was completed without any problems, but a few issues arose regarding the rock samples.

For flysch rock, slaking is a known issue, which posed a challenge as water is used for preparing UCS and Brazil specimens. After submerging some smaller sections of the different rock material which almost immediately showed signs of disintegration, it was evident that the clay flysch rock could not be prepared for these tests.

The sand and conglomerate flysch did not visibly slake, even after 24 hours of submersion and was prepared for UCS specimens. However, as some sections had pieces fall off or broke completely during preparation, it was decided that the Brazil test could not be performed, as the risk of losing a significant portion of the material in the preparation process was too great.

Rock sample F6 and F7 were prepared for UCS testing by coring out a smaller rock cylinder of 50 mm. From this, four specimens were prepared. It was noted by Gunnar Vistnes during the coring process that the mud produced was unusually clayey, suggesting a significant clay content in the rock. As pieces of rock were easily broken off from sample F10, it was decided not to attempt coring out UCS specimens.

### 5.3 Uniaxial compression strength test and deformability

Five specimens of the rock core material, eleven specimens of sprayed concrete and a total of four specimens from the material from the F-series were tested in line with ISRM (1979*a*) to find the uniaxial compression strength and the deformability of the materials. The tests were conducted on specimens with a diameter,  $D$  ranging from 44.16 to 50.13 mm, given as the mean of six measurements on each specimen.

Tested specimens were of various heights,  $h$  and  $h/D$  ratios as reported in Appendix A. According to ISRM (1979*a*) a  $h/D$  ratio of 2.5-3 is recommended to avoid end effects which may result in a artificially high UCS value (Hawkes and Mellor, 1970). A suggested absolute minimum  $h/D$  ratio is 2.0 (Hawkes and Mellor, 1970). None of the tested cores meet the ISRM (1979*a*) criteria, but all cores have a  $h/D > 2.0$  to minimise end effects. As the grain size in tested conglomerate specimens and sprayed concrete aggregate where ranging up to cm scale, maintaining a diameter to largest grain ratio of 10:1 as required by ISRM (1979*a*) was impossible for these specimens.

Core samples from Figure 5.1 were tested in laboratory conditions. In addition to these, specimens F6 and F7 were tested in both dry and wet conditions to assess the influence of saturation on the compression strength. The saturated specimens (F6W and F7W) were submersed in water for respectively one and two weeks before testing. It was discovered that specimen F6W had a rather dry interior after it was broken during testing, which led to the decision to leave specimen F7W submersed for another week.

The GCTS Rapid Triaxial Test System (RTR-4000) was used for testing the specimens. Both sprayed concrete and rock specimens were loaded with an increased axial pressure while the axial and radial deformations were registered as displayed in Appendix A. The uniaxial compression strength,  $\sigma_c$ , Young's modulus,  $E$ , and Poisson's ratio,  $\nu$  were calculated using the software used to log the deformations. Table 5.2 show the mean values for both rock and sprayed concrete, while Table 5.3 shows the UCS of sample F6 and F7 in both laboratory and submersed condition with the resulting decrease in strength.

Table 5.2. Mean UCS, Young's modulus and Poisson's ratio together with standard deviation for laboratory condition flysch rock and sprayed concrete specimens.

Material type	Uniaxial compressive strength [MPa]	Young's modulus [GPa]	Poissons ratio
Flysch rock*	132.3 ± 22.0	55.8 ± 17.1	0.29 ± 0.02
Sprayed Concrete	39.9 ± 11.7	18.2 ± 5.3	0.18 ± 0.05

\*Only sandstone and conglomerate flysch were tested for uniaxial compression strength.

Table 5.3. Uniaxial compression strength of specimen F6D, F6W, F7D and F7W, and the resulting percentage strength reduction due to submersion.

Test condition	Uniaxial compression strength [MPa]	
	F6	F7
Laboratory conditions (D)	117.3	90.3
Submersed in water* (W)	105.0	74.2
Strength reduction	10%	18%

\*F6W was submersed in water for one week and F7W for two weeks.

The dry cores from the instrumented area had a similar UCS ranging from 121.2 to 158 MPa, which gives a classification of very high strength according to Table 3.1. The flysch rock from the F series have lower UCS values, both in dry and wet condition. The dry specimens could still be classified as having very high strength. During preparation of these specimens, a significant clay content was noted. A combination of the clay content and different storage conditions could explain the difference. Wet specimens are weaker than dry, in line with the theory presented in Section 3.2.4. The strength reduction in the wet specimens reduced the strength classification to high strength.

The sprayed concrete cores displayed varied strengths ranging from 25.1 to 60.2 MPa without any apparent correlation to the visual characteristics of the specimens. It is possible that the distribution of fibres could affect the strength in the concrete at the measured scale as they are of a length that is near half of the core diameter. The failure to fulfil the diameter grain ration may also contribute to the varying strength.

## 5.4 Point load index test

The point load test is performed on both the rock and the sprayed concrete material described in Table 5.1 in accordance with ISRM (1985). A total of 28 tests on sprayed concrete and 25 tests on flysch rock were performed. 12 out of the flysch rock tests were conducted on clay flysch, 9 on sandstone flysch and 2 on conglomerate flysch. With the exception of the F10, the tests were performed using the NTNU Point Load index machine equipment in Figure 5.3. Due to the larger diameter of F10 it was tested using the GCTS Point Load Tester (Enerpac PLT-100). For the tests it was attempted to manually maintain a constant load increase of 0.2 MPa and 0.2 kN/s depending on the equipment used.



Figure 5.3. The setup of the point load strength test for diametral testing on a rock core.

The loading direction is of importance when conducting a point load index test as rocks are weaker along the foliation. By loading the core parallel to the orientation of the foliation in a diametral test and perpendicular to the foliation in subsequent axial test, the strength an isotropy index of the rock can be found. Figure 5.4 shows the shape requirements for the diametral and axial tests ISRM (1985).

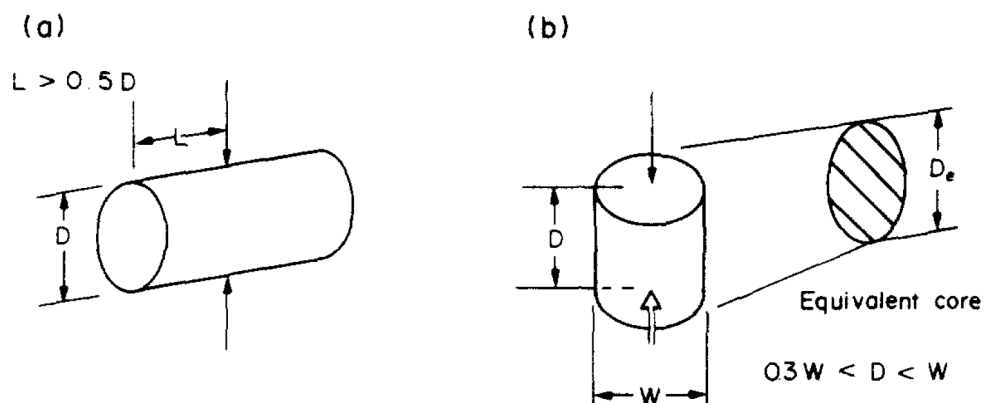


Figure 5.4. Specimen shape requirements for (a) the diametral test and (b) the axial test (ISRM, 1985).

When failure occurs during the PLi test, the plane of failure must pass through both loading points. Figure 5.5 shows valid failure modes for the diametral and axial test. If the plane of failure only passes through one of the loading points, the result is not considered valid.

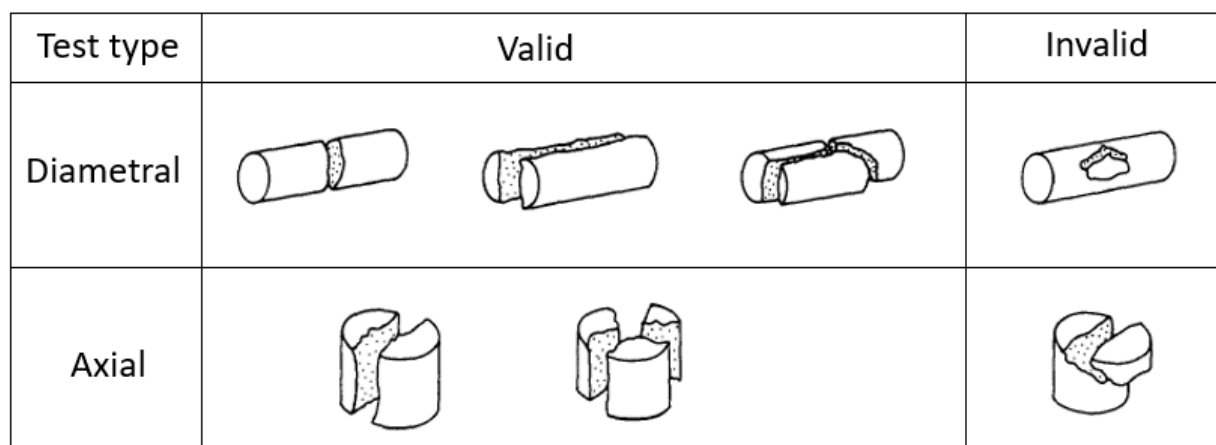


Figure 5.5. Typical valid and invalid modes of failure for diametral and axial tests (Modified from ISRM (1985)).

ISRM (1985) states the following on reporting results. When ten or more specimens are tested, the two highest and lowest values are omitted when the mean value of  $I_{s(50)}$  is calculated. When fewer than ten specimens are tested, only the highest and lowest value is disregarded. The calculated mean values and standard deviation are displayed in Table 5.4. Complete table of core measurements and results for the rock and sprayed concrete specimens are found in Appendix A

Sprayed concrete is not thought to have an anisotropy index so all test data is grouped together. For the flysch rock, weaker samples generally broke along the foliation regardless of the loaded orientation and resulted in a high level of invalid results. Specimens with visible borders between weak and strong rock, were especially prone to failure or flaking along this border during testing. Calculating an accurate anisotropy index based on the collected data was thus not possible.

Two conglomerate specimens were tested, but with severely different results, respectively 0.96 and 6.66. A reliable mean  $I_{s50}$  could thus not be calculated.

Table 5.4. Mean and standard deviation values for  $I_{s(50)}$ , classification and estimated UCS of rock and sprayed concrete specimens depending on k values.

Material type	$I_{s(50)}$ [MPa]	Classification	k value	Estimated UCS [MPa]
Clay flysch	$0.72 \pm 0.28$	Very low strength	11	$8 \pm 3$
Sandstone flysch	$4.87 \pm 0.57$	High strength	24	$117 \pm 14$
Sprayed concrete	$3.42 \pm 0.60$	Medium strength	12	$41 \pm 7$

The values for Flysch is an average of claystone, sandstone and conglomerate.  $I_{s(50)}$  values are adjusted to UCS with an appropriate factor depending on the rock type.

For the different material types an estimated UCS was found by using Equation 3.3. k values was determined in consultation with supervisor Krishna Panthi and Table 3.9. Although Bieniawski (1973) suggests that the point load strength test should not be used for rocks with a

lower UCS than 25 MPa, it is in this case the only tool available to indicate the strength of the clay flysch. From this analysis, a strength of 8 MPa is suggested.

The  $k$  value for the sandstone is on the high end if one is to use Table 3.9 as a recommendation. However, even with a  $k$  set to 24, the estimated UCS is significantly lower than the measured one. A possible reason could be that stronger specimens were chosen for the UCS test due to size requirements.

## 5.5 Brazil test

Tensile strength can be found indirectly through the Brazil test. Due to lack of suitable rock material, this test was only performed on sprayed concrete. The test was conducted in accordance with ISRM (1978*b*).

Disks of approximately 44 mm diameter and 20 mm thickness were prepared for the test. These were placed in the GCTS Rapid Triaxial Test System (RTR-4000), fitted with two steel loading jaws. The automated software kept the load increase at 0.2 kN/s, which was maintained until failure. The failure of the disks occurred in a soft manner. Failure did not cause audible cracks and had to be observed through a reduction in the load sustained by the specimen. For most of the specimens, the tensile failure was visible as a hairline fracture.

A total of 17 disks of sprayed concrete was tested. The tensile strength was then calculated using Equation 3.6 and ranged from 3.2 to 6.3 MPa. Similarly to the point load index test, the failure plane must go through the two loading points. All the performed tests had valid results. Table 5.5 shows the mean tensile strength of the material. A full list with disk measurements and calculated tensile strength can be found in Appendix A.

Table 5.5. Mean strength of sprayed concrete samples and standard deviation.

Material type	Tensile strength, $\sigma_t$ [MPa]
Sprayed concrete	$4.9 \pm 0.8$

## 5.6 Density and velocity

The density,  $\rho$  and velocity,  $v$  of the rock and sprayed concrete samples were found by weighing and measuring the cores prepared for the UCS test. After the volume of the cores were found as described in Section 5.3, the samples were weighed. The density was then calculated using Equation 5.1 where  $V$  is the volume and  $m$  is the mass of the specimens.

$$\rho = \frac{m}{V} \quad (5.1)$$

Seismic velocity,  $v$  through a rock mass can be used as an indication of quality. Good quality rock mass typically has seismic velocities over 5000 m/s, while weakness zones have velocities lower than 4000 m/s (Nilsen and Palmström, 2000). Equation 5.2 was used to find  $v$ , where  $s$  is the length of the core and  $t$  is the travel time of the sound waves.

$$v = \frac{s}{t} \quad (5.2)$$

Table 5.6. Mean and standard deviation values for sound velocity and density of sand/conglomerate flysch and sprayed concrete in dry laboratory condition.

<b>Material type</b>	<b>Velocity [m/s]</b>	<b>Density [g/cm<sup>3</sup>]</b>
Sand/conglomerate flysch	5601 ± 134	2.67 ± 0.03
Sprayed concrete	4514 ± 121	2.21 ± 0.10

# Chapter 6

## Methodology of numerical modelling

### 6.1 Introduction to methods of analysing stability

In order to ensure safe construction and long term stability of an underground structure, it is necessary to perform a stability analysis. Three categories of such an analysis may be utilised; mathematical/analytical methods, empirical methods and numerical methods (Trinh and Holmøy, 2012). Mathematical methods are suitable for simple geometries and are known to be precise, but have the disadvantage of being time consuming and complex when taking multiple parameters into account. The industry has thus long favoured empirical methods based on experience gathered from all over the world (Rahmani et al., 2012). Methods as the Q system and GSI are easy and efficient tools to characterise the rock mass in the field and offer a suitable support regime (Nilsen and Palmström, 2000). Similarly, equations based on empirical knowledge are used to estimate in-situ rock mechanical properties based on laboratory values as previously discussed in Chapter 3.

A significant advantage of numerical tool is the possibility to perform sensitivity analysis (Rahmani et al., 2012). This way, the effect of changing unknown parameters can be evaluated with minimal effort. As both the in-situ stresses and swelling pressure exerted on the tunnel support is unknown, this is a powerful tool to evaluate different possible situations. Additionally, the rock mass differs in quality, which further increases the uncertainties that must be evaluated. Numerical modelling is the tool chosen to evaluate the effect of swelling in this thesis. Thus a further description of the method used is warranted.

### 6.2 Numerical analysis

Compared to conventional tools, numerical modelling has several advantages. One is the possibility to model increasingly complex situations, such as complicated profiles, geological conditions and construction procedures. It can also help when dealing with previously



uncharted territory, when no similar projects have been constructed. Additionally, numerical tools are useful for obtaining more detailed information about the rock and rock support performance (Trinh and Holmøy, 2012).

### 6.2.1 Types of numerical models

Nilsen and Palmström (2000) states that there are two main methods of numerical methods, continuous and discontinuous models, as seen in Figure 6.1. A common factor for continuous models is that they regard the rock mass as a uniform medium. Thus only a few discontinuities or heavily jointed rock mass or soil can be modelled. Several methods of continuous models exists, but they are mostly separated by the mathematics used to solve the equations. This is most commonly used category of numerical methods (Nilsen and Palmström, 2000).

Discontinuous models separates the rock mass into individual blocks which are interacting along their boundaries. As the nature of the rock mass is discontinuous this type of model has obvious advantages (Nilsen and Palmström, 2000). Such models require knowledge if joint locations and orientation, which often become apparent at the construction stage (Trinh and Holmøy, 2012).

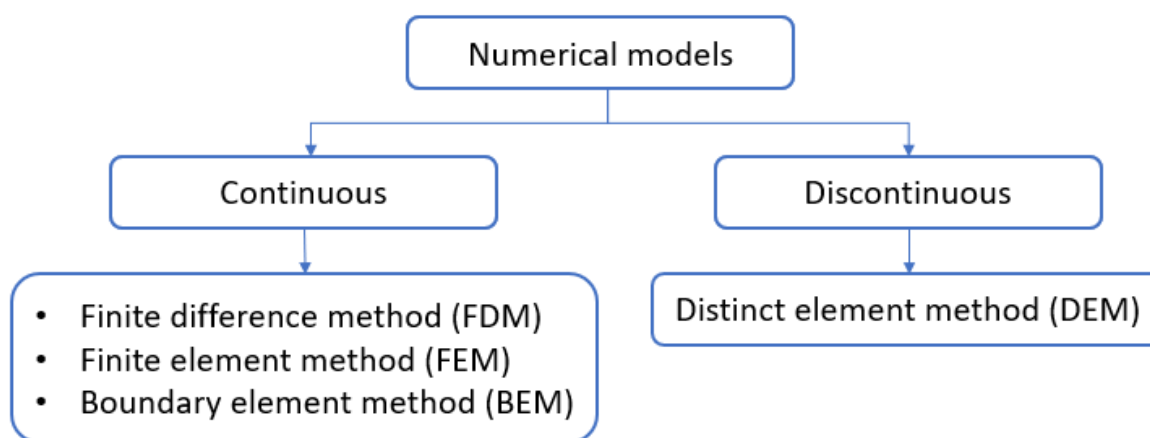


Figure 6.1. General types of numerical methods (Based on Nilsen and Palmström (2000) and Trinh and Holmøy (2012)).

### 6.2.2 The process of a numerical analysis

In Trinh and Holmøy (2012) a general procedure is recommended when working with numerical models. By following this procedure Trinh and Holmøy (2012) states that the tool will be used more effectively and fewer uncertainties will be encountered. Numerical modelling is an interactive process, where several steps call for verification and adjustments as the model is created, evaluated and as more information is revealed during construction. Figure 6.2 outlines the 8 steps of the process.

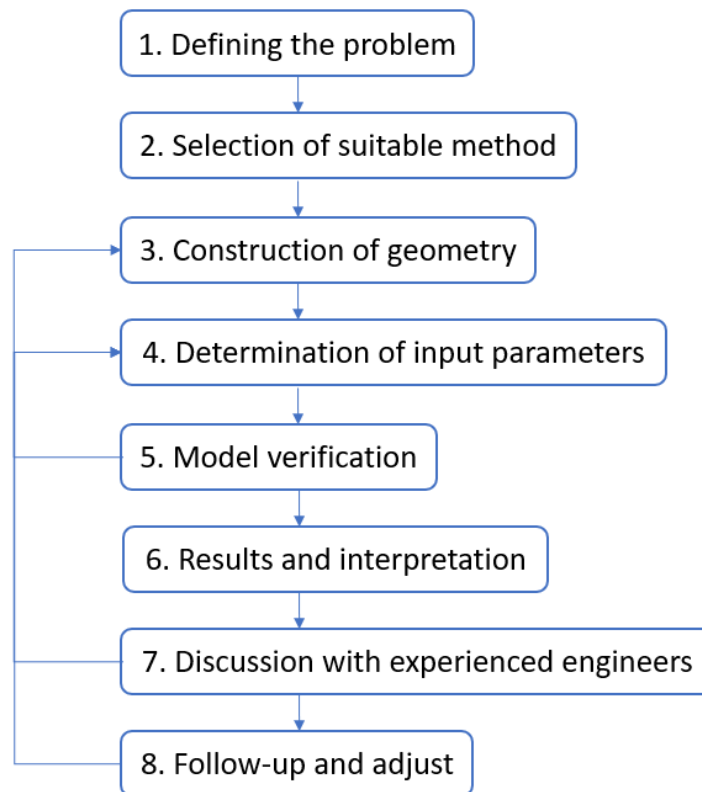


Figure 6.2. Flowchart outlining the process of solving a problem by use of numerical modelling. (Based on Trinh and Holmøy (2012))

### **Step 1. Defining the problem to be analysed.**

The purpose of this step is to correctly identify the problem, the most important goals or targets and thus help identify a suitable method to solve it. Among such a problems are the stability of tunnels, both in soft or hard rock, excavation in jointed rock and slope stability issues.

### **Step 2. Selection of suitable method(s).**

Based on the findings in step 1, a method for analysis can be chosen. As previously discussed, there are several methods with different advantages and limitations. In additions to the different methods, the engineer may also consider if the problem is static or dynamic, 2D or 3D when selecting the method. Complicated situations may call for a combination of multiple methods.

### **Step 3. Construction of the geometry for the problem.**

In most cases the exact geometry is too complex to model accurately. Both mines and tunnel profiles are often rough due to imperfect blasting. An idealised shape is often used. When the geometry is constructed, it is important to keep in mind the actual planned construction sequence. Excavation and support installation should be in the same order as planned in reality.

**Step 4. Obtaining inputs for the model.**

Although numerical models are a useful tool, Nilsen and Palmström (2000) stresses that numerical analysis often has the character of parameter or sensitivity analysis rather than exact calculations with definitive answers.

A common pitfall of such tools is that the result may look pretty and decisive, independent of the input parameters values, summarised in the expression "Garbage in, garbage out". The quality of the result is hence significantly reliant on the quality of the input data. Trinh and Holmøy (2012) thus considers this to be the most important step of a numerical analysis. Site investigations and mapping and laboratory measurements as well as data from reference projects are sources of good quality input data.

**Step 5. Verification of the model.**

Verification and input data is in it self a loop that might take many iterations to complete. By running the model with some known situations, the engineer can observe if the results are reasonable. When some stages of construction are completed, the model can be compared to results and observations made in-situ. Revisions of the model input is necessary if the results are unreasonable.

**Step 6. Presenting the results and interpretation.**

Numerous results can be extracted from a numerical analysis. A common way to present the results is by use of contour plots related to stress, strain, displacement, etc. Concise and understandable figures with relevant information, simplifies the interpretation process. Both results for the overall situation and local areas may be presented depending on the investigated problem.

**Step 7. Discuss the results with experienced engineers.**

Discussions with experienced engineers is useful to verify that the necessary considerations are made in the model. By comparing the results with their general experience, uncertainties can be reduced. If discrepancies are found, the model may need a revision.

**Step 8. Following up and adjustments.**

During the construction process, observations may be made, which presents a need to further revise the model. In complicated or critical situations, the underground structure may be monitored by use of extensometers, loading cells or sensors. The numerical model should in such cases be compared with the data from these tools and altered when necessary throughout the construction process.

# Chapter 7

## Evaluating the effect of swelling by use of RS<sup>2</sup>

### 7.1 Problem definition

At Moglice HPP, the flysch rock is known to have a swelling characteristic. The level of swelling has been investigated in the lab during the preliminary project (Frengen, 2019). However, as the in-situ swelling pressures are known to be different to laboratory values, the effect of the swelling on the rock support is unknown and has to be investigated. Changes in the support design has been implemented as the swelling characteristics were initially evaluated. Thus, the effect on the different support regimes is to be evaluated.

As flysch is a heterogeneous rock, the material parameters varies greatly. In the laboratory both strong sandstone and conglomerate flysch as well as weak claystone flysch were tested. The mechanical properties found in the laboratory will be the foundation for the material input in the numerical analysis.

Additionally, the long term stability is of interest. Attention is thus also directed to the supports capacity to limit displacement of the tunnel contour compared to an unsupported case.

### 7.2 Choice of numerical method

For this thesis, RS<sup>2</sup> is the preferred software used for the numerical analysis as it is a powerful and user-friendly tool which is readily available for NTNU students. This software uses the finite element method in two dimensions. This type of model is suitable as the flysch rock is severely jointed and weak, where the deformations rather than the joint characteristics are of interest.

A three-dimensional version of the software exists. This software would have been ideal, as the

reinforced ribs of sprayed concrete which are used as support cannot be accurately described in two dimensions. Unfortunately, the analysis had to be limited to a 2D analysis due to time and computational restrictions. Thus, some calculations must be done to approximate the 3D structures.

### 7.3 Model geometry

The headrace tunnel is excavated both by TBM and drill and blast. At the location of interest, between H3 and H4 as indicated in Figure 4.2 drill and blast is used. Figure 7.1a shows the theoretical outline of the tunnel. The sole of the tunnel is flat while the wall and crown has a radius of 3.15 m.

Figure 7.1b shows the geometry as constructed in the RS<sup>2</sup> software. The excavation outline is constructed using the information provided in Figure 7.1a.

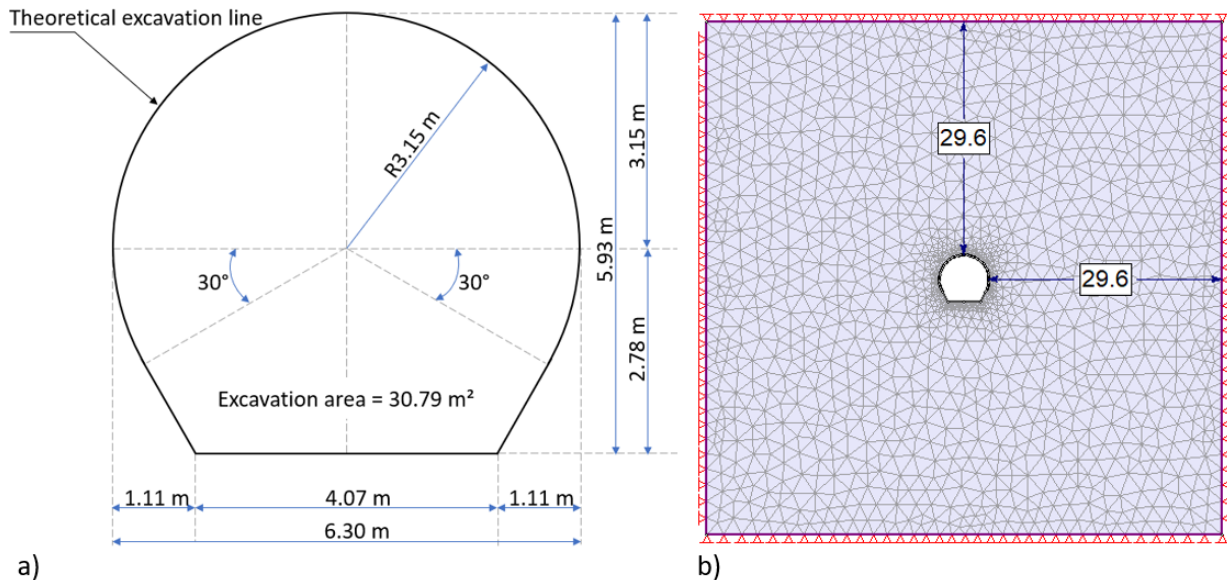


Figure 7.1. a) Theoretical excavation outline diagram for the DHP headrace tunnel in the H3 to H4 region. b) Headrace geometry and boundary condition of the model in RS<sup>2</sup>.

#### 7.3.1 Mesh and boundary conditions

A graded mesh type with 3 noded triangles is used in the model. The gradation factor and number of nodes on excavations are left at the suggested values and are 0.1 and 110 respectively. A gradation factor of 0.1 means that the length between the nodes on the boundary of the model is 10 times the length between nodes on the excavation boundary. A low gradation factor allows a higher density of nodes around the excavation profile, which is useful as this area has a higher stress gradient, while areas far away from the excavation consume less computational power.

Trinh and Holmøy (2012) suggests that the distance from the excavation to the model boundary should be at least 4 to 5 times the underground opening to avoid boundary effects near the excavation. An expansion factor of 5 is thus chosen. As a constant stress field is used, the boundary is restrained in both the x and y direction.

### 7.3.2 Stages

Stages in a numerical model should follow and closely resemble the construction stages (Trinh and Holmøy, 2012). For this project, the four main stages present in Figure 7.2 have been identified and modelled. The initial condition serves as a tool to make the verification process easier, as the initial stress distribution can be visualised. Secondly, the excavation takes place before the support is installed in stage 3. At last, when the headrace tunnel is filled with water, the swelling is introduced in stage 4 and increased gradually in subsequent stages.

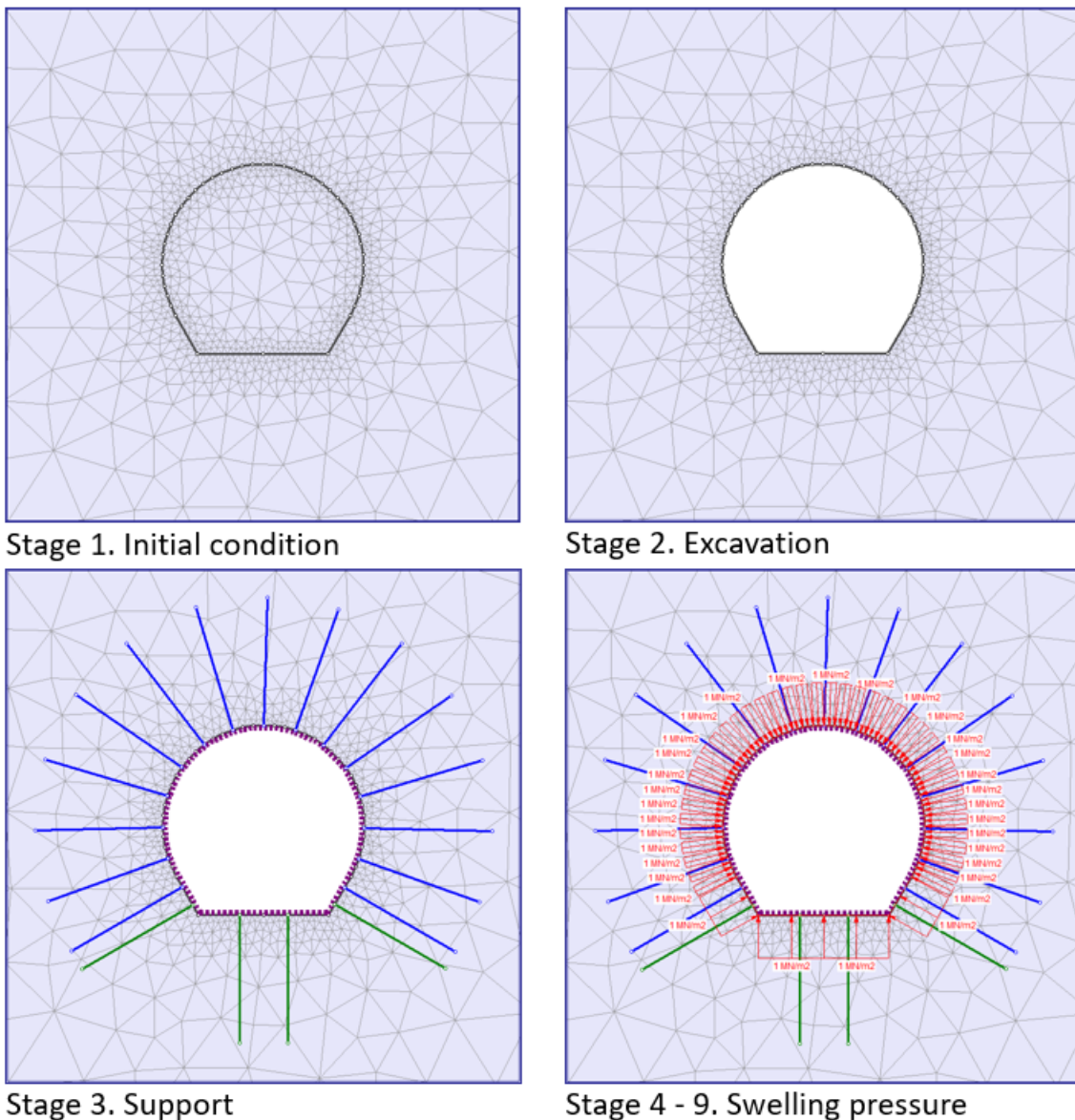


Figure 7.2. Model stages used in the numerical analysis.

## 7.4 Determining input parameters

The quality of the input parameters used in a numerical model, is as previously discussed of paramount importance. For the rock material parameters and swelling pressures, the result of the laboratory investigation and relevant literature has been used. Different technical documents have been provided by Statkraft, describing the installed support along the headrace tunnel and the material parameters of these.

### 7.4.1 Material parameters

#### Failure criterion

Several failure criterion are available for use in the RS<sup>2</sup> software. Figure 3.13 offers an overview of when some criteria are suitable. Due to the severe jointing and poor rock quality present, the generalised Hoek-Brown criterion is preferred in this model. The necessary parameters for this criterion is thus UCS,  $m_b$ ,  $a$  and  $s$ , as described in Section 3.5.

#### Rock material parameters

Three qualities of flysch were investigated in the laboratory; Conglomerate, sandstone and claystone flysch. However, as the conglomerate and sandstone flysch were of similar character, the results from these have been combined, and are in this analysis denoted as strong flysch. The material input in Table 7.1 for the strong flysch is gathered from the laboratory investigation described in Chapter 5.

From Table 5.2, UCS of the rock is  $132.3 \pm 22$  MPa. Using Equation 3.7, the UCS can be corrected to that of a 50mm core, resulting in a reduction to 128.3 MPa. A further strength reduction is warranted as the material was tested in a dry condition, while the the rock is saturated in-situ. By use of Equation 3.9, the resulting UCS for the saturated strong flysch is set to 98 MPa.

To calculate the  $m_b$ ,  $a$  and  $s$  parameter, the GSI and  $m_i$  of the rock mass must be determined. In the list of suggested values for  $m_i$ , sandstone has a value of  $17 \pm 4$ . During the preparation of the F-series rock it was noted that the mud water was unusually clayey, suggesting a significant content of clay. Thus a  $m_i$  value of 13 was chosen. Devoll HPP (2011) suggests a a GSI value of 15 to 50 in the modelled region. Considering this is strongest rock tested it is reasonable to assume that the GSI can be set to 50.

Table 7.1. Material Parameters of the strong flysch.

<b>Input parameters</b>	<b>Peak values</b>	<b>Residual values</b>
Intact Compressive Strength <sup>1)</sup> (USC) [MPa]	98	-
E-modulus <sup>1)</sup> (Ei) [MPa]	55 800	-
Poisson's Ratio <sup>1)</sup>	0.29	-
Geological Strength Index (GSI) <sup>2,3)</sup>	50	25
Intact Rock Constant (mi) <sup>3)</sup>	13	-
<b>Calculated parameters</b>		
E-modulus (Erm) [MPa]	17141	3339.9
mb	2.1798	0.892595
s	0.003866	0.00024
a	0.505734	0.531267

<sup>1)</sup>Laboratory investigation <sup>2)</sup> Devoll HPP (2011) <sup>3)</sup>Appendix B

A pure sandstone flysch, is however not reasonable. Thus a more appropriate rock mass must be estimated using the suggested method by Marinos and Hoek (2001). For the claystone flysch, some tests could not be performed. Thus material parameters used for this rock is partly from the laboratory investigation, but relies also on values from the research conducted by Malaj et al. (2017) shown in Table, where a similar analysis has been performed on Flysch rock from the same region. The midpoint values from this research are chosen for this analysis.

Table 7.2. Material parameters for claystone flysch from Malaj et al. (2017)

<b>Parameter</b>	<b>Range of values for claystone flysch</b>	<b>Midpoint value</b>
UCS [MPa]	8.00 - 17.00	12.5
Poissons ratio	0.31 - 0.46	0.39
E-modulus [GPa]	5.00 - 10.00	7.50

According to the geological report from the site, Devoll HPP (2011), the approximate percentage of weak and strong flysch is  $50\% \pm 10\%$ . In order to model a scenario where a weak section denoted as weak flysch is encountered, the following relation has been used for estimating the input value for the intact rock strength:

$$UCS_{weak\ flysch} = 0.6 \cdot UCS_{claystone\ flysch} + 0.4 \cdot UCS_{strong\ flysch}$$

The E-modulus and Poisson's ratio was determined in the same manner. The GSI for the weak rock was set in conference with Devoll HPP (2011) and Appendix B.1 for flysch rock. The sandstone values have been reduced in line with Table 3.5. For a flysch rock of such proportions of weak and strong layers a GSI of 35 is suggested.



Table 7.3. Material Parameters for weak flysch rock.

<b>Input parameters</b>	<b>Peak values</b>	<b>Residual values</b>
Intact Compressive Strength (USC) <sup>1,4)</sup> [MPa]	60.8	-
E-modulus <sup>1,4)</sup> (Ei) [MPa]	31 650	-
Poisson's Ratio <sup>1,4)</sup>	0.34	-
Geological Strength Index (GSI) <sup>2,3)</sup>	35	22
Intact Rock Constant (mi) <sup>3)</sup>	8.5	-
<b>Calculated parameters</b>		
E-modulus (Erm) [MPa]	3041.6	1358.0
mb	0.785	0.493
s	0.0007302	0.0001722
a	0.5159	0.5382

<sup>1)</sup>Laboratory investigation <sup>2)</sup>Devoll HPP (2011) <sup>3)</sup>Appendix B <sup>4)</sup>Malaj et al. (2017)

### Post-peak behaviour

A method to determine post-peak behaviour of a rock material is suggested by Cai et al. (2007), based on the GSI system. Earlier studies have suggested that the residual geological strength index  $GSI_r$  of a rock mass post-peak is 36% of the original (Russo et al. (1998) in Cai et al. (2007)). However, this relationship tend to underestimate the residual values for poor rock masses and over estimate residual values for strong rock. Cai et al. (2007) argues that for very low rock masses the residual GSI should be equal to the peak GSI. By combining this statement with empirical data, Equation 7.1 <sup>5</sup> is used to determine the  $GSI_r$  for the generalised Hoek-Brown criterion. UCS and mi values should be kept constant when using this relation.

$$GSI_r = GSI \cdot e^{-0.0134 \cdot GSI} \quad (7.1)$$

### 7.4.2 In-situ stresses

Ideally, the in-situ stresses in an area would have been known. This is however an unknown parameter. Thus, a terrain analysis has been conducted to valuate a likely magnitude and orientation for the principal stresses at the location of the tunnel cross section.

In lieu of terrain data, the surface of the terrain model is created by extracting height data along a line perpendicular to the tunnel in google earth, shown in Figure 7.3. It was made by adjusting the geological map in Figure 4.2 to fit the map in the Google Earth Pro application and a path was added perpendicular to the headrace tunnel at the approximate location. An elevation profile was then extracted.

<sup>5</sup>For future confused readers of Cai et al. (2007), who cannot make sense of why their calculations are unreasonable, it is noted that the article has a tiny error in the equation (where -0.134 is used instead of -0.0134 in the exponentiation). A close look at the graph associated to the equation in Cai et al. (2007) reveals that Equation 7.1 as used in this thesis is correct.

Care was taken to ensure that relevant nearby terrain features that might influence the stress in the tunnel region were included. The depth of the model is set to approximately two thirds of the length. This is a somewhat arbitrary length, but should be sufficient to avoid boundary effects at the tunnel location. The final terrain as modelled in RS<sup>2</sup> is shown in Figure 7.4.

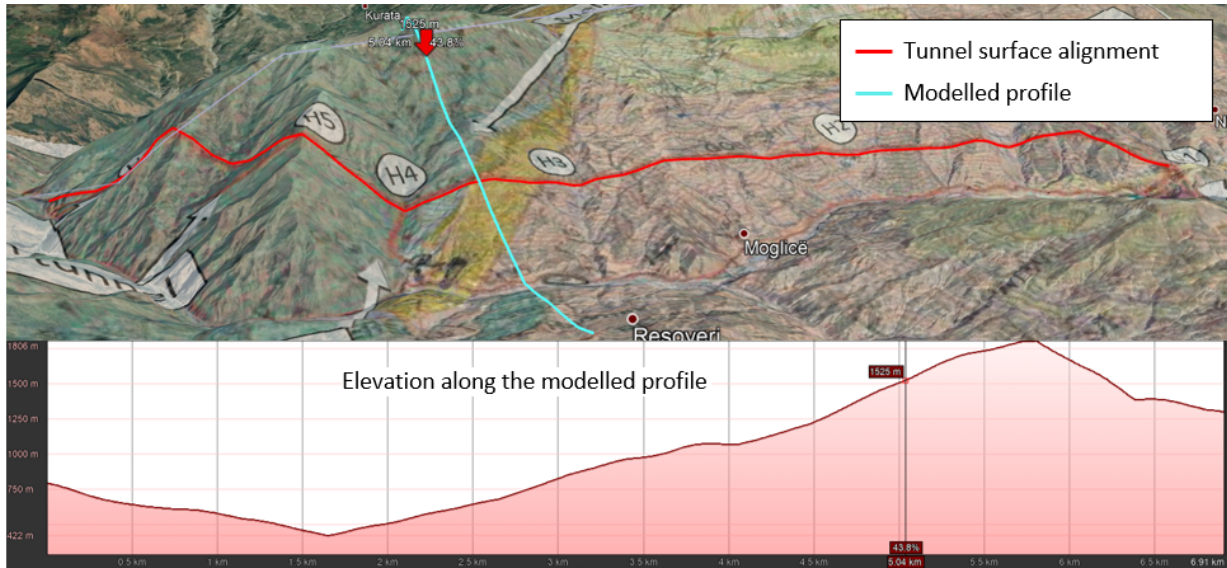


Figure 7.3. Extract from the terrain overlay created in Google Earth Pro, from which the elevation data for the terrain model was created. The location of the red arrow corresponds to the highlighted point in the elevation profile.

The field stress type chosen in this model is gravity, as the material weight is the dominant influence on the stress magnitude. The material used in the model is that of strong flysch described in Table 7.1, but set to elastic as only the resulting stresses from the valley geometry and material density is of interest. As the location is dominated by valleys and rather steep mountain sides of approximately 20°, topographic effects are likely to have a significant influence on the stress direction and magnitude (Nilsen and Palmström, 2000). Initially, a horizontal to vertical stress ratio of 2, which is common at such depths, was decided after conferring with supervisor Bjørn Nilsen. However, the resulting stresses caused the weak rock in the main analysis to yield before any excavation took place. For materials of low stiffness, it is reasonable to believe that the horizontal stresses are lower, due to a low E modulus for this material. The k value was thus reduced to 1.

In addition to topographic effects, the area might also be under influence of tectonic stress. However, such effects are neglected in this model as no decisive data indicating the magnitude was found either in literature or the world stress map.

Along the horizontal and vertical boundaries, rollers were placed to allow movement along the boundary. To avoid leakage out of the model, the corners are fixed using pins. The mesh type is set to graded and the element type to three noded triangles. The number of nodes on the external boundary was left at 120 as suggested by the software. To increase the density of nodes around the tunnel location, a line of six points were added from the tunnel location to

the surface. Along the longitudinal profile seen in Figure 4.2 the maximum overburden is 260 m. The tunnel is thus set to this depth.

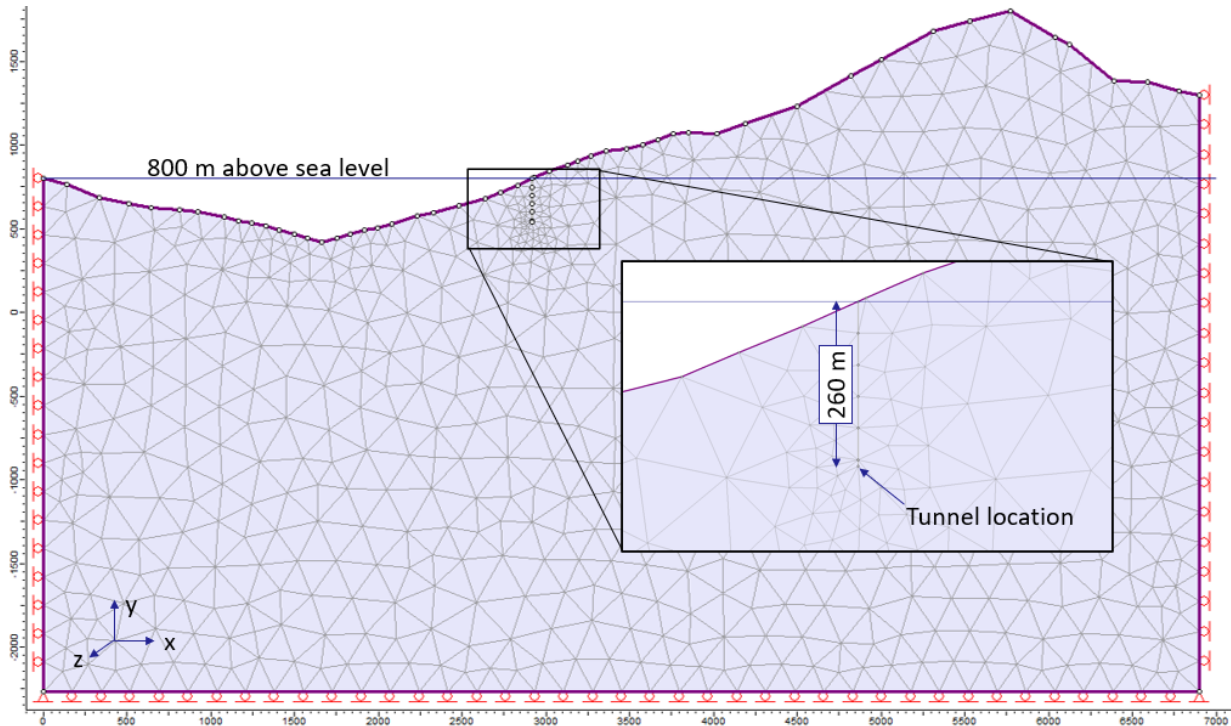


Figure 7.4. Cross section of the Moglice valley perpendicular to the headrace tunnel.

Figure 7.5 shows the magnitude of the principle stresses after running the model. The major principle stress,  $\sigma_1$  is 23.4 and angled  $10^\circ$  to the horizontal. Table 7.4 displays the two principle stresses in the plane as well as the out of plane stress,  $\sigma_z$ .

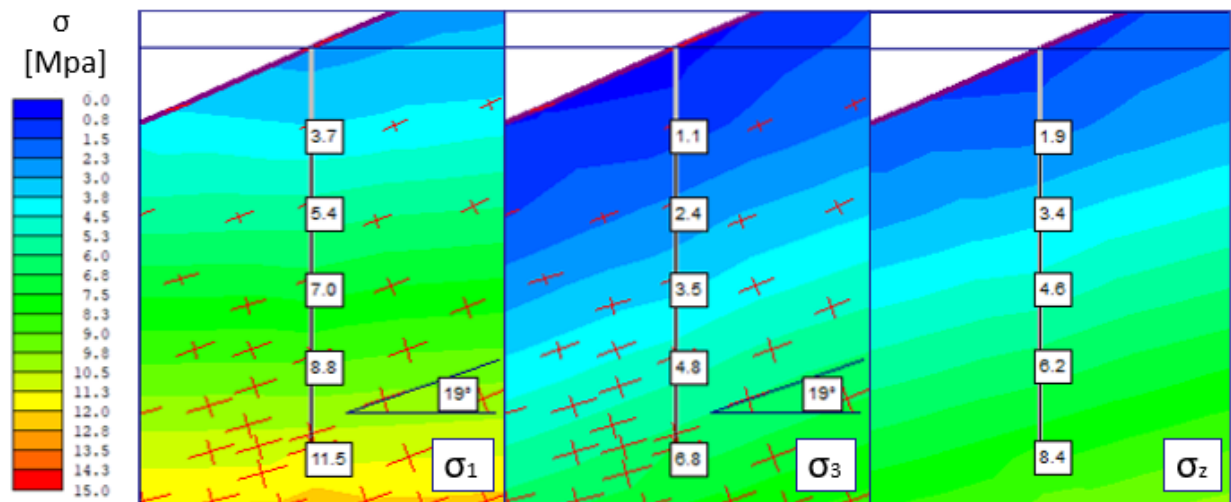


Figure 7.5. Resulting principal stresses,  $\sigma_1$  and  $\sigma_3$  and the out of plane stress  $\sigma_z$ .  $\sigma_1$  is angled  $19^\circ$  from the horizontal.

Table 7.4. Principal stresses

Parameter	Description	Stress [MPa]
$\sigma_1$	Major in plane stress	11.5
$\sigma_3$	Minor in plane stress	6.8
$\sigma_z$	Out of plane stress	8.4

### Model stresses

In RS<sup>2</sup>, a constant stress field must be chosen in order to apply principal stresses at an angle to the horizontal. The values from Table 7.4 were used. The stress block was angled accordingly at 19° degrees counterclockwise to the horizontal.

### 7.4.3 Support

Due to the variable rock mass quality along the tunnel profile, the tunnel support varies along the headrace tunnel. At the location of interest, the support consists of reinforced ribs of sprayed concrete (RRS), held in place by bolts as seen in Figure 7.6. The base layer of the support consists of a smoothing layer of fibre reinforced concrete. In the second layer, rebars of 20mm diameter in groups of 6 are installed in arches. These are fastened with fully bonded rock bolts and covered in plain sprayed concrete. The initial design placed the ribs at 1.5 m distance. A later update reduced the spacing to 0.75 m. Both cases are modelled to see the consequence of the design alteration. A separate case without support is also used in comparison to evaluate the support effect.

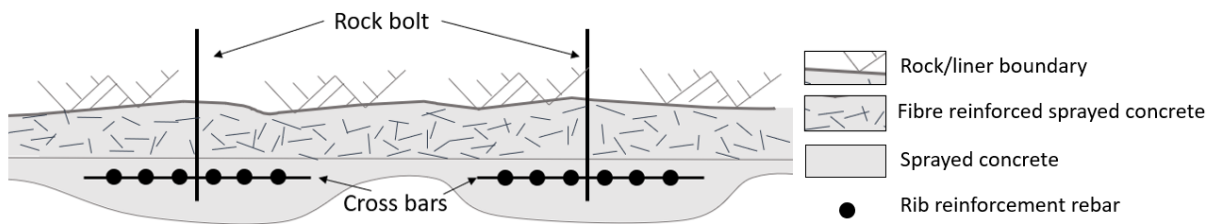


Figure 7.6. Principal sketch of two reinforced ribs of sprayed concrete.

### Liner

Sprayed concrete ribs are not standard support structures in the RS2 software. Because the ribs are 3D structures they cannot accurately be represented in the model. To combat this issue, the support of the ribs have been smoothed along the tunnel wall to a structure that can be modelled in 2D. In the two support cases the distance between the ribs are 1.5 m and 0.7 m. Each rib is composed of 6 rebars, which equals an average spacing of 0.25 m and 0.125 m in the model. The rebar tensile strength is left as suggested in the software.

Table 7.5. Actual and equivalent RRS support. Two cases distances between the ribs and subsequent equivalent rebar spacing are modelled.

Actual support		Equivalent support	
Rebar in RRS	6 x Ø20 mm	Rebar diameter	20 mm
RRS, c/c distance	1.5 (0.75) m	Rebar Spacing	0.25 (0.125) m
		Rebar tensile strength	400 MN

The material parameters of the sprayed concrete is based on the values obtained in the laboratory investigation and are displayed in Table 7.6. The UCS test provided the value for compressive strength as well as providing data to calculate the Youngs modulus and poisson ratio of the sprayed concrete. In the tested specimens of sprayed concrete there were visible specs of fibres, thus the tensile strength for the reinforced concrete is based on the brazil test results. For the plain sprayed concrete, the standard value for concrete is used. This is somewhat lower due to the lack of fibres. The thickness of the layers are as specified by Table 7.6.

Table 7.6. Material properties of fibre reinforce sprayed concrete ( $S_{fr}$ ) and plain sprayed concrete (S). Thickness for the improved support is shown in parenthesis.

Parameter	$S_{fr}$	S
Thickness [mm]	200	150 (200)
Youngs Modulus [MPa]	18 000	30 000
Poisson Ratio	0.18	0.15
Compressive strength [MPa]	40	40
Tensile strength [MPa]	4.9	3.0

Material parameters for the fibre reinforced sprayed concrete are from the laboratory investigation, while values suggested by the RS<sup>2</sup> software is used for the plain sprayed concrete.

The invert as supported on site is a complex structure with rebars of different size and spacing perpendicular and parallel to the profile, with drainage pipes and a layer of compacted gravel. For simplicity, the lining has been placed around the entire profile.

### Bolts

Two types of rock bolts are used in the design of the tunnel, 20 mm bolts along the crown and the wall and 25 mm bolts on the invert and corners. Along the wall and crown of the wall, rock bolts are incorporated in the RRS structures and are spaced accordingly. The distance between the bolts in the modelled profile is 1.0 and 1.5 m as indicated in Figure 7.7.

Table 7.7 displays the properties of the two types of bolts used in the Model. The type of bolt used is a fully grouted bolt. In the model, this type of bolt is not an option, thus the bolt type is set to end anchored. Early iterations of the models included fully bonded bolts Bolt capacity is set based on technical requirements for the support design, calling for a minimum yield strength of 500N/mm<sup>2</sup>, while the bolt modulus is as suggested by the RS<sup>2</sup> software.

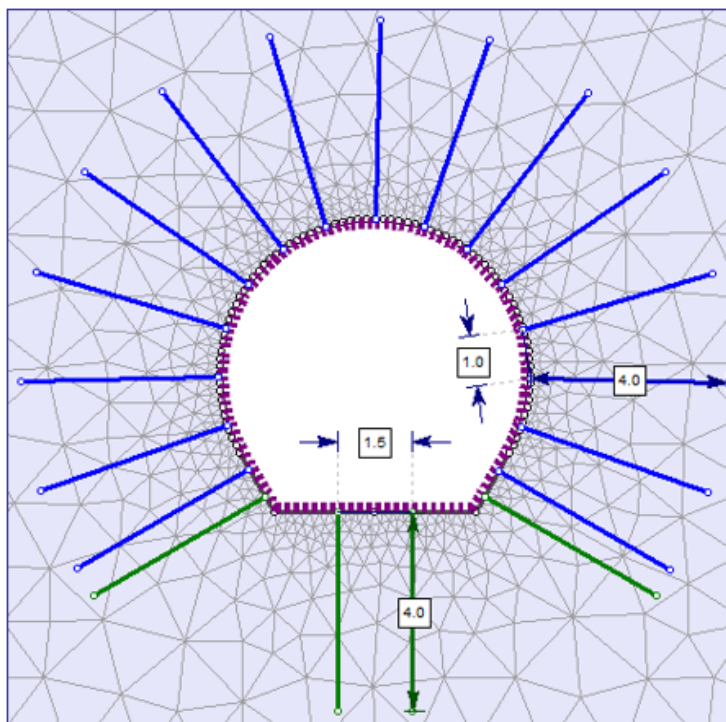


Figure 7.7. Rock support as modelled in RS2. The violet lining is a composite, containing the fibre reinforced sprayed concrete layer and the rebar reinforced layer. 20 mm bolts are coloured blue and 25 mm bolts are coloured green.

Table 7.7. Bolt parameters for rock bolts in the crown/wall and invert. Values for the improved support are in parenthesis.

Parameter	Crown and wall	Invert and corner
Bolt diameter [mm]	20	25
Bolt length [m]	4	4
Bolt modulus, E [MPa]	200 000	200 000
Tensile capacity [MN]	0.16	0.25
Residual tensile capacity [MN]	0.016	0.025
Out of place spacing [m]	1.5 (0.75)	1

#### 7.4.4 Load splitting

In the model the excavation and support installation is conducted in two separate stages. An unfortunate consequence of this, is that all of the deformation occurs before the support is installed. Alternatively, the support could be installed simultaneously as the excavation. In this case, the support carries a higher than realistic load. A common rule of thumb is that the radial displacement during excavation of a tunnel starts roughly half a tunnel diameter in front of the advancing face, and has reached a third of the final value at the face (Hoek, 2000). This effect is further illustrated in Figure 7.8.

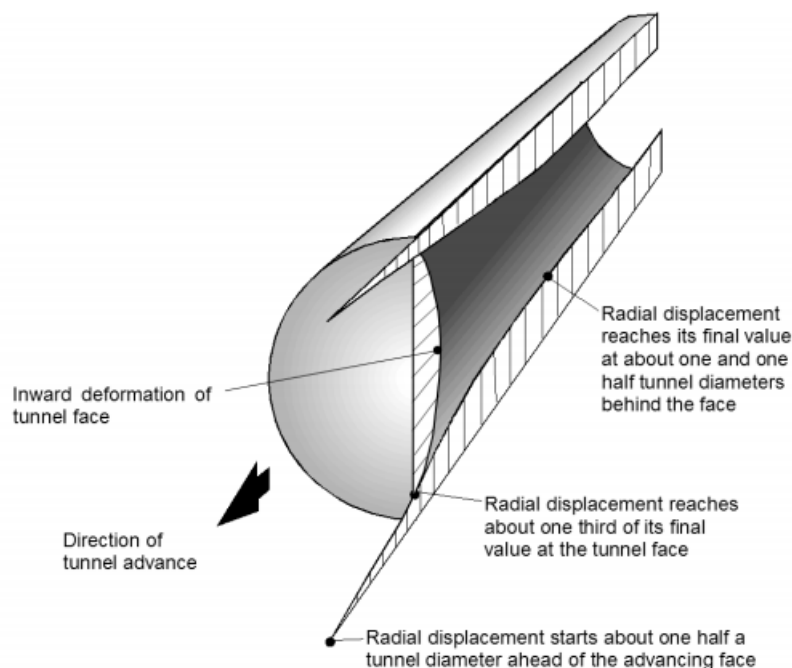


Figure 7.8. Pattern of deformation in the rock mass surrounding an advancing tunnel (Hoek, 2000)

As the main goal of this thesis is to evaluate the effect swelling has on the installed support, the load on the support must be realistic before the swelling pressure is added. A way to adapt to the deformation that happens in front of the tunnel face, is to implement load splitting in the model as seen in Table 7.8. With this function, the rock stresses can be increased over several stages. In the model there are four stages. The initial stage serves the purpose of confirming that the initial stresses are correct. Thus this stage must include the full load and has a split factor of 1. At the excavation stage the split factor is reduced by 0.7 to a total of 0.3. This way 30% of the deformation occurs at this stage. The split factor is increased by 0.7 in the support stage, bringing the principal stress back to the initial condition. No changes are made in the swelling stages.

Table 7.8. Load splitting factors during different stages of excavation.

Stage	Initial condition	Excavation	Support	Swelling pressure
Stress behaviour	Initialise	add	add	add
Split factor	1	-0.7	0.7	0
Percentage of total stress	100	30	100	100

### 7.4.5 Swelling pressure

In the model it is assumed that the swelling pressure materialises when the tunnel is filled with water. Hence the pressure is added in a separate stage after the tunnel support is added. The pressure from swelling is simulated by distributing a uniform load radially from the rock mass to the tunnel lining. To model different possible levels of swelling, the load is increased over six stages.

During the preliminary project, the swelling pressure of the flysch rock at Moglice HPP was tested in the laboratory, and found to be  $0.18 \pm 0.006$  MPa, with a maximum of 0.25 MPa and minimum of 0.07 MPa. However, it is not reasonable to directly use these values as the swelling pressure in the model, as the swelling pressure test was performed on crushed rock, instead of intact specimens.

In the case of the Chingaza project discussed in Chapter 2, the swelling pressure measured on a disk was 10 and 75 times greater than that of the equivalent powder, indicating that in-situ rock values may be significantly higher than powdered laboratory values Brattli and Broch (1995). However Selen (2017) found great variation in the relationship between powder and intact samples, where the powdered specimens showed both higher and lower levels of swelling than intact ones. Statens vegvesen (2020) states that only 30% of the swelling pressure measured in the laboratory affects the tunnel support. However, this recommendation is based on swelling soil specimens which may act different than swelling rock.

The uncertainty in relating laboratory values to the swelling pressure exerted on the tunnel profile, calls for a sensitivity analysis. Using the recommendation of Statens vegvesen (2020) the minimum value is set to 0.06 MPa, 30% of the mean value. Determining a likely maximum is difficult. The powder-disk comparison in Brattli and Broch (1995) is not necessarily analogous to a comparison between swelling pressures experienced in powder and rock. Still, it is an indication that higher swelling pressures than that found in the lab may be possible. A maximum of 5 MPa, 20 times the maximum value found in the lab is thus chosen to represent an extreme level of swelling. Still, a lower level is more probable, so uneven intervals are chosen. An overview of the tested swelling pressures is displayed in Table 7.9.

Table 7.9. Values for swelling pressure used in the sensitivity analysis.

<b>Case nr.</b>	<b>1</b>	<b>2</b>	<b>3</b>	<b>4</b>	<b>5</b>	<b>6</b>
Swelling pressure [MPa]	0.06	0.25	0.5	1.5	3.0	5.0





# Chapter 8

## Results from the numerical model

A total of 6 simulations with 9 stages each have been performed in this thesis. For both the strong and weak flysch two cases of support and a version without support have been created. Out of the simulations, the case with the final support and weak flysch is the one that is most true to life. For all comparisons the weak flysch with the final support is set as the standard other cases are evaluated against.

There are multiple aspects of the results that are important, but due to the sheer amount of data, only the most relevant findings can be presented. The most critical aspect of the analysis is the effect of swelling on the support and deformations. The difference in how swelling and deformations materialises in weak and strong rock is also of importance.

First the resulting stresses and effect on the general rock mass after excavation is evaluated. Secondly the general deformation in the cases measured. At last the effect of swelling on the support and the rock mass is assessed.

### 8.1 General stresses and deformations prior to swelling

#### 8.1.1 Stresses and yielded zones

When a rock is excavated, stresses are redistributed around the profile. This leads to a concentrated higher stress at points around the profile that is parallel to the major principal stress which attenuates back to the in-situ stresses further away from the excavation as described by the Kirsch solutions. Similarly, points at the profile parallel to the minor principle stress may display a stress lower than the initial minor stress Li (2017).

In Figure 8.1 the redistributed stresses for the two rock types with the final rock support is visualised. There was no significant difference in the stresses or yielded zone when comparing the original, final support or the unsupported case, hence a comparison is not presented.

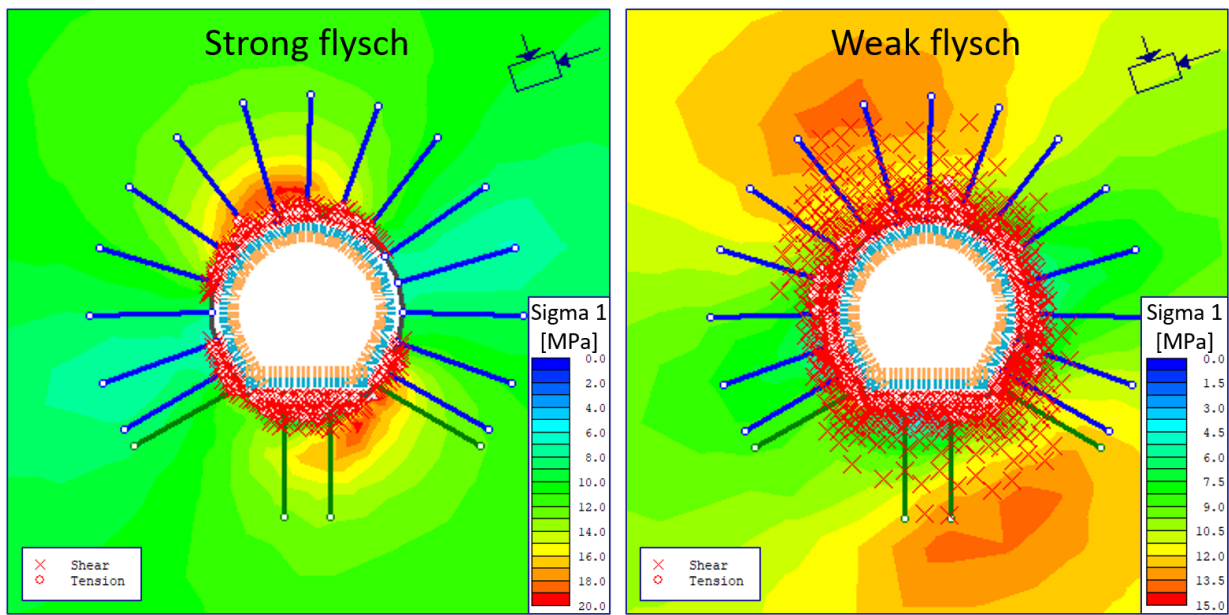


Figure 8.1. Major stress  $\sigma_1$  after excavation for the strong and weak flysch with the final support. Failure around the opening is due to shear or tension indicated by crosses or circles. Note that the legend for the figures are different to make the stress concentration in the weak flysch visible.

The differences in the rock mass strength is evident in that the weak rock yields at a greater radius than for the strong flysch as seen in Figure 8.3. In general the weak flysch has a much greater yielded zone than the strong version. For the strong flysch, the yielded zone has a maximum thickness of 1.8 m, while the weak flysch has a yielded zone of 5 m at the sole the tunnel. For both cases the yielded zone above the tunnel crown is 1 m shorter.

Due to the plastic quality of the rock, it still carries some load after failure. An effect of the yielded zone is that the stresses redistribute at a greater distance from the excavation in the weak flysch. Due to the increased distance from the excavation the resulting stresses are also lower.

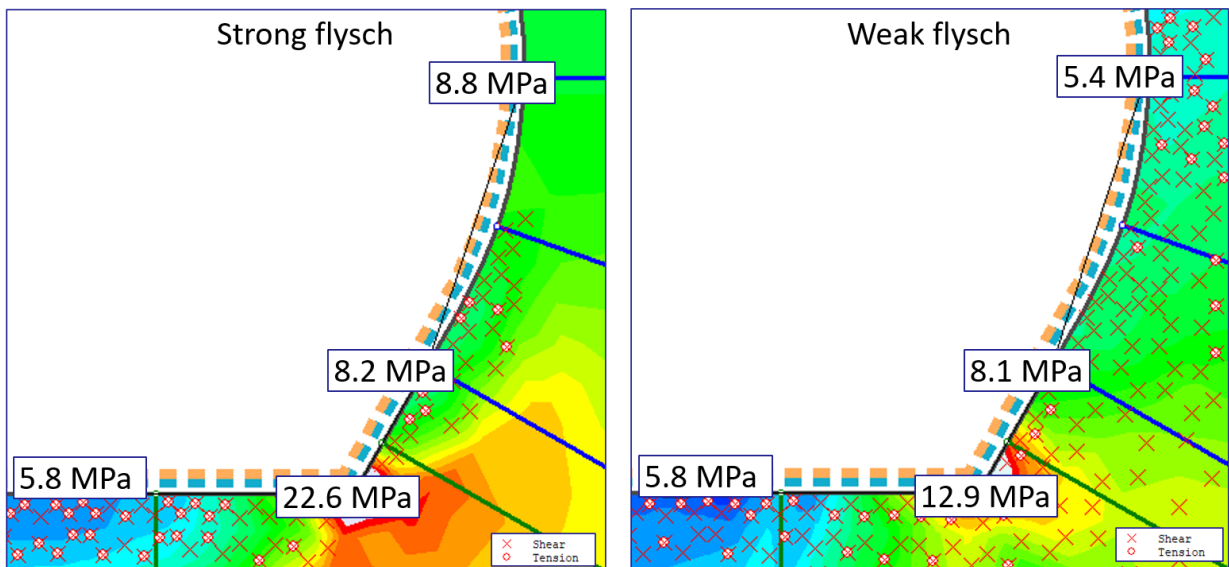


Figure 8.2. Close up of the lower right corner.

Because the stress field is at an angle to the horizontal, a concentration builds up at the lower right corner. A close up is provided in Figure 8.2. The increased distance to the area of concentrated stress causes this effect to be reduced in the weak flysch rock.

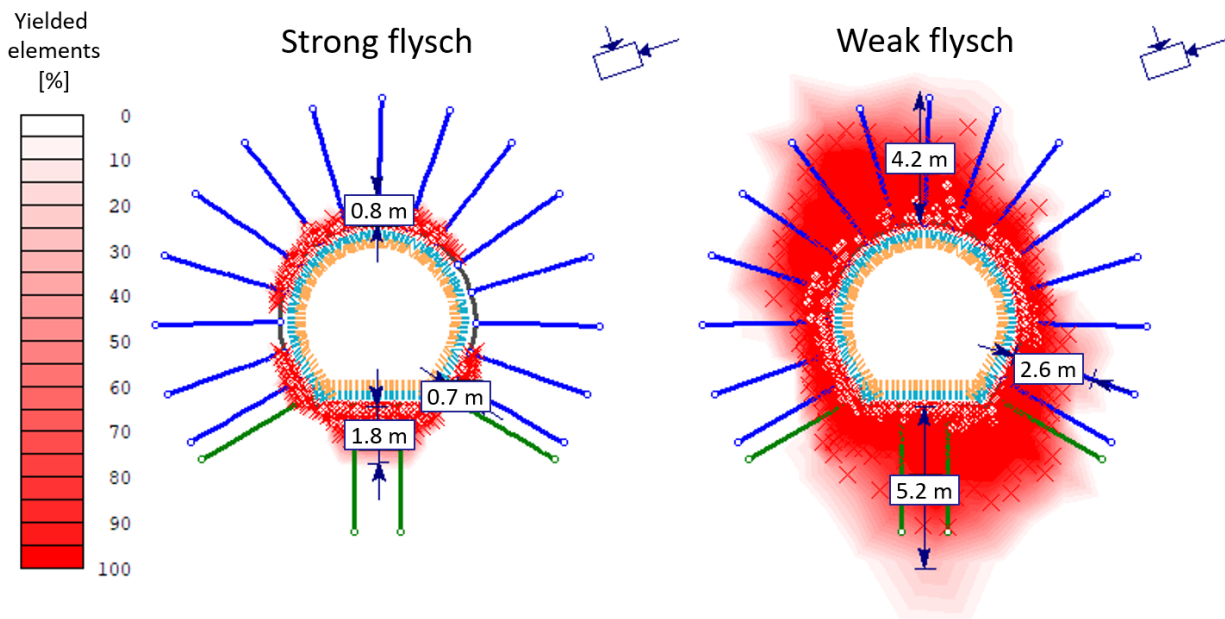


Figure 8.3. Yielded elements around the excavation for the strong and weak flysch with the final support. The dimensions shows the distance from the tunnel that is up to 50% yielded.

### 8.1.2 Deformation reduction due to the additional support

When comparing the difference in the deformation of the tunnel profile between the two support cases, no significant differences was found, and the difference was generally less than 1 mm. The deformation of the cases with the final support are thus compared to the unsupported to see the effect of the support.

At the excavation stage of the unsupported and the supported cases naturally have the same level of deformations as the models of the same rock type are identical at this stage. This stage is affected by 30% of the final stresses in order to mimic the deformations that has happened at the face of the excavation.

In  $RS^2$  the total displacement at the nodes and the displacement vector can be visualised as a contour plot. However, creating comparable plots was not possible due to the vast differences in displacements. Figure 8.4 shows a contour plot of the total displacements and displacement vectors in the weak flysch rock, with the final support. The general contour pattern and vector directions are comparable for the other cases, while the magnitude are from 1mm to 10 cm. Due to the difficulty of making visual representations of the different cases, deformations at the indicated locations are plotted in Figure 8.5 and 8.6.

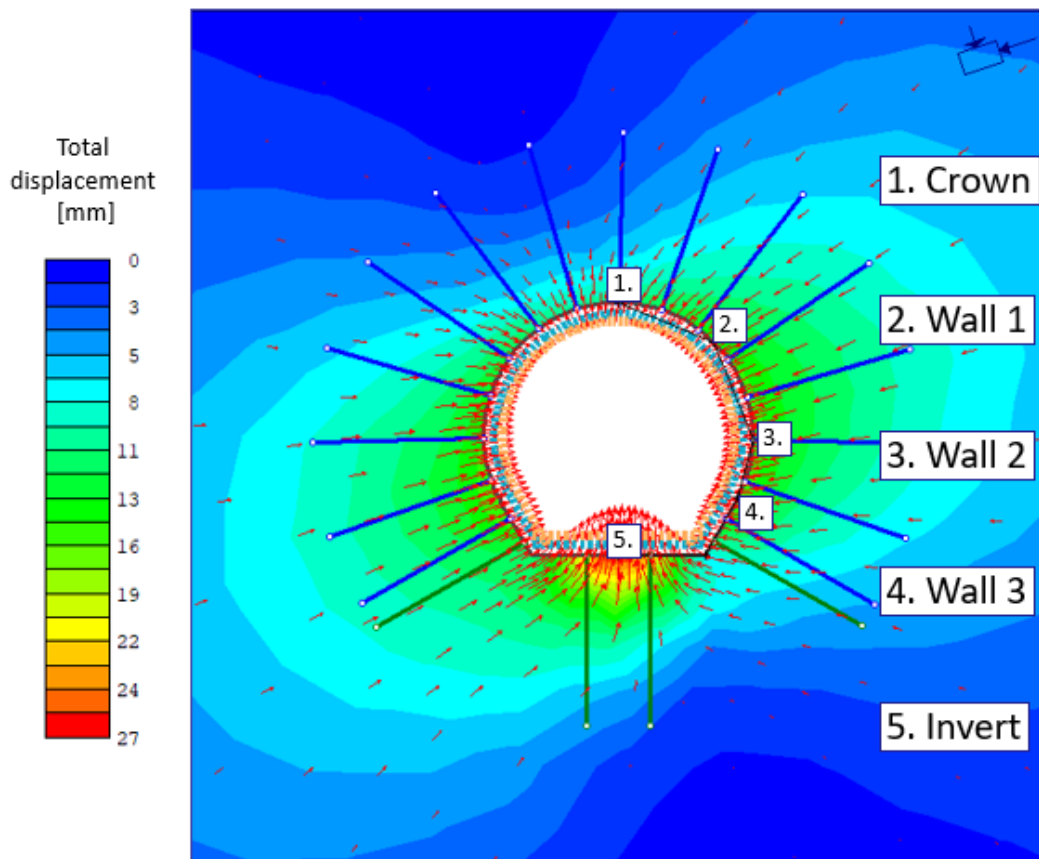


Figure 8.4. Displacements contour plot for the support stage in weak flysch with the final support.

For both flysch qualities, the unsupported and supported cases are evaluated against each other. For each case the overall displacement from the excavation and liner stage is displayed alongside the experienced displacement. The experienced displacement is the deformations that happens after excavation, that in theory could be measured in the tunnel. The difference between the supported and unsupported case shows the effect the support has on the deformations.

The highest level of deformations for the unsupported cases are found in the crown and invert of the tunnel. Comparing the unsupported case the crown displayed the most drastic reduction and the lowest resulting deformation in the supported cases. A likely reason is that the bolts and lining reinforce and support the rock, creating an arc effect, which better withstands the inward movement of rock. Due to the flat invert construction, the effect is not equally strong at the invert. This could be due to shorter bolt spacing or the flat character of the geometry at this location.

The effect of the support is most evident in the weak flysch. At the crown of the headrace tunnel, the experienced displacement is reduced from 87 to 2 mm, a total of 66 mm. The lowest reduction was found at location wall 2, where the reduction was 55 mm. The mean reduction at the selected points is 68 mm. In Section 4.2.3 two convergence readings of 7.6 and 44 mm are presented. These measurements are taken at a height comparable to Wall 2. where the inward displacement is 7 mm. The equivalent convergence measurement considering the

displacement on the opposing side would then be 14 mm, which is in the range of the actual measurements.

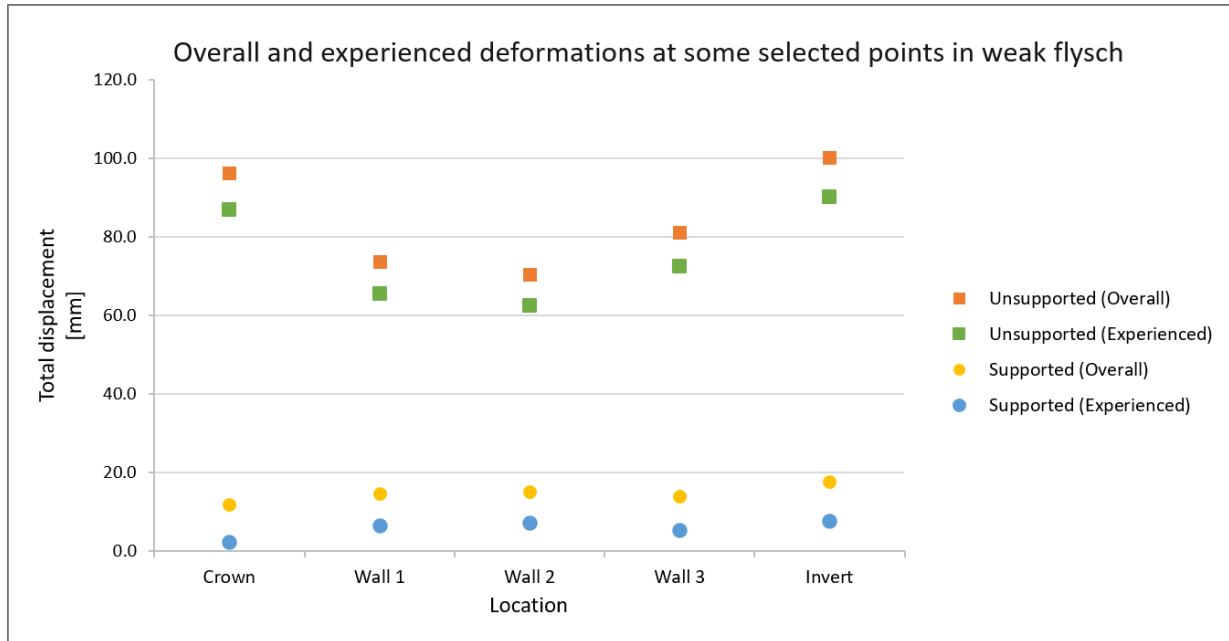


Figure 8.5. Displacements at selected points in weak flysch.

It can be argued that both the material parameters, and the support regime for the strong flysch is unrealistic. A tunnel constructed through flysch rock mass of this strength and low stresses is likely to be constructed with a milder support regime. Deformations in the rock mass are low compared to the weak flysch, even in the unsupported case. Even the unsupported overall displacements are all less than 6 mm. Hence, the effect of the support is not as extreme. In this case the deformation at Wall 2 is 2 mm which would give a convergence of 4 mm.

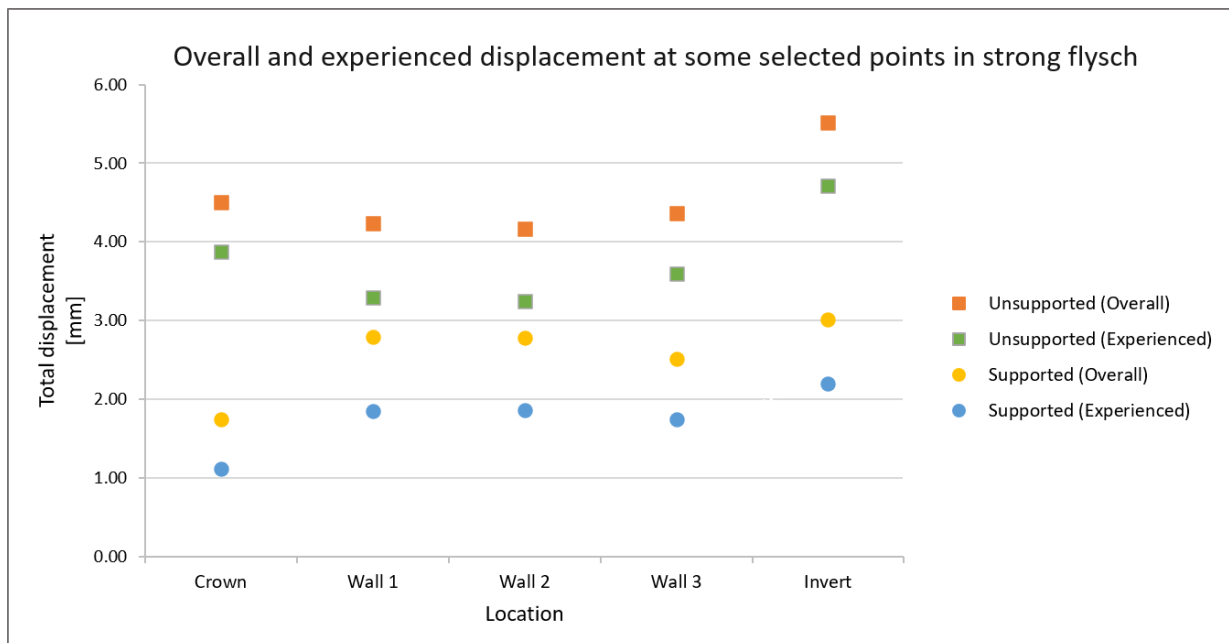


Figure 8.6. Displacements at selected points in strong flysch.

### 8.1.3 Yielded bolts

The invert experiences the highest stress concentrations and the highest deformations. The support in this region is a simplification of the actual support and is thus applying a lower support pressure. An unfortunate effect is illustrated in Figure 8.7. For both the original and final support in weak rock, these bolts yield due to tension, possibly due to the high deformations. Yielding does not occur at the support stage for strong flysch where the deformations are one order of magnitude lower, indicating that the stress conditions are not the cause for the bolt yielding.

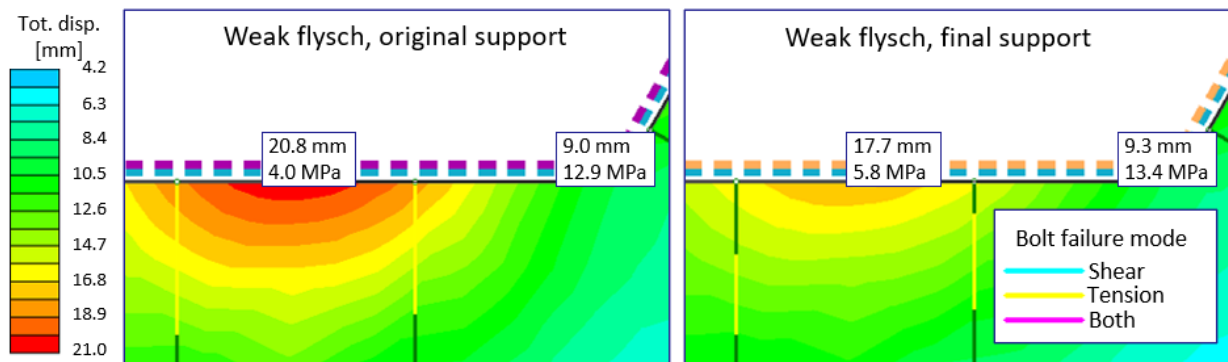


Figure 8.7. Yielded invert bolts at the support stage for the original and final support in weak rock. The major stress and deformations at the centre of the invert and the right corner is indicated at the respective locations.

## 8.2 Swelling

Swelling was in this analysis implemented as a uniform load applied directly onto the sprayed concrete lining which is increased over the course of 6 stages as indicated in Figure 7.2. The lowest swelling pressure added is 0.06 MPa, increasing with unequal intervals to 5 MPa. In the following figures, the load is not displayed, because it covers stress and deformation plots. Instead, the pressure is indicated on the respective figures.

### 8.2.1 Deformations and yielded support in weak rock

Figure 8.8 shows how the deformations increase with the swelling pressure when the new support is installed. All lining elements remain intact throughout the swelling stages, however, the invert bolts continue to yield further as the swelling pressure increases. At the final stage, where the swelling pressure is 5 MPa, the remaining bolts also yield at the elements closest to the tunnel. The main difference that can be seen between the two support versions, is that four of the wall bolts, two on each side display yielding in a few elements at 2.0 MPa.

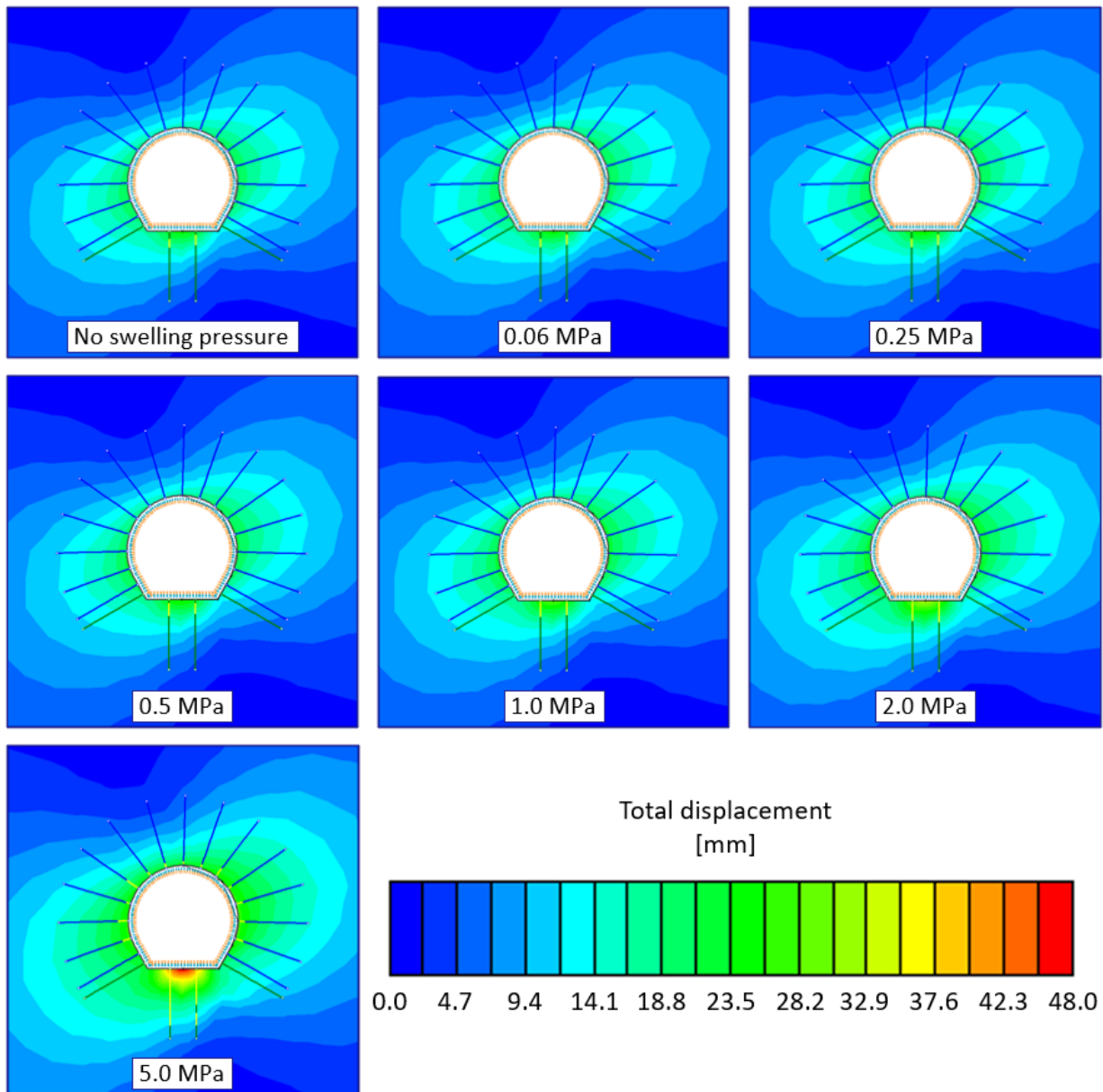


Figure 8.8. Displacement due to swelling for flysch rock. The displacement is the total displacement, including those present at the face of the excavation. Yielding bolt elements are indicated in yellow.

The experienced deformations at the previously defined points have been plotted for the support stage to the final swelling stage in Figure 8.9. To visualise the wall and crown deformations, the invert had to be plotted in a separate sub plot as the deformations at this point was notably larger. Lines of the same colour describe deformations at the same points, with a solid line for the initial support and a dotted line for the final. For all points, the deformations are lower, when a higher support pressure is installed.

The magnitude of the reduction is however variable. At all of the investigated locations, the reduction in the experienced displacement due to the increased support  $\Delta D$  is larger for higher levels of swelling. However,  $\Delta D$  is generally lower than 0.5 mm for swelling pressures of 2 MPa and below. At the invert,  $\Delta D$  is 0.6 mm at 0.25 MPa, increasing to 14.1 mm when the swelling pressure is increased to 5 MPa. For the remaining locations a  $\Delta D$  ranging from 1.0 to



1.4 mm is observed for the highest swelling pressure.

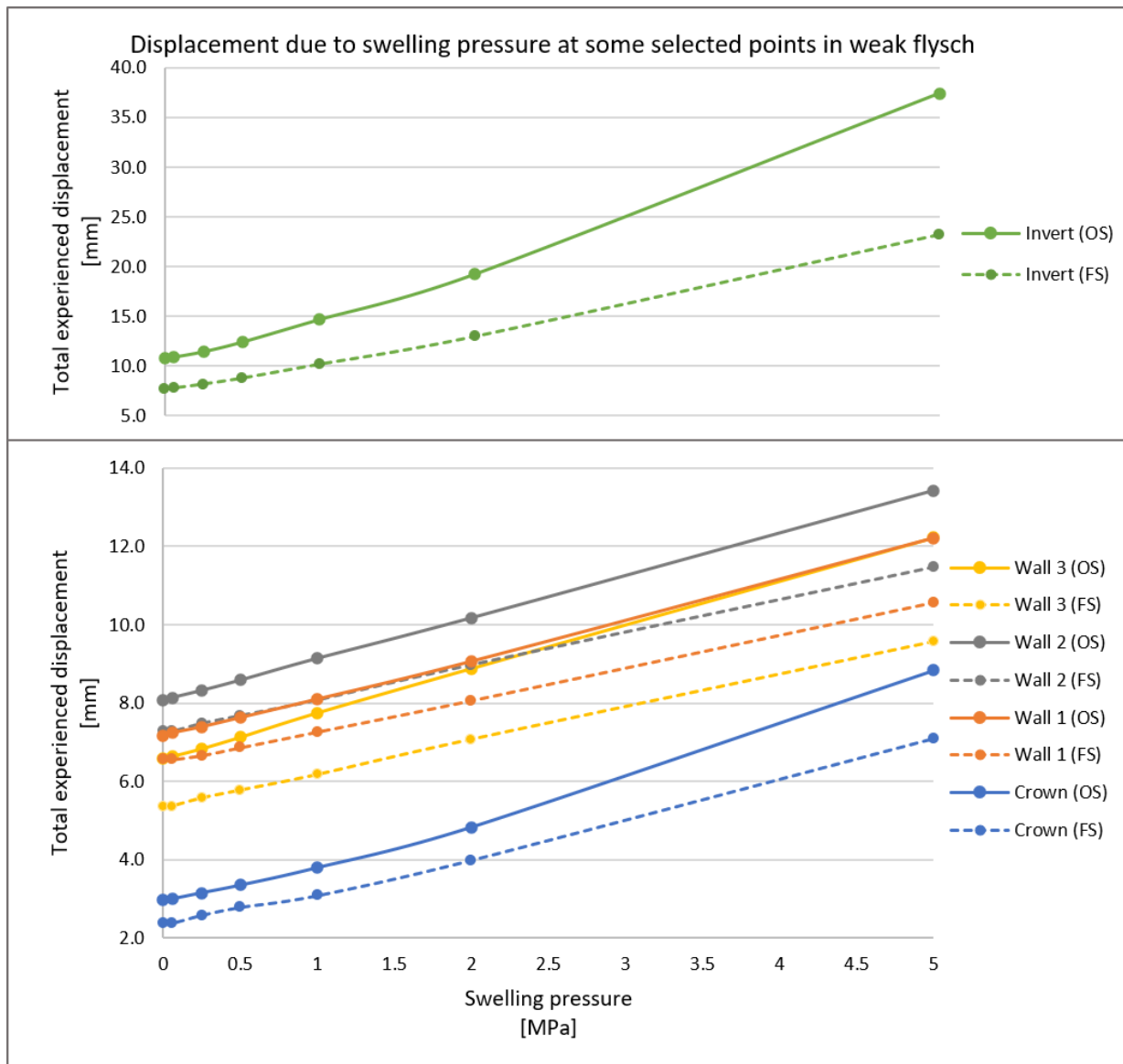


Figure 8.9. Displacements due to swelling for some selected points in weak flysch. The displacements are plotted for both the original support (OS) and the final support (FS).

### 8.2.2 Deformations and yielded support in strong flysch

Deformations in strong flysch is generally lower than in the weak flysch, thus the total experienced displacements are also lower in this rock quality which can be seen in Figure 8.10. Similarly to the weak flysch,  $\Delta D$  is below 0.5 mm for the crown and wall at swelling pressures lower than 2MPa. Only at location Wall 2 and 3 is  $\Delta D$  higher than 0.5 mm at 2MPa, 0.8 mm and 1.0 mm respectively. At a swelling pressure of 5 MPa  $\Delta D$  ranges from 1.2 mm to 1.4 mm for the Crown, Wall 1 and 3. Wall 2 has a  $\Delta D$  of 1.9mm at this pressure. Again the invert has both the highest deformations overall, but also the highest  $\Delta D$  between the support versions at 16.7 mm.

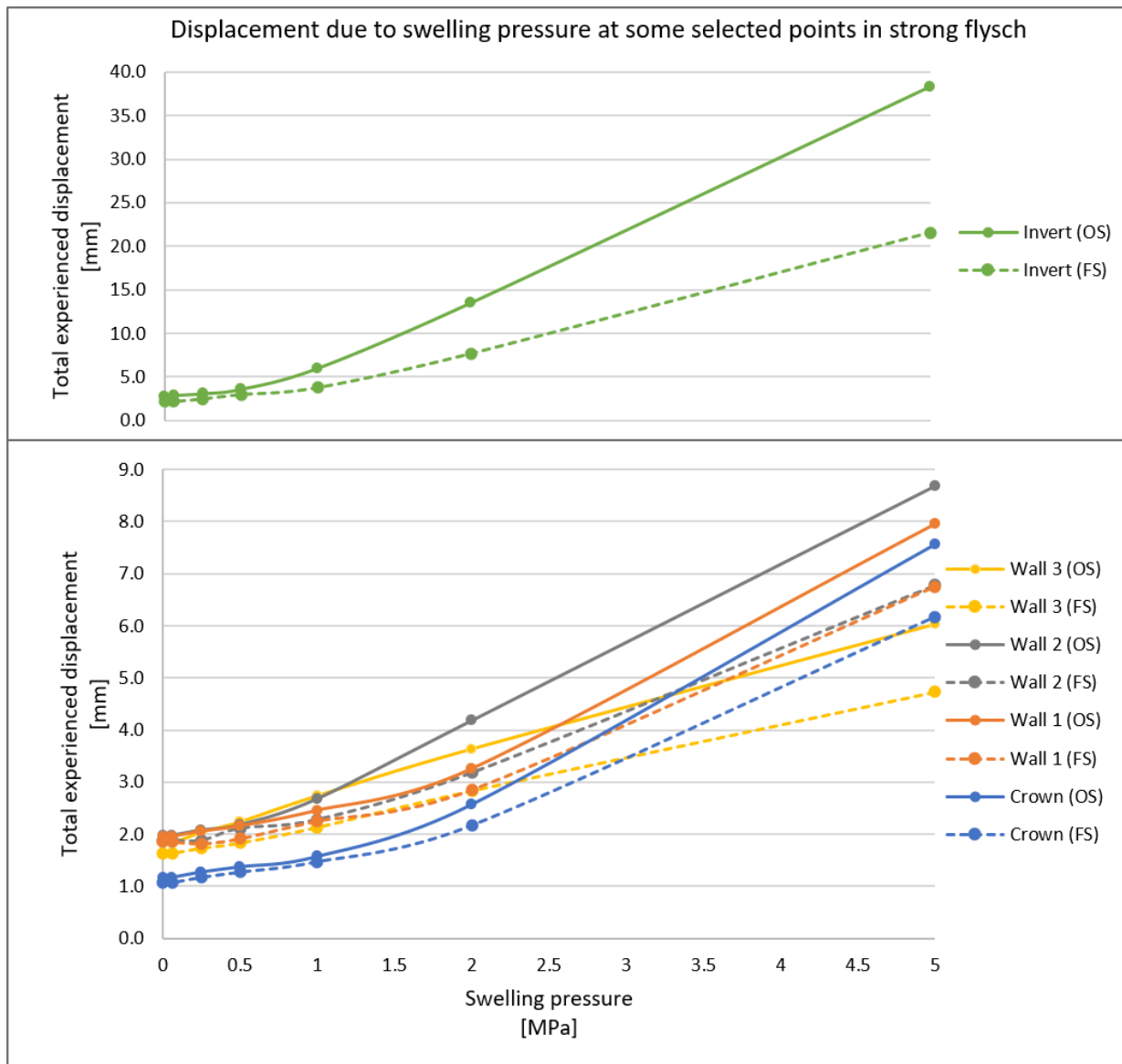


Figure 8.10. Displacements due to swelling for some selected points in strong flysch. The displacements are plotted for both the original support (OS) and the final support (FS).

As with the weak flysch, the liner elements remain intact for all levels of swelling pressure for both support designs. For the original support, all bolts remain intact up to 1 MPa, where the invert bolts start to yield. At 2 MPa six wall bolts show a few yielded elements before all wall and crown bolts yield when the swelling pressure reaches 5 MPa. The final support improves the situation. The invert bolts start to yield at 2 MPa, before all but two wall bolts start yielding at 5 MPa. Figure 8.11 shows the situation with a swelling pressure of 5 MPa. The resulting yielded zone is reduced, as is the number of yielded bolt elements. The extent of the yielded zone and yielding of invert bolts may also explain why the deformations at the invert in strong rock is equal to that in weak rock.

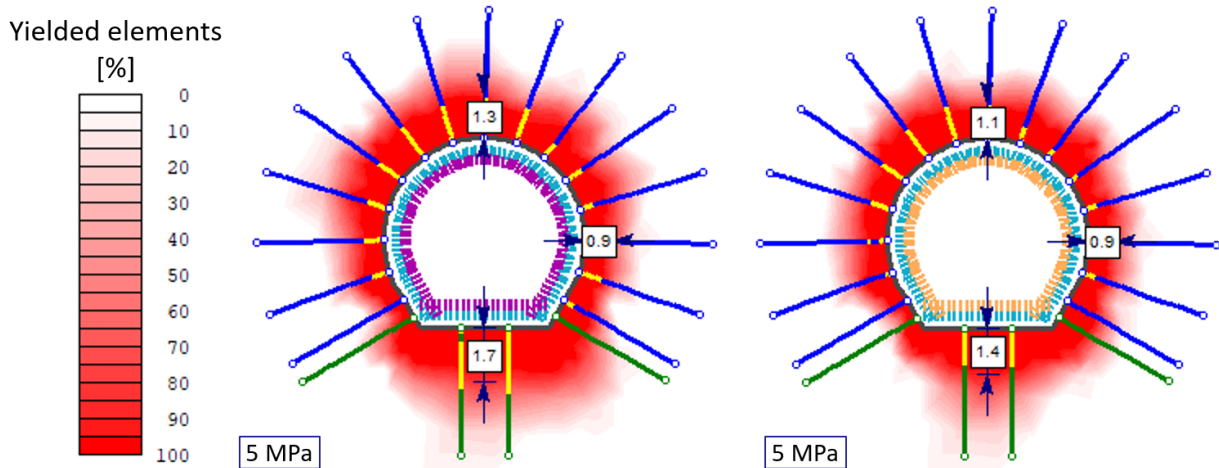


Figure 8.11. Yielded zone around the excavation in strong flysch rock for the original (left) and final (right) support. Dimension arrows display the thickness of the 100%yielded zone in meters. The lining is subjected to a swelling pressure of 5 MPa.

### 8.2.3 Comments on the effect of swelling in weak and strong flysch

One of the major differences between the effect on swelling in weak and strong rock lies in the yielded zone around the excavation. For the weak rock, the yielded zone is thicker before the swelling pressure is added, while more additional yielding of rock occurs when swelling pressure is added in strong rock. A possible reason could be that the intact rock is further away in the weak flysch and is thus not as affected.

The reason may also be artificial due to the manner the swelling pressure is applied. In the model, it is directly applied to the lining, meaning the rock is not influenced. The effect is apparent in Figure 8.12. For both cases the major stress in the rock is reduced significantly from what was seen in Figure 8.1. In the strong rock, an area experiencing a stress situation lower than 2 MPa extends to the same degree as the fully yielded region in Figure 8.11.

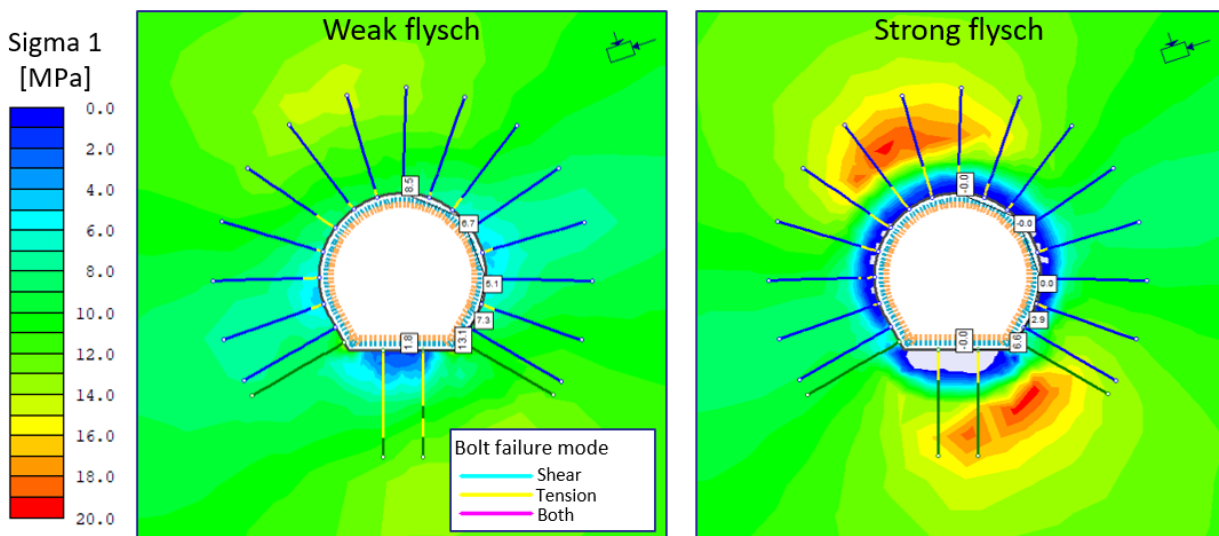


Figure 8.12. Major principal stress distribution around the excavation supported by the final design. The swelling pressure on the lining is 5 MPa. Grey areas indicate a major stress lower than 0 MPa.

A sharp gradient is visible in the strong rock mass, indicating that the rock mass is self supporting beyond the yielded region. In the weak rock, the yielded region extends further. Because the rock mass is not self supporting the yielded rock is forced towards the lining. Thus, the stresses remain compressive around the profile in the weak rock.

The yielding of the wall and crown bolts in the strong rock also seems to be attributed to the tensile stresses induced by the swelling pressure. This suspicion is supported by the fact that the only two bolts remaining intact are the ones with compressive stresses. A matching, although reduced effect, is seen in the weak rock mass. The wall and crown bolts are generally yielding to a larger extent when the rock stress is lower, but to a lesser degree. On the other hand, the invert bolts in the weak rock is severely yielded. As previously discussed, the most likely reason for this is the high deformations in the region.



# Chapter 9

## Discussion

In this thesis and the specialisation project, aspects of flysch rock and the stability of such have been evaluated by considerable laboratory testing of the mineralogical, water affected properties and mechanical characteristics. The results of these are important in the context of the long term stability of the headrace tunnel constructed in Moglice, Albania. The effect of swelling and rock stresses have been evaluated by use of numerical modelling. To assess the effect swelling and slaking has on the long term stability of the headrace tunnel, the uncertainties in both the laboratory investigations and the numerical analysis must be discussed to reach a conclusion on the validity of the results in order to assess the long term implications of swelling.

### 9.1 General rock characteristics

The heterogeneity of flysch rock has been stated repeatedly in this thesis and is observable from the conducted laboratory investigation. Great variations are found in the results from the various tests.

From the specialisation project all tested specimens displayed some level of swelling potential, with an average of  $0.18 \pm 0.06$  MPa. The slake durability of the specimens varied greatly from 43.3 to 97% and is related to the amount of weak rock constituents such as amorph material and sheet silicates. A weakness to the study on the swelling and slaking properties of flysch rock is the relatively few specimens tested. It is possible that the range of both swelling and slaking values may be greater. Slaking tests must be conducted on specimens of a given size, which is larger than the crumbled rock pieces found in some cores. Furthermore, as rock cores were selected for the purpose of slake durability testing, there may be rocks of higher swelling potential due to higher clay content.

Investigating the material properties of flysch rock is a challenge. The weak layers are often of too poor quality to obtain valid results. Cores used in this thesis were extracted during the

installation of flat jacks, causing most of the cores to have a crescent shape, which further reduced the test material. Tests such as the UCS test and Brazil test require specimens of a defined geometry which could not be satisfied by the clay flysch.

Preparing cores for these tests often require water for cutting, which may damage rocks that are susceptible to slaking. Long term storage at laboratory conditions may also damage the structural integrity of the rock and cause fissures due to drying that may reduce the rock strength. During the laboratory investigation the cores were opened and prepared over the course of a few weeks, which may have had a negative effect on the rock strength. Despite these considerations, the conglomerate and sandstone flysch could be classified as having high strength with an average UCS of  $137 \pm 22.0$  MPa. Point load testing of the clay flysch indicated very low strength at  $8 \pm 3$  MPa. Other rock mass parameters for the clay flysch had to be obtained from external sources due to lack of intact material, which adds a level of uncertainty to the values used in the numerical analysis.

## 9.2 Numerical analysis

The method used to analyse the effect of swelling has been that of numerical modelling in RS<sup>2</sup>. This is a two-dimensional tool utilising the finite element method. By use of procedure visualised in Figure 6.2 the analysis have been conducted in a structured manner.

### 9.2.1 Input values

Garbage in, garbage out, is a known term in numerical analysis. The quality of the input data hence determines the quality of the output. The following considerations have to be made regarding the construction of the model

#### **Rock mass values**

In this analysis the material data has been based on the laboratory investigations, technical documents provided by Statkraft and external sources for additional rock properties. Empirical relations discussed in Chapter 3 have been used to correct the material values for the analysis.

Two rock masses have been modelled, to evaluate if the effect of swelling is depended on the rock mass. A strong flysch based on the obtainable data from the laboratory investigation and a weak flysch modelled to best describe the local conditions where the rock mass is a weighted average of strong and weak layers.

A character of the rock mass which was not considered in this analysis was the effect of jointing and layering. An interesting task would have been to evaluate the effect of swelling when

layers of weak and strong rock is examined. To perform this type of analysis the joint characteristics would have to be evaluated as well as the rock mechanical properties.

A feature that could have been added is a radius around the tunnel affected by blast damage, by giving the rock mass a disturbance factor according to appendix B3. Due to the extensive yielded zone in the weak rock, the zone would be unlikely to cause a significant difference.

### **Rock support**

The support, geometry and location has been interpreted from technical documents supplied by Statkraft. Simplification has been made where data has been missing, uncertain or impossible to model in 2D. The main caveat is the 2D representation of a 3D RRS support and geometry. Conducting a 3D analysis would be beneficial to better understand the effect swelling has on RRS structures. An additional benefit of conducting a 3D analysis would be that the deformations affecting the support could be more accurate than what was attempted using the load split function.

The invert was especially difficult to model correctly, and the same lining has been applied as the one constructed for the wall and crown. High levels of deformations and bolt yielding at installation in the weak flysch suggests that the modelled invert support was an insufficient approximation.

### **Swelling**

Swelling has in this analysis been applied as an uniform load around the profile. This had an unintended consequence regarding the stress distribution around the profile, and subsequent bolt yielding. For the strong rock, the rock mass yielded by tension at a distance of up to 1.4 m from the tunnel. Because the rock mass was already yielded in the weak rock, the effect was not as strong. No levels of swelling caused any damage on the lining for either support case.

An attempt was made to rather increase the stress block equivalently to the swelling pressure, but naturally, the stress was redistributed around the profile, rather than acting directly on the lining. A better solution would be to apply a stress that acts perpendicular onto the lining, which attenuates to zero at some distance away from the tunnel. This way the tension in the rock material and bolts may have been solved. However, this was not a possibility in the RS<sup>2</sup> software.

In the model it is assumed that swelling occurs after the tunnel is filled with water. Because the headrace tunnel is below the water table it is reasonable to believe that swelling may also occur at an earlier stage.



## 9.2.2 Iterations and changes to the model

Throughout the modelling process, iterations and changes have been made to approximate available data and in discussions with supervisor Bjørn Nilsen. Initially the model stresses were obtained from a terrain analysis where the ratio of horizontal to vertical stresses were set to 2. However, this resulted in the weak material yielding before any excavation could occur. After discussing the capability of weak rock to transfer stresses, it was decided to reduce the ratio to 1. It could be argued that a rock mass with the qualities of strong flysch would have higher horizontal stresses, but it was decided to keep the lower stresses for this rock mass as well to keep the results comparable.

The weak rock mass was modelled to be a representation of the actual rock mass. Changes to the input parameters and stresses were thus made to approximate a reasonable deformation in line with the measured convergence readings of 7.6 and 46 mm presented in Chapter 4. Early editions displayed low deformations when the dry laboratory values was used for the rock mass parameters. Correcting for the fact that the rock is saturated in-situ resulted in a reasonable convergence of 14 mm.

## 9.3 Long term stability

Deformations due to stress and swelling are the main indicators of long term stability investigated in this thesis. Effective support is essential in maintaining structural integrity of the headrace tunnel, especially since the weak flysch is too weak to be self supporting. Swelling may also cause further deformations which in combination with slaking has the potential to cause collapse if the support is insufficient.

### 9.3.1 Deformations at the excavation and support stage

In both the weak and strong rock, the reduction in deformations of the profile compared to the unsupported case is clear from Figures 8.6 and 8.5. The strong flysch is to an extent self supporting. In this case the support reduces the displacements by 50%, but as they are low even in the unsupported strong flysch, the difference is on average 2 mm.

The reduction was the largest in the weak rock, where the rock mass yields at a greater extent. In this case the support consisting of RRS's and bolts create an artificial arc effect, supporting the profile. For both cases the deformations found in the analysis are acceptable and is not likely to be a stability issue on their own. However, the convergence in the tunnel should be monitored during inspections to observe plausible changes in the profile.

#### **Deformation reduction due to load splitting**

An attempt was made to better describe the deformations affecting the support using the load

split function. For the unsupported case in weak flysch, a disproportionate amount of the displacements stem from the second application of the remaining stress in stage 3, indicating that this method does not work for severely unsupported yielded rock.

In the supported cases the displacements happening in the third stage are reduced. In the strong rock the displacements at the face, ie. the difference in displacements between the overall and the experienced displacement, accounts for 30% of the displacement. In the weak rock the roughly half of the displacement has occurred at the face, while the remaining displacement occurs after the support is installed. If load splitting is not used, bolts are either affected by all or none of the deformations due to excavation. For both cases adjusting the displacements affecting the support to a more accurate degree was thus achieved.

### **9.3.2 The effect of swelling**

Figures 8.9 and 8.10 shows a general increase in deformation as a higher swelling pressure is applied. In weak rock, the trend is linear for the wall locations. For the invert and crown and the strong flysch in general, the trend displays a slightly exponential character, but it is uncertain if this is an effect due to the manner the swelling pressure is applied and the resulting reduced stresses.

Six different levels of swelling pressure have been modelled, and the additional displacement for high swelling pressures are comparable to the displacements happening due to excavation. To what extent swelling will occur, is however uncertain. Most literature suggests that swelling in-situ is lower than what is found in the laboratory (Statens vegvesen (2020) and Selen (2017)). Higher values were also modelled because there are indications by Brattli and Broch (1995) and Selen (2017) that rock disks swell more than powder, which leaves a plausible case where the in-situ swelling in rock may be higher than the laboratory values from powdered specimens. Due to the weak character of the rock, and the extensive yielding of the material seen in the model, it is reasonable to believe that the swelling pressures may be on the lower end of the scale. The resulting deformations due to 0.5 MPa, twice the laboratory values, are less than 0.5 mm for all modelled cases. If the swelling pressures manifests the same way in the headrace tunnel, there is little chance it will influence the stability.

However, it is possible that the swelling pressures would be higher if the suggested changes in how swelling is included in the model are implemented. The stresses on the lining and in the near proximity to the tunnel would be higher, which may result in higher levels than those found in this analysis.

### **9.3.3 Swelling and slaking**

The combined effect of swelling and slaking has not been evaluated in this thesis, but may have a potential effect on the long term stability. The slake durability of flysch rock varies from low to very high, and may thus over time with periodical differences in water levels and pressures in the tunnel degrade the rock mass over time. In the case study from Chingaza, drying of the material caused fissuring in the rock mass which increased the surface area where water rock interaction led to swelling of the material. It is a possibility that similar problems may occur in this hydropower tunnel. Inspections of the sprayed concrete lining should be prioritised during inspections to detect possible damage caused by compounding slaking and swelling.

# Chapter 10

## Conclusion and recommendations

### 10.1 Conclusion

Both quantifying the qualities of flysch rock and the modelling of such rock masses are tasks where several considerations have to be made regarding the validity of the results. The heterogeneity and difficulty in preparing viable rock specimens creates uncertainty in the mechanical properties of the rock. Different methods for quantifying swelling, and uncertain relations between laboratory values and swelling pressures in the field makes it difficult to predict to what extent swelling will be an issue in an underground construction.

A numerical analysis have been conducted using the mechanical and swelling properties of flysch rock to evaluate the effect on the installed lining and long term stability at the head-race tunnel at Moglice. Two rock mass types based on the laboratory results obtained in the specialisation project and this master's thesis have been modelled. A rock mass based on the strong sandstone and conglomerate specimens have been compared to a more realistic weak rock mass created by combining the mechanical properties of both the strong specimen, and values for claystone flysch obtained from Malaj et al. (2017). Two versions of a support based on reinforced ribs of concrete have been tested for each of the rock masses.

Based on discussions of the laboratory investigations and the numerical analysis, the following conclusions may be drawn:

1. The deformations due to excavation as evaluated by the numerical analysis is not likely to be a cause for concern regarding the long term stability. Inspections should be conducted periodically to ensure that the tunnel remains intact.
2. Deformations due to swelling as applied in the model are low, and does not damage the lining. Due to the method of which swelling has been applied in the model the stresses on the tunnel lining is lower than what's realistic. Hence the deformations may be more severe than what these results indicate.

3. The results indicate yielding of rock bolts and tensile failure of the encompassing rock mass. The results of the analysis are uncertain due to the manner in which swelling pressure has been applied in the model. In order to determine the degree of bolt yielding and the extent of deformations due to swelling, further analysis is required.
4. Flysch rock displays a range of mechanical properties with UCS values ranging from less than 8 MPa to 137 MPa depending on the grain content of the tested layer. All the tested specimens from Moglice headrace tunnel displayed some level of swelling. together with the periodically low slake durability, the rock mass stability may experience deterioration over time. The sprayed concrete lining should be evaluated for signs of cracking and deformations should be monitored during inspections to ensure continuous safe operation.

## 10.2 Recommendations for further work

There are many limitations in the analysis performed in this thesis that may be improved upon. Some suggestions for further numerical analysis of swelling ground and recommendations for further work are the following:

1. A 3D analysis should be conducted due to the 3D characteristics of the support and the gradual deformation effects due to excavation.
2. The application of swelling in the model should be changed in order to illustrate a more accurate stress concentration around the tunnel. A suggestion would be to create a pressure gradient normal to the lining, where the pressure dissipated with increased distance to the tunnel
3. When readings from the flat jacks are available, the measured stresses could be used to verify and/or improve the analysis, both regarding the initial stress situation and the swelling pressures.

# Bibliography

- Aasen, O., Ødegaard, H. and Palmström, A. (2013), Planning of pressurized headrace tunnel in albania, *in* 'Norwegian Hydropower Tunneling II', Norwegian Tunneling Industry (NFF).
- ASTM (1992), Standard test method for slake durability of shales and similar weak rocks, *American Society for Testing and Materials*.
- Barton, N. (2002), Some new q-value correlations to assist in site characterisation and tunnel design, *International Journal of Rock Mechanics and Mining Sciences* 39(2), 185–216.
- Barton, N., Lien, R. and Lunde, J. (1974), Engineering classification of rock masses for the design of tunnel support, *Rock Mechanics Felsmechanik Mecanique des Roches* 6, 189–236.
- Bieniawski, Z. (1973), Engineering classification of jointed rock masses, *Civil Engineer in South Africa* 15(12).
- Bieniawski, Z. (1978), Determining rock mass deformability: experience from case histories, *International Journal of Rock Mechanics and Mining Sciences & Geomechanics Abstracts* 15(5), 237 – 247.
- Bieniawski, Z. (1984), *Rock mechanics design in mining and tunneling*, A. A. Balkema, Rotterdam.
- Bieniawski, Z. (1993), "classification of rock masses for engineering: the rmr system and future trends", *in* 'Rock Testing and Site Characterization', Elsevier, pp. 553–573.
- Brattli, B. and Broch, E. (1995), Stability problems in water tunnels caused by expandable minerals. swelling pressure measurements and mineralogical analysis, *Engineering Geology* 39(3), 151 – 169.
- Brekke, T. L. (1965), On the measurement of the relative potential swellability of hydrothermal montmorillonite clay from joints and faults in pre-cambrian and paleozoic rocks in norway, *International Journal of Rock Mechanics and Mining Sciences and Geomechanics Abstracts* 2(2), 155,IN11,161–160,IN12,165.
- Brekke, T. and Selmer-Olsen, R. (1965), Stability problems in underground constructions caused by montmorillonite-carrying joints and faults, *Engineering Geology* 1(1), 3–19.
- Broch, E. (1979), Changes in rock strength caused by water, *in* '4th ISRM Congress', International Society for Rock Mechanics and Rock Engineering.
- Broch, E. (1984), Lekkasje- og stabilitetsproblemer i noen colombianske tunneler, *in* 'Fjellsprengningsteknikk, Bergmekanikk, Geoteknikk 1984', Norsk jord- og fjellteknisk forbund, Tapir, Oslo.
- Bråtveit, K., Bruland, A. and Brevik, O. (2016), Rock falls in selected norwegian hydropower tunnels subjected to hydropeaking, *Tunnelling and Underground Space Technology* 52, 202 – 207.

- Cai, M., Kaiser, P., Tasaka, Y. and Minami, M. (2007), Determination of residual strength parameters of jointed rock masses using the gsi system, *International Journal of Rock Mechanics and Mining Sciences* 44(2), 247–265.
- Devoll HPP (2011), Geological report hpp moglicë. [unpublished].
- Dyar, M. D. (2008), *Mineralogy and optical mineralogy*, Mineralogical Society of America, Chantilly, Va.
- Einstein, H. H. (1996), Tunnelling in difficult ground — swelling behaviour and identification of swelling rocks, *Rock Mechanics and Rock Engineering* 29(3), 113–124.
- EU (2014), EU Action on Climate Change.  
Available from: [https://ec.europa.eu/clima/sites/clima/files/eu\\_climate\\_action\\_factsheet\\_en.pdf](https://ec.europa.eu/clima/sites/clima/files/eu_climate_action_factsheet_en.pdf) [Accessed: 25.5.2019]
- Forouzan, A. J. (2016), Prediction of swelling behavior of expansive soils using modified free swell index, methylene blue and swell oedometer test, *Middle East Technical University*.
- Franklin, J. and Chandra, R. (1972), The slake-durability test, 9(3), 325–328.
- Frashëri, A. (2005), Geothermal regime and hydrocarbon generation in the albanides, *Petroleum geoscience* 11(4), 347–352.
- Frengen, R. B. (2019), Study on the swelling and slaking properties of rocks from moglice hydropower project, Specialisation project, NTNU, Trondheim.
- Hawkes, I. and Mellor, M. (1970), Uniaxial testing in rock mechanics laboratories, *Engineering Geology* 4(3), 179–285.
- Hawkins, A. and McConnell, B. (1992), Sensitivity of sandstone strength and deformability to changes in moisture content, *Quarterly Journal of Engineering Geology and Hydrogeology* 25(2), 115–130.
- Hoek, E. (1994), Strength of Rock and Rock Masses, *ISRM News Journal* 2(2), 4–16.
- Hoek, E. (2000), *Practical rock engineering*, Rocscience, Toronto.
- Hoek, E. and Brown, E. (2019), The hoek-brown failure criterion and gsi - 2018 edition, *Journal of Rock Mechanics and Geotechnical Engineering* 11(3), 445 – 463.
- Hoek, E. and Brown, E. T. (1980), *Underground excavations in rock*, London: institution of mining and metallurgy.
- Hoek, E. and Brown, E. T. (1997), Practical estimates of rock mass strength, *International journal of rock mechanics and mining sciences* 34(8), 1165–1186.
- Hoek, E., Carranza-Torres, C. and Corkum, B. (2002), Hoek-brown failure criterion-2002 edition, *Proceedings of NARMS-Tac* 1(1), 267–273.
- Hoek, E. and Marinos, P. (2000), Predicting tunnel squeezing problems in weak heterogeneous rock masses, *Tunnels and tunnelling international* 32(11), 45–51.
- IISD (2014), A Summary Report of the UN Climate Summit 2014, *Climate Summit Bulletin* 172(18). Published by the International Institute for Sustainable Development (IISD) in collaboration with the Executive Office of the UN Secretary-General.  
Available from: <http://enb.iisd.org/CLIMATE/CS/2014/> [Accessed on: 06.05.19]
- ISRM (1978a), International society for rock mechanics commission on standardization of laboratory and field tests: Suggested methods for the quantitative description of discontinuities in rock masses, *International Journal of Rock Mechanics and Mining Sciences & Geomechanics Abstracts* 15(6), 319 – 368.

- ISRM (1978*b*), Suggested methods for determining tensile strength of rock materials, *International Journal of Rock Mechanics and Mining Sciences and Geomechanics Abstracts* 15(6), 124–124.
- ISRM (1979*a*), Suggested methods for determining the uniaxial compressive strength and deformability of rock materials, *International Journal of Rock Mechanics and Mining Sciences & Geomechanics Abstracts* 16(2), 138–140.
- ISRM (1979*b*), Suggested methods for determining water content, porosity, density, absorption and related properties and swelling and slake-durability index properties: Part 2: Suggested methods for determining swelling and slake-durability index properties, *International Journal of Rock Mechanics and Mining Sciences & Geomechanics Abstracts* 16(2), 151 – 156.
- ISRM (1985), "suggested method for determining point load strength", *International Journal of Rock Mechanics and Mining Sciences & Geomechanics Abstracts* 22(4), 112–112.
- Labuz, J. and Zang, A. (2012), Mohr-coulomb failure criterion, *Rock Mechanics and Rock Engineering* 45(6), 975–979.
- Li, C. C. (2017), *Rock Mechanics*, Norwegian University of Science and Technology (NTNU), Trondheim.
- Madsen, F. T. and Müller-Vonmoos, M. (1989), The swelling behaviour of clays, *Applied Clay Science* 4(2), 143–156.
- Malaj, A., Rusi, I., Meço, A., Faca, D. and Allkja, S. (2017), The characterization of flysch rock in albania with field and laboratory testing, *Procedia Engineering* 191, 104–111.
- Marinos, P. and Hoek, E. (2001), Estimating the geotechnical properties of heterogeneous rock masses such as flysch, *Bulletin of Engineering Geology and the Environment* 60(2), 85–92.
- Marinos, P., Hoek, E. and Marinos, V. (2006), Variability of the engineering properties of rock masses quantified by the geological strength index: The case of ophiolites with special emphasis on tunnelling, *Bulletin of Engineering Geology and the Environment* 65, 129–142.
- NAE (2003), *The National Strategy of Energy and Plan of Action (Updated 2005)*, Ministry of Industry and Energy, National Agency of Energy (NAE), Tirana.
- NGI (2015), Using the q-system. rock mass classification and support design, Technical report, NGI, Oslo.
- Nilsen, B. and Broch, E. (2012), *Ingeniørgeologi-Berg Grunnkurskompendium*, NTNU - Institutt for geologi og bergteknikk, Trondheim.
- Nilsen, B. and Palmström, A. (2000), *Handbook No 2 Engineering geology and rock engineering*, Norwegian Group for Rock Mechanics (NBG), Oslo.
- Palmstrom, A. (1996), Engineering geology and rock engineering applied in the design of norwegian tunnels, in 'Materials of the conference on Tunnels for the third Millennium, Prievidza Slovakia'.
- Palmström, A. (1995), *RMi - a rock mass characterization system for rock engineering purposes*, Department of Geology, Faculty of Mathematics and Natural Sciences, University of Oslo, Oslo.
- Palmström, A. and Stille, H. (2010), *Rock Engineering*, Thomas Telford.
- Panthi, K. K. (2006), *Analysis of Engineering Geological Uncertainties Related to Tunnelling in Himalayan Rock Mass Conditions*, Fakultet for ingeniørvitenskap og teknologi.



- Panthi, K. K. (2017), Review on the prevailing methods for the prediction of potential rock burst / rock spalling in tunnels.
- Rahmani, N., Nikbakhtan, B., Ahangari, K. and Apel, D. (2012), Comparison of empirical and numerical methods in tunnel stability analysis, *International Journal of Mining, Reclamation and Environment* 26(3), 261–270.
- Rauh, F., Thuro, K. and Spaun, G. (2006), The powder swelling test-advantages and limitations, *Engineering Geology for Tommorrow's cities Geological Society London, Engineering Geology Special Publication* 22.
- Rickerson, W. and Perroy, R. (2005), Renewable energy development on the edge of the european union: A case study of albania.  
Available from: [https://www.researchgate.net/publication/323666236\\_Renewable\\_Energy\\_Development\\_on\\_the\\_Edge\\_of\\_the\\_European\\_Union\\_A\\_Case\\_Study\\_of\\_Albania](https://www.researchgate.net/publication/323666236_Renewable_Energy_Development_on_the_Edge_of_the_European_Union_A_Case_Study_of_Albania) [Accessed on: 06.05.19]
- Russo, G., Kalamaras, G. and Grasso, P. (1998), A discussion on the concepts of geomechanical classes behavior categories and technical classes for an underground project, *Gallerie e grandi opere sotterranee* 54, 40–51.
- Selen, L. (2017), Study on material properties of various rock types, development of investigation procedure and test methodology for future projects, master thesis, NTNU, Trondheim.
- Selen, L. (2019), Communication and discussions during the project work, [Oral communication].
- Selen, L., Panthi, K. K. and Vergara, M. R. (2018), Swelling pressures of some rocks using different test procedures, in 'Geomechanics and Geodynamics of Rock Masses, Volume 1: Proceedings of the 2018 European Rock Mechanics Symposium', CRC Press, p. 401.
- Selen, L., Panthi, K. K. et al. (2018), Influence of slaking and disintegration effect on the stability of water tunnels for hydropower, in 'ISRM International Symposium-10th Asian Rock Mechanics Symposium', International Society for Rock Mechanics and Rock Engineering.
- Selmer-Olsen, R., Palmstrom, A. and Stromme, B. (1989), Tunnel collapses in swelling clay zones, *Tunnels & Tunnelling International* 21, 49–51.
- Sheorey, P. (1994), A theory for in situ stresses in isotropic and transverseley isotropic rock, *International Journal of Rock Mechanics and Mining Sciences & Geomechanics Abstracts* 31(1), 23 – 34.
- Singh, T. N., Kainthola, A. and A, V. (2012), Correlation between point load index and uniaxial compressive strength for different rock types, *Rock Mechanics and Rock Engineering* 45(2), 259–264.
- Sivapullaiyah, P. V., Sitharam, T. G. and Rao, K. S. (1987), Modified free swell index for clays, *Geotechnical Testing Journal* 10(2), 80–85.
- Statens vegvesen (2014), Laboratorieundersøkelser Håndbok R210.
- Statens vegvesen (2020), Tunnelveiledning: Håndbok V520.
- Statkraft (2014), Benefits to albania, online.  
Available from: [http://www.devollhydropower.al/new/?page\\_id=7805](http://www.devollhydropower.al/new/?page_id=7805) [Accessed on: 06.05.19]
- Statkraft (2015), 120 years in pure energy.  
Available from: <https://www.statkraft.com/about-statkraft/historyweb/#2005-2015> [Accessed: 26.05.2019]

- Statkraft (2017), Hydropower sustainability assessment assessment protocol devoll hydropower project.  
Available from: <http://www.hydrosustainability.org/IHAHydro4Life/media/ProtocolAssessments/PDF%20Reports/Devoll-Protocol-Assessment-Final-with-appendices.pdf?ext=.pdf> [Accessed on: 26.05.19]
- Statkraft (2019), Devoll.  
Available from: <https://www.statkraft.com/about-statkraft/Projects/albania/devoll/> [Accessed on: 06.05.19]
- Sweco (2018), Devoll Hydropower Project HPP Moglicë, Permanent rock support in HRT3, Technical report, Sweco Norge AS. [Unpublished].
- Taylor, R. and Spears, D. (1970), The breakdown of british coal measure rocks, *International Journal of Rock Mechanics and Mining Sciences & Geomechanics Abstracts* 7(5), 481 – 501.
- Theng, B. (2012), Chapter 1 - the clay minerals, in B. Theng, ed., 'Formation and Properties of Clay-Polymer Complexes', Vol. 4 of *Developments in Clay Science*, Elsevier, pp. 3 – 45.
- Trinh, N. Q. and Holmøy, K. H. (2012), Numerical modelling in rock engineering: What can it do, advantages and disadvantages, and software limitations, *Fjellsprenningsdagen 2012*.
- Vásárhelyi, B. (2003), Some observations regarding the strength and deformability of sandstones in dry and saturated conditions, *Bulletin of Engineering Geology and the Environment* 62(3), 245–249.
- Waseda, Y., Matsubara, E. and Shinoda, K. (2011), *Scattering and Diffraction*, Springer Berlin Heidelberg, Berlin, Heidelberg, pp. 67–106.
- Will, G. (2006), *Powder Diffraction : The Rietveld Method and the Two Stage Method to Determine and Refine Crystal Structures from Powder Diffraction Data*, Springer-Verlag, Berlin, Heidelberg.

---

## **Appendix A: Laboratory Results**

- Point Load strength (Rock material)
- Point Load strength (Sprayed concrete)
- Density and Velocity (Rock material)
- Density and Velocity (Sprayed concrete)
- Uniaxial compression strength (Rock material)
- Uniaxial compression strength (Sprayed concrete)
- Brazil test (Sprayed concrete)
- Swelling and slaking (Rock material)
- Mineral content and swelling clay identification (Rock material)

<b>Point Load index test</b>							Date:	14.11.19			
<b>Test apparatus:</b> NTNU point load test machine and GCTS Point Load Tester (Enerpac PLT-100)							<b>Location:</b>	NTNU Rock mechanics lab			
<b>Test material:</b> Rock material (flysch rock)							<b>Performed by:</b>	Runa Berstad Frengen			
<b>Test condition:</b> Laboratory conditions (dry)							<b>Assisted by:</b>	Gunnar Vistnes			
<b>Information:</b> Flysch rock is composed of alternating layers of different sedimentary composition. Sections dominated by conglomerate (Cl) and sandstone (s) and conglomerate (Cgl) have been tested. Non-valid results are striked through and the highest and lowest valid value of each flysch type are marked with a grey background. The pressure p displayed by the NTNU PLT machine is adjusted to the load P, by mulitiplying with the constant c = 0.956 Mpa/kN as stated on the machinery. Specimens from the F-series were tested with the GCTS machine due to size constraint.											
ID	Flysch type	A/D	D [mm]	W [mm]	p [MPa]	P [kN]	De <sup>2</sup> [mm <sup>2</sup> ]	Is	F	I <sub>s(50)</sub>	
5.1	<del>Cl</del>	<del>D</del>	<del>44.33</del>		<del>no value</del>						
5.2	<del>Cl</del>	<del>D</del>	<del>44.33</del>		<del>no value</del>						
8.1	Cl	D	44.31		2.98	2.88	1963.38	1.46	0.95	1.39	
8.2	Cl	D	44.43		0.78	0.75	1974.02	0.38	0.95	0.36	
<del>8.3</del>	<del>Cl</del>	<del>D</del>	<del>44.33</del>		<del>0.72</del>	<del>0.69</del>	<del>1965.15</del>	<del>0.35</del>	<del>0.95</del>	<del>0.33</del>	
<del>8.4.1</del>	<del>Cl</del>	<del>D</del>	<del>44.32</del>		<del>0.88</del>	<del>0.85</del>	<del>1964.26</del>	<del>0.43</del>	<del>0.95</del>	<del>0.41</del>	
8.4.2	Cl	D	44.32		0.38	0.37	1964.26	0.19	0.95	0.18	
11.1	Cl	D	43.75		2.10	2.03	1914.06	1.06	0.94	1.00	
11.2	Cl	D	43.75		2.12	2.05	1914.06	1.07	0.94	1.01	
<del>13</del>	<del>Cl</del>	<del>A</del>	<del>33.42</del>	<del>42.9</del>	<del>6.10</del>	<del>5.89</del>	<del>1825.47</del>	<del>3.22</del>	<del>0.93</del>	<del>3.00</del>	
F10.1	Cl	D	85		N/A	2.33	7225.00	0.32	1.27	0.41	
F10.2	Cl	A	79.8	85	N/A	3.68	8636.38	0.43	1.32	0.56	
F10.3	Cl	A	53.2	85	N/A	4.55	5757.59	0.79	1.21	0.95	
<del>F10.4</del>	<del>Cl</del>	<del>D</del>	<del>85</del>		<del>N/A</del>	<del>2.01</del>	<del>7225.00</del>	<del>0.28</del>	<del>1.27</del>	<del>0.35</del>	
<del>9.1</del>	<del>S</del>	<del>D</del>	<del>43.74</del>		<del>7.72</del>	<del>7.45</del>	<del>1913.19</del>	<del>3.89</del>	<del>0.94</del>	<del>3.67</del>	
9.2	S	A	43.4	43.75	10.88	10.50	2417.56	4.34	0.99	4.31	
9.3	S	D	43.72		8.70	8.40	1911.44	4.39	0.94	4.13	
9.4.1	S	D	43.74		11.56	11.16	1913.19	5.83	0.94	5.49	
9.4.2	S	D	43.74		12.14	11.72	1913.19	6.12	0.94	5.77	
<del>9.5</del>	<del>S</del>	<del>D</del>	<del>43.75</del>		<del>2.34</del>	<del>2.26</del>	<del>1914.06</del>	<del>1.18</del>	<del>0.94</del>	<del>1.11</del>	
10.1.1	S	D	43.67		6.90	6.66	1907.07	3.49	0.94	3.29	
10.1.2	S	A	31.58	43.67	10.76	10.38	1755.92	5.91	0.92	5.46	
10.1.3	S	A	32.87	43.67	10.10	9.75	1827.65	5.33	0.93	4.97	
3	Cgl	A	33.68	43.36	1.98	1.91	1859.39	1.03	0.94	0.96	
4	Cgl	D	44.43		14.36	13.86	1974.02	7.02	0.95	6.66	

Point Load index test						Date:	04.11.19			
Test apparatus: NTNU point load test machine						Location: NTNU Rock mechanics lab				
Test material: Sprayed concrete						Performed by: Runa Berstad Frengen				
Test condition: Laboratory conditions (dry)						Assisted by: Jon Runar Drotninghaug				
Information:						All tests had valid results. The two highest and lowest valid values are marked with a grey background. The load p displayed by the -NTNU PLT machine is adjusted to P, by multiplying with the constant c = 0.956 Mpa/kN as stated on the machinery.				
ID	A/D	D [mm]	W [mm]	p [MPa]	P [kN]	De <sup>2</sup> [mm <sup>2</sup> ]	Is	F	I <sub>s(50)</sub>	
4.1	D	43.3		5.78	5.58	1874.89	2.97	0.94	2.79	
4.2	D	43.3		4.88	4.71	1874.89	2.51	0.94	2.35	
4.3	D	43.5		7.00	6.76	1892.25	3.57	0.94	3.35	
9.1	D	43.7		5.56	5.37	1909.69	2.81	0.94	2.64	
9.2	D	43.8		6.28	6.06	1918.44	3.16	0.94	2.98	
9.3	D	43.8		6.92	6.68	1918.44	3.48	0.94	3.28	
9.4	D	43.8		7.24	6.99	1918.44	3.64	0.94	3.43	
10.1	D	44.4		3.82	3.69	1971.36	1.87	0.95	1.77	
10.2	D	43.7		6.50	6.27	1909.69	3.28	0.94	3.09	
10.2	D	43.7		7.02	6.77	1909.69	3.55	0.94	3.34	
11.1	D	43.8		3.98	3.84	1918.44	2.00	0.94	1.89	
13.2	D	43		6.26	6.04	1849.00	3.27	0.93	3.05	
4.1.1	A	30.2	43.3	5.83	5.63	1664.96	3.38	0.91	3.08	
4.1.2	A	28.18	43.3	10.06	9.71	1553.60	6.25	0.90	5.61	
4.1.3	A	33.51	43.3	7.48	7.22	1847.45	3.91	0.93	3.65	
4.2.1	A	30.13	43.5	9.40	9.07	1668.78	5.44	0.91	4.96	
9.1.1	A	21.68	43.5	7.18	6.93	1200.77	5.77	0.85	4.89	
9.2.1	A	26.11	43.7	6.48	6.25	1452.78	4.30	0.89	3.81	
9.2.2	A	27.4	43.6	6.48	6.25	1521.06	4.11	0.89	3.68	
9.3.1	A	32.15	43.8	6.82	6.58	1792.94	3.67	0.93	3.41	
9.4.1	A	26.63	43.8	6.34	6.12	1485.10	4.12	0.89	3.66	
9.4.2	A	24.87	43.8	6.32	6.10	1386.95	4.40	0.88	3.85	
10.2	A	27.4	43.6	5.56	5.37	1521.06	3.53	0.89	3.15	
10.3.1	A	32.6	43.9	6.40	6.18	1822.18	3.39	0.93	3.16	
11.1.1	A	22.09	43.8	5.92	5.71	1231.91	4.64	0.85	3.95	
11.1.2	A	25.7	43.8	5.62	5.42	1433.23	3.78	0.88	3.34	
13.2.1	A	24.2	43.1	5.86	5.65	1328.01	4.26	0.87	3.69	
13.2.2	A	24.9	42.9	6.12	5.91	1360.09	4.34	0.87	3.79	

<b>Density and velocity</b>		<b>Date:</b> 17.11.19
		<b>Location:</b> NTNU Rock mechanics lab
<b>Test apparatus:</b> Pundit apparatus for sound velocity	<b>Performed by:</b> Runa Berstad Frengen	
<b>Test material:</b> Rock material (flysch rock)	<b>Assisted by:</b>	
<b>Test condition:</b> Laboratory conditions (dry)		
<b>Information:</b>	Flysch rock is composed of alternating layers of different sedimentary composition. Sections dominated by conglomerate (Cgl) and sandstone (s) have been measured. The diameter is an average of six measurements on the specimen. Images of the measured cores are provided under the table. The same specimens were used for the UCS test.	

ID	Flysch type	Diameter, D [mm]	Length, L [mm]	Mass [g]	Sound velocity [m/s]	Density [g/cm <sup>3</sup> ]
3.0	Cgl	43.36	88.79	352.59	6166	2.69
4.1	Cgl	43.43	88.06	351.89	6335	2.70
4.3	Cgl	43.45	105.51	421.07	6243	2.69
10.0	S	43.67	88.45	356.96	5936	2.69
11.0	S	43.67	95.18	384.46	5986	2.70
F6D	S	50.10	127.30	657.29	4405	2.62
F7D	S	50.12	127.30	657.22	4133	2.62
F6W	S	50.11	127.30	659.77	4405	2.63
F7W	S	50.13	127.30	659.18	4133	2.62

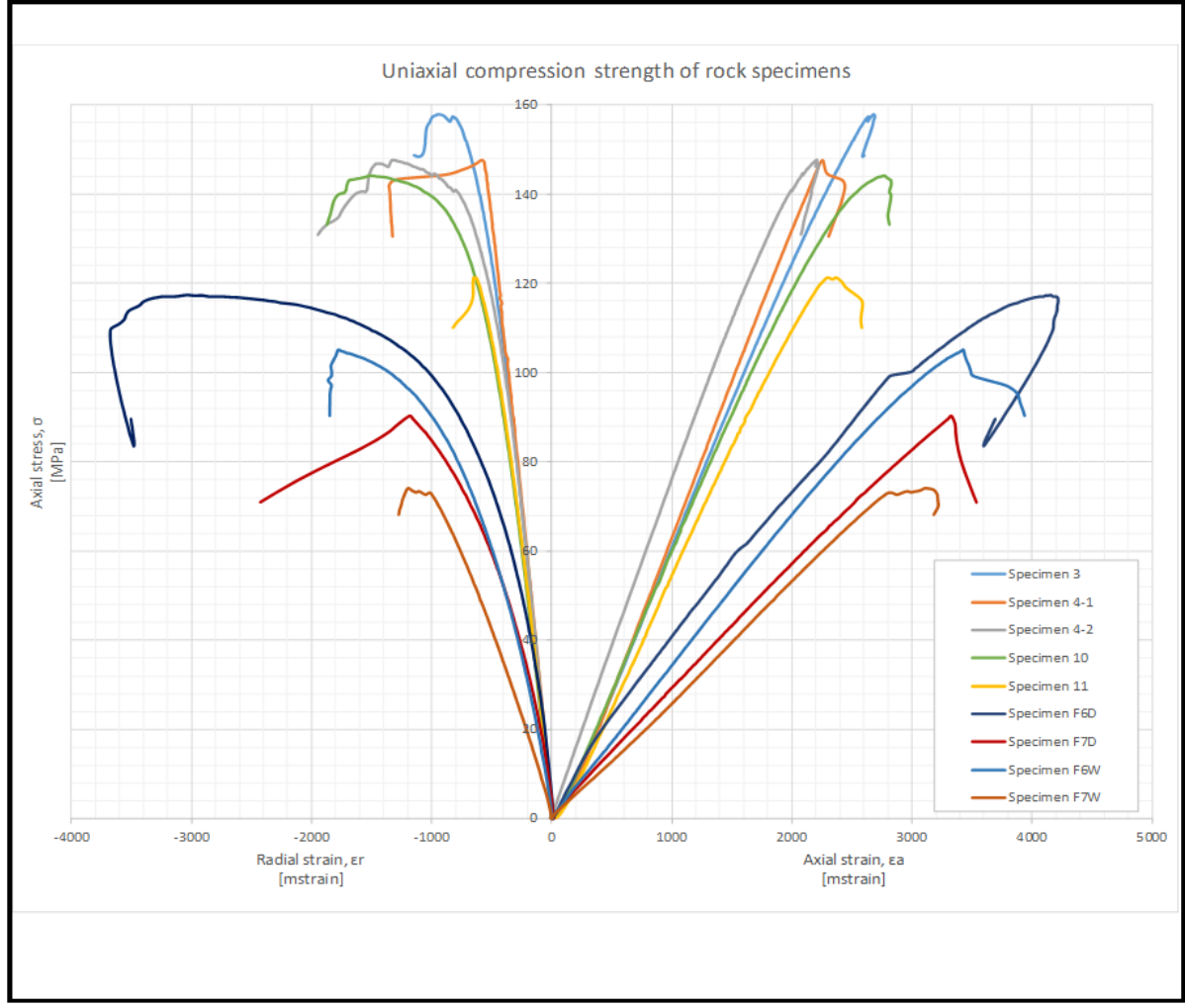


<b>Density and Velocity</b>		<b>Date:</b> 07.11.19
		<b>Location:</b> NTNU Rock mechanics lab
<b>Test apparatus:</b>	Pundit apparatus for sound velocity	<b>Performed by:</b> Runa Berstad Frengen
<b>Test material:</b>	Sprayed concrete	<b>Assisted by:</b>
<b>Test condition:</b>	Laboratory conditions (dry)	
<b>Information:</b>	The diameter is an average of six measurements. An image of the measured cores is provided under the table. The same specimens were used for the UCS test.	

ID	Diameter, D [mm]	Length, L [mm]	Mass [g]	Sound velocity [m/s]	Density [g/cm <sup>3</sup> ]
4.0	43.44	101.66	332.42	4439	2.21
6.0	44.26	101.66	310.82	4439	1.99
7.1	44.18	92.58	345.20	4430	2.43
7.2	43.31	87.05	277.66	4374	2.17
7.3	43.37	87.40	282.59	4414	2.19
8.1	44.30	92.58	314.13	4652	2.20
8.2	44.31	101.66	347.52	4459	2.22
9.0	43.67	101.66	344.30	4642	2.26
10.0	43.53	87.40	292.32	4750	2.25
11.0	43.64	87.40	293.57	4624	2.25
13.0	43.18	92.58	299.60	4430	2.21



<b>Uniaxial Compression Strength</b>		Date:	18.11.19		
<b>Test apparatus:</b> GCTS Rapid Triaxial Test System (RTR-4000)		Location:	NTNU Rock mechanics lab		
<b>Test material:</b> Rock material (flysch rock)		Performed by:	Runa Berstad Frengen		
<b>Test condition:</b> Laboratory conditions (dry) + wet		Assisted by:	Gunnar Vistnes		
<b>Information:</b> Flysch rock is composed of alternating layers of different sedimentary composition. Sections dominated by conglomerate (Cgl) and sandstone (s) have been tested. Specimens from the F-series are tested both in laboratory (D) and wet (W) condtion. Curves from the test is provided below the table. The relationship between specimen length, L and diameter, D is stated in the comment column.					
ID	Flysch type	UCS [Mpa]	E modulus, E [Gpa]	Poissons ratio, v	Comment
3.0	Cgl	158	65.76	0.26	L=2.0xD
4.1	Cgl	147.6	69.83	0.27	L=2.0xD
4.3	Cgl	147.6	75.2	0.32	L=2.4xD
10.0	S	144.1	61.58	0.31	L=2.0xD
11.0	S	121.2	58.23	0.27	L=2.2xD
F6D	S	117.3	32.07	0.31	L=2.5xD
F7D	S	105	34.11	0.38	L=2.5xD
F6W	S	90.3	28.13	0.31	L=2.5xD
F7W	S	74.2	27.66	0.37	L=2.5xD





# Uniaxial Compression Strength

Date: 08.11.19

Location: NTNU Rock mechanics lab

Test apparatus: GCTS Rapid Triaxial Test System (RTR-4000)

Performed by: Runa Berstad Frengen

Test material: Sprayed concrete

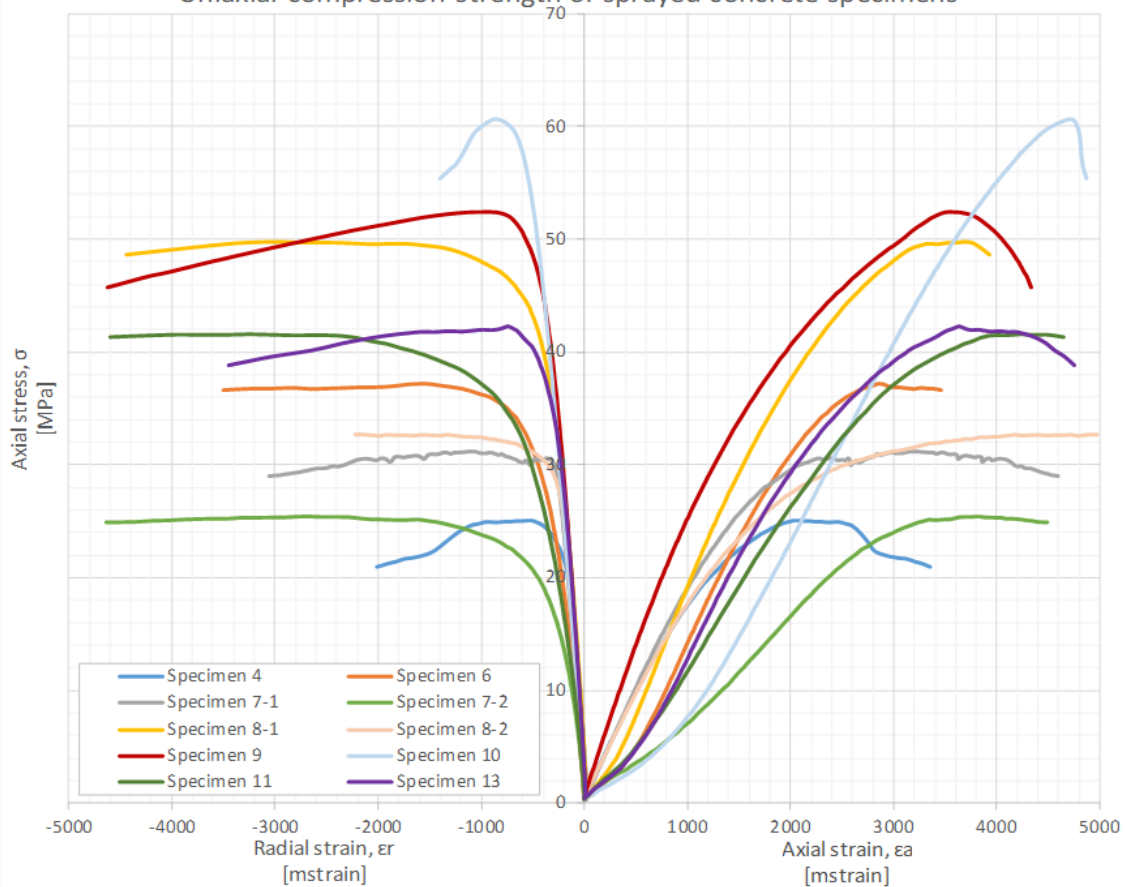
Assisted by: Jon Runar Drotninghaug

Test condition: Laboratory conditions (dry)

Information: Curves from the test is provided below the table. The relationship between specimen length, L and diameter, D is stated in the comment column.

ID	UCS [Mpa]	E modulus, E [Gpa]	Poissons ratio, $\nu$	Comment
4.0	25.1	18.27	0.13	L=2.3xD
6.0	37.1	20.29	0.24	L=2.1xD
7.1	31.2	19.68	0.16	L=2.3xD
7.2	25.4	9.89	0.24	L=2.0xD
7.3	41	16.34	0.18	L=2.0xD
8.1	49.8	22.96	0.19	L=2.1xD
8.2	32.8	17.42	0.15	L=2.3xD
9.0	52.5	23.88	0.17	L=2.3xD
10.0	60.5	17.51	0.16	L=2.0xD
11.0	41.6	15.08	0.26	L=2.0xD
13.0	42.2	18.67	0.14	L=2.2xD

Uniaxial compression strength of sprayed concrete specimens



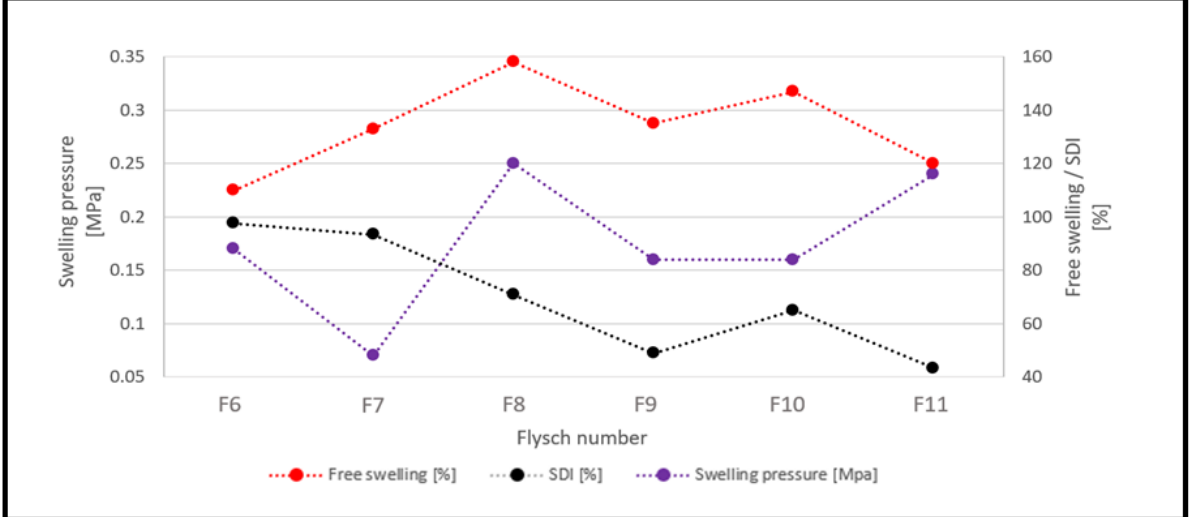
<b>Brazil test</b>		<b>Date:</b> 09.11.2019
		<b>Location:</b> NTNU Rock mechanics lab
<b>Test apparatus:</b>	GCTS Rapid Triaxial Test System (RTR-4000)	<b>Performed by:</b> Runa Berstad Frengen
<b>Test material:</b>	Sprayed concrete	<b>Assisted by:</b> Gunnar Vistnes
<b>Test condition:</b>	Laboratory conditions (dry)	
<b>Information:</b>	The GCTS system was fitted with a loading jaws after the ISRM requirement. Image of cores prior to testing is provided under the table.	

ID	Diameter, D [mm]	Thickness, T [mm]	Load, P [kN]	Tensile strength, $\sigma_t$ [Mpa]
2.1	44.3	21.7	8.3	5.7
2.2	44.4	21.2	9.0	6.3
2.3	44.3	21.5	7.8	5.4
5.0	43.6	21.3	6.5	4.6
6.1	44.3	21.4	6.3	4.4
6.2	44.2	21.5	6.3	4.4
6.3	44.3	20.4	7.3	5.3
9.0	43.7	21.3	7.0	4.9
10.1	43.6	22.0	8.8	6.0
10.2	43.6	22.0	8.0	5.5
10.3	43.6	21.8	4.6	3.2
10.4	43.5	19.6	6.6	5.1
11.1	43.7	21.8	7.2	5.0
11.2	43.8	21.7	7.8	5.4
11.3	43.7	21.6	5.1	3.5
11.4	43.7	21.4	7.1	5.0
11.5	43.7	21.2	6.1	4.3



<b>Swelling and slaking</b>		<b>Date:</b> Spring 2019
		<b>Location:</b> NTNU Rock mechanics lab
<b>Test apparatus:</b>	NTNU odeometer NTNU slaking apparatus	<b>Performed by:</b> Runa Berstad Frengen Lena Selen
<b>Test material:</b>	Rock material (flysch)	<b>Assisted by:</b>
<b>Test condition:</b>	Laboratory conditions	
<b>Information:</b>	Swelling tests have been performed by Runa, while Lena has performed the slaking tests. The test material has been flysch rock of sandy to clayey character.	

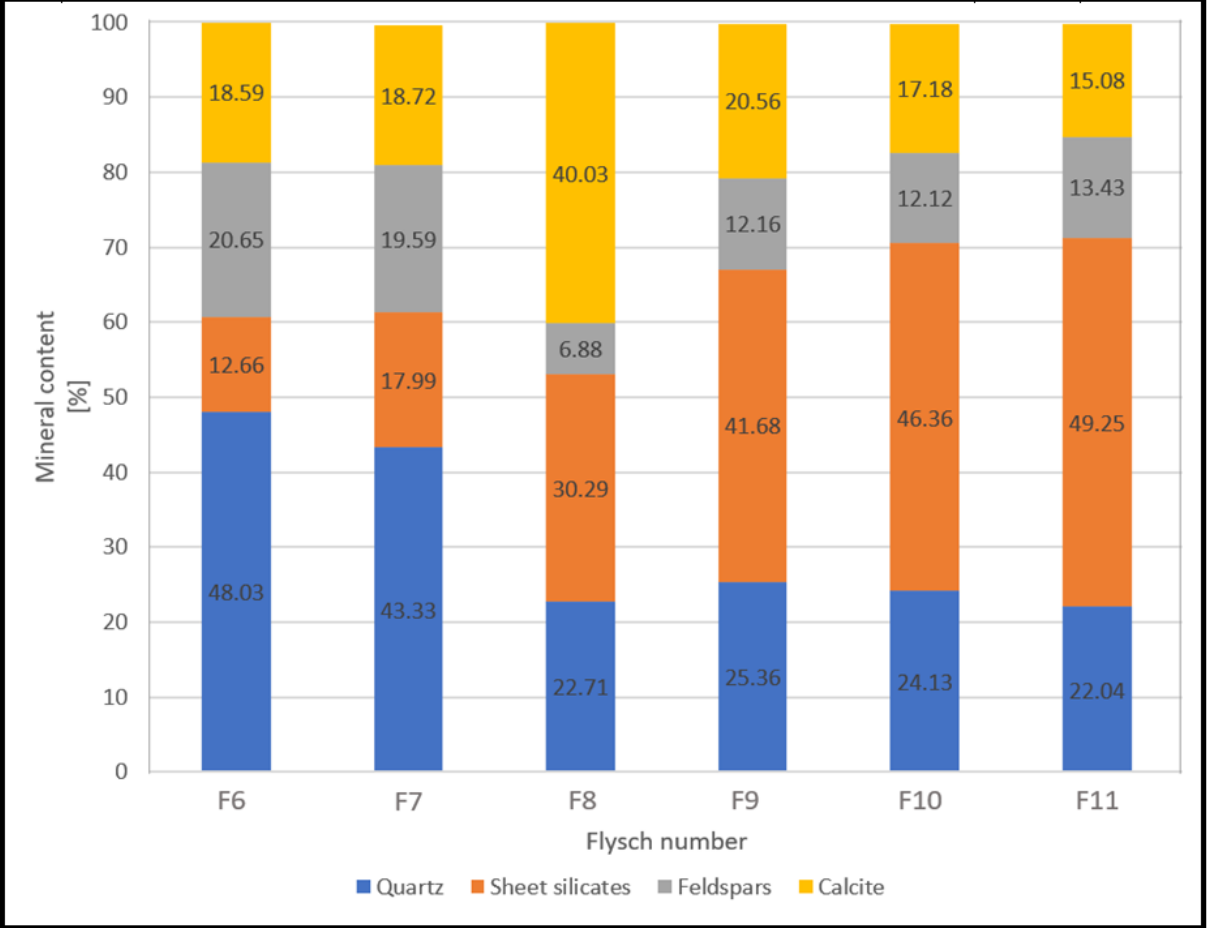
ID	Swelling pressure [Mpa]	Free swelling [%]	Slake durability index, SDI [%]
F6	0.2	110	97.6
F7	0.1	133	93.4
F8	0.3	158	70.8
F9	0.2	135	48.9
F10	0.2	147	64.9
F11	0.2	120	43.3



<b>XRD and swelling ID</b>		Date: Spring 2019
		Location: NTNU Mineralogical laboratory
Test apparatus: Bruker D8 ADVANCE	Performed by: Runa Berstad Frengen	
Test material: Rock material (flysch)	Assisted by: Laurentius Tjihuis	

**Information:** The test material is flysch rock of clayey to sandy character. The mineral classification was determined using the DIFFRAC.SUITE.EVA software combined with PDF-4+ database. The curves of glycolated and non-glycolated specimens were compared to determine the presence of swelling clays. Curves from the test are provided on the pages after this spreadsheet.

ID	Mineral content [%]							Amorph [%]	Swelling [yes/no]
	Quartz	Plagioclase	Muscovite	Chlorite	Calcite	K-feldtspat	Pyrite		
F6	48.0	17.2	4.6	8.1	18.6	3.5	0.1	22.9	yes
F7	43.3	17.1	6.4	11.6	18.7	2.5	0.4	27.6	yes
F8	22.7	5.8	6.9	23.4	40.0	1.1	0.1	37.1	yes
F9	25.4	10.7	14.4	27.2	20.6	1.5	0.2	39.7	no
F10	24.1	10.7	14.4	32.0	17.2	1.4	0.2	43.3	yes
F11	22.0	12.1	19.4	29.8	15.1	1.4	0.2	47.9	no



# Appendix B: Standard Charts and Figures

## B1: The GSI system tables







<p><b>GEOLOGICAL STRENGTH INDEX FOR JOINTED ROCKS (Hoek and Marinos, 2000)</b></p> <p>From the lithology, structure and surface conditions of the discontinuities, estimate the average value of GSI. Do not try to be too precise. Quoting a range from 33 to 37 is more realistic than stating that GSI = 35. Note that the table does not apply to structurally controlled failures. Where weak planar structural planes are present in an unfavourable orientation with respect to the excavation face, these will dominate the rock mass behaviour. The shear strength of surfaces in rocks that are prone to deterioration as a result of changes in moisture content will be reduced if water is present. When working with rocks in the fair to very poor categories, a shift to the right may be made for wet conditions. Water pressure is dealt with by effective stress analysis.</p>		<p><b>SURFACE CONDITIONS</b></p> <p><b>VERY GOOD</b> Very rough, fresh unweathered surfaces</p> <p><b>GOOD</b> Rough, slightly weathered, iron stained surfaces</p> <p><b>FAIR</b> Smooth, moderately weathered and altered surfaces</p> <p><b>POOR</b> Slickensided, highly weathered surfaces with compact coatings or fillings or angular fragments</p> <p><b>VERY POOR</b> Slickensided, highly weathered surfaces with soft clay coatings or fillings</p>				
<p><b>STRUCTURE</b></p>		<p><b>DECREASING SURFACE QUALITY</b> →</p>				
 <p><b>INTACT OR MASSIVE</b> - intact rock specimens or massive in situ rock with few widely spaced discontinuities</p>	90			N/A	N/A	
 <p><b>BLOCKY</b> - well interlocked undisturbed rock mass consisting of cubical blocks formed by three intersecting discontinuity sets</p>	80	70				
 <p><b>VERY BLOCKY</b>- interlocked, partially disturbed mass with multi-faceted angular blocks formed by 4 or more joint sets</p>		60	50			
 <p><b>BLOCKY/DISTURBED/SEAMY</b> - folded with angular blocks formed by many intersecting discontinuity sets. Persistence of bedding planes or schistosity</p>			40	30		
 <p><b>DISINTEGRATED</b> - poorly interlocked, heavily broken rock mass with mixture of angular and rounded rock pieces</p>				20		
 <p><b>LAMINATED/SHEARED</b> - Lack of blockiness due to close spacing of weak schistosity or shear planes</p>	N/A	N/A			10	

Figure B.1. GSI for jointed rock (Hoek, 2000).

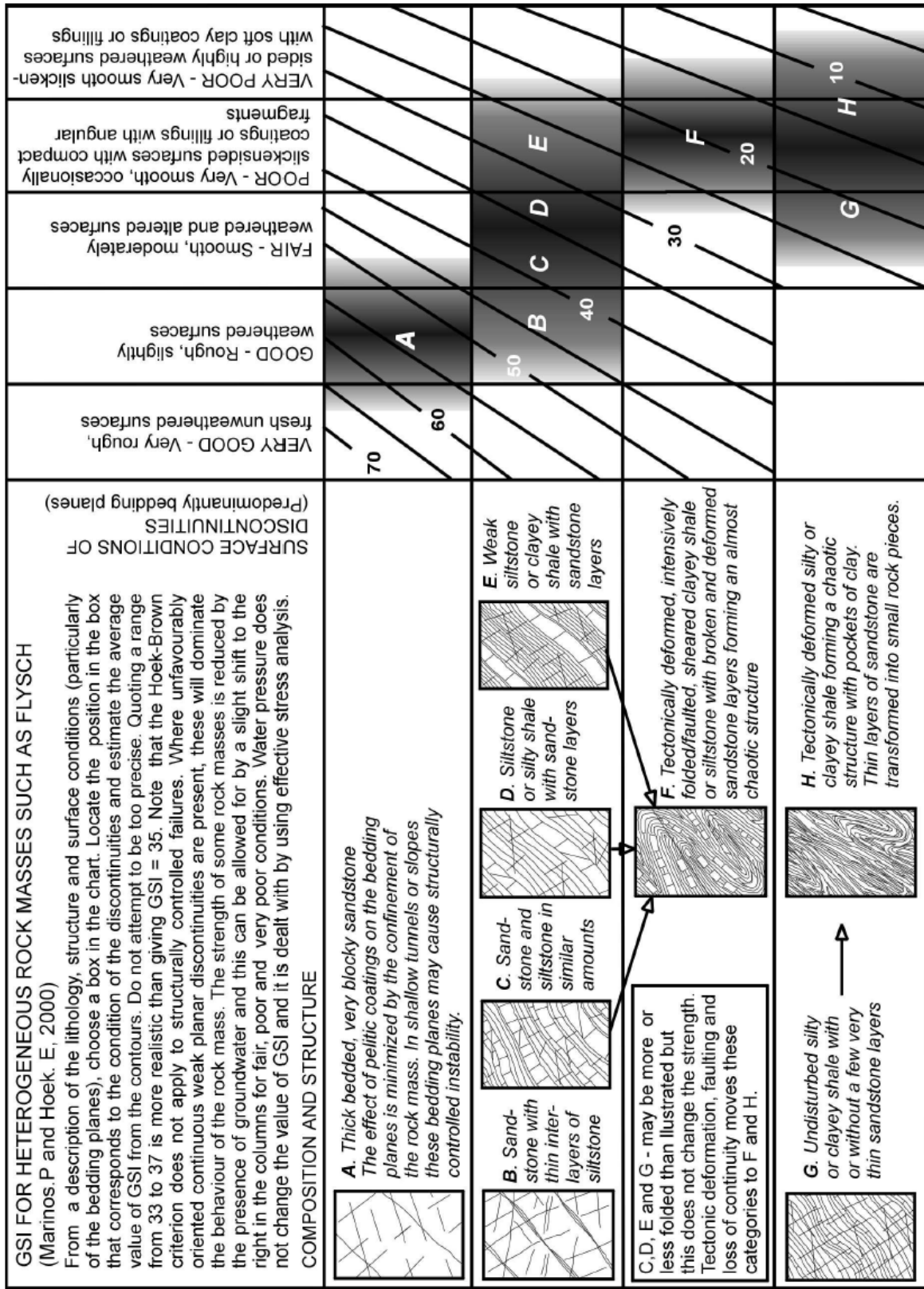


Figure B.2. GSI estimates for heterogenous masses such as flysch (Marinos and Hoek, 2001).

## B2: Suggested $m_i$ values for some rock types

Rock type	Class	Group	Texture			
			Coarse	Medium	Fine	Very fine
SEDIMENTARY	Clastic		Conglomerates* (21 ± 3)	Sandstones 17 ± 4	Siltstones 7 ± 2	Claystones 4 ± 2
			Breccias (19 ± 5)		Greywackes (18 ± 3)	Shales (6 ± 2) Marls (7 ± 2)
	Non-Clastic	Carbonates	Crystalline Limestone (12 ± 3)	Sparitic Limestones (10 ± 2)	Micritic Limestones (9 ± 2)	Dolomites (9 ± 3)
		Evaporites		Gypsum 8 ± 2	Anhydrite 12 ± 2	
		Organic			Chalk 7 ± 2	
METAMORPHIC	Non Foliated		Marble 9 ± 3	Hornfels (19 ± 4) Metasandstone (19 ± 3)	Quartzites 20 ± 3	
	Slightly foliated		Migmatite (29 ± 3)	Amphibolites 26 ± 6		
	Foliated**		Gneiss 28 ± 5	Schists 12 ± 3	Phyllites (7 ± 3)	Slates 7 ± 4
IGNEOUS	Plutonic	Light	Granite 32 ± 3	Diorite 25 ± 5		
			Granodiorite (29 ± 3)			
	Dark	Gabbro 27 ± 3	Dolerite (16 ± 5)			
		Norite 20 ± 5				
	Hypabyssal		Porphyries (20 ± 5)		Diabase (15 ± 5)	Peridotite (25 ± 5)
Volcanic	Lava		Rhyolite (25 ± 5) Andesite 25 ± 5	Dacite (25 ± 3) Basalt (25 ± 5)	Obsidian (19 ± 3)	
	Pyroclastic	Agglomerate (19 ± 3)	Breccia (19 ± 5)	Tuff (13 ± 5)		

\* Conglomerates and breccias may present a wide range of  $m_i$  values depending on the nature of the cementing material and the degree of cementation, so they may range from values similar to sandstone to values used for fine grained sediments.

\*\* These values are for intact rock specimens tested normal to bedding or foliation. The value of  $m_i$  will be significantly different if failure occurs along a weakness plane.

Figure B.3. Values of the constant  $m_i$  for intact rock, by rock group. Note that values in parenthesis are estimates (Hoek, 2000).

### B3: Guidelines for estimating disturbance factor D




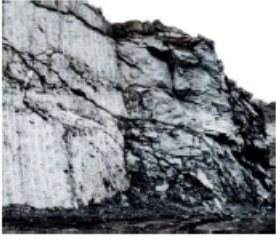

Appearance of rock mass	Description of rock mass	Suggested value of D
	Excellent quality controlled blasting or excavation by Tunnel Boring Machine results in minimal disturbance to the confined rock mass surrounding a tunnel.	D = 0
	Mechanical or hand excavation in poor quality rock masses (no blasting) results in minimal disturbance to the surrounding rock mass.  Where squeezing problems result in significant floor heave, disturbance can be severe unless a temporary invert, as shown in the photograph, is placed.	D = 0  D = 0.5 No invert
	Very poor quality blasting in a hard rock tunnel results in severe local damage, extending 2 or 3 m, in the surrounding rock mass.	D = 0.8
	Small scale blasting in civil engineering slopes results in modest rock mass damage, particularly if controlled blasting is used as shown on the left hand side of the photograph. However, stress relief results in some disturbance.	D = 0.7 Good blasting  D = 1.0 Poor blasting
	Very large open pit mine slopes suffer significant disturbance due to heavy production blasting and also due to stress relief from overburden removal.  In some softer rocks excavation can be carried out by ripping and dozing and the degree of damage to the slopes is less.	D = 1.0 Production blasting  D = 0.7 Mechanical excavation

Figure B.4. Guidelines for estimating disturbance factor D (Hoek, 2000).



